A Szilikátipari Tudományos Egyesület lapja

építőanyag

Journal of Silicate Based and Composite Materials

A TARTALOMBÓL:

2022/5

Invitation to CMCEE-14

The 14th International Conference on Ceramic Materials and Components for Energy and Environmental Applications (CMCEE-14) will be held in the beautiful city of Budapest, Hungary. The conference series began in 1980s and has established a strong reputation for state-of-the-art presentations and information exchange on the latest emerging ceramic technologies and their wide ranging applications. CMCEE-14 will contain more than 30 symposia covering wide range of topics, which will facilitate global dialogue and discussion with leading world experts to ceramic technologies for sustainable development of society.

We would like to invite all of you to actively participate in the conference and visit the city of Budapest. We are quite hopeful that this conference will provide excellent forum for interaction and friendship with participants from various continents.

We hope to meet you all in 2024!

About Budapest

Budapest is famous not only for the monuments reflecting its own 1,000-year-old culture, but also for the relics of others who settled here. Remains from both Roman occupation and much later ruled by the Turks can still be seen in the city. After the Ottoman Empire the union with Austria has a particular influence on the city's form and style.

Conference venue

Budapest Congress Center & Novotel Budapest City****Budapest Congress Center is the largest, most convenient, modern event facility in Budapest. It has over 20 meeting rooms in various shapes and sizes, adjustable for every possible need, as well as an exhibition space of over a 4000 m^2, which means it can hold separate events at the same time without them interfering with each other. International congresses, exhibitions, professional conferences, corporate meetings, gala dinners, tradeshows, fairs, concerts, plays or graduation ceremonies – Budapest Congress Center is perfect for them all!

https://akcongress.com/cmcee14

építőanyag

Journal of Silicate Based and Composite Materials

2022/5

TARTALOM

CONTENT

A finomkerámia-, üveg-, cement-, mész-, beton-, tégla- és cserép-, kő- és kavics-, tűzállóanyag-, szigetelőanyag-iparágak szakmai lapja
Scientific journal of ceramics, glass, cement, concrete, clay products, stone and gravel, insulating and fireproof materials and composites

A folyóiratot referálja · The journal is referred by:

ProQuest · Google Scholar · INDEX COPERNICUS INTERNATIONAL · THOMSON REUTERS

A folyóiratban lektorált cikkek jelennek meg.
All published papers are peer-reviewed.
Kiadó · Publisher: Szilikátipari Tudományos Egyesület (SZTE)
Elnök · President: ASZTALOS István
1034 Budapest, Bécsi út 120.
Tel.: +36-1/201-9360 ▪ E-mail: epitoanyag@szte.org.hu
Tördelő szerkesztő · Layout editor: NÉMETH Hajnalka
Címlapfotó · Cover photo: GYURKÓ Zoltán

WWW.EPITOANYAG.ORG.HU
EN.EPITOANYAG.ORG.HU

Online ISSN: 2064-4477
Print ISSN: 0013-970x
INDEX: 2 52 50 ▪ 74 (2022) 163–206

Synthesis of geopolymer binder from the partially de-aluminated metakaolinite by-product resulted from alum industry

Nabil A. ABDULLAH
Director of Research & Development at Aluminum Sulphate Co. of Egypt. Ph.D. in Environmental science, Faculty of science, Ain Shams University, Egypt.

Tarek M. EL-SOKKARY
Head of Institute of Raw Building Materials Technology and Processing Research Institute, Housing & Building National Research Center (HBRC), Cairo, Egypt. Professor at the Raw Building Materials Technology and Processing Research Institute, Housing & Building National Research Center (HBRC), Cairo, Egypt. Ph.D. Geop, Zagazig University, Cairo, Egypt.

Mahmoud GHARIEB
Researcher (Assistant Professor), Institute of Raw Building Materials Technology and Processing Research, Housing & Building National Research Center (HBRC), Cairo, Egypt. Ph.D., Ain Shams University, Cairo, Egypt.

Nabil Ahmed ABDULLAH ▪ Research Supervisor, Aluminum sulphate Co. of Egypt ▪ nabilxp9@gmail.com
T. M. EL-SOKKARYB ▪ Raw Building Materials Technology and Processing Research Institute, Housing & Building National Research Center (HBRC), Egypt
Mahmoud GHARIEBB ▪ Raw Building Materials Technology and Processing Research Institute, Housing & Building National Research Center (HBRC), Egypt

Érkezett: 2022. 05. 02. ▪ Received: 02. 05. 2022. ▪ https://doi.org/10.14382/epitoanyag-jsbcm.2022.25

Abstract
In this study an experimental work has been done to test the feasibility of using partially de-aluminated metakaolin (PDK) with metakaolin (MK) in the production of geopolymer binder. The chemical composition and physical properties of de-aluminated metakaolin was tested. For this purpose, metakaolin (MK) was partially substituted with partially de-aluminated metakaolin (PDK) at ratios of 0-60% by weight. The alkaline activator was NaOH. Geopolymer pastes were cured at room temperature. The compressive strength was measured by testing standard cubes at 7 and 28 days. Satisfactory results have been achieved by using 15, 20, 30, 35 wt.% of PDK. Hence it was suggested to use the local metakaolin with added proportions of PDK up to 35% of metakaolin to produce economic geopolymer binder. It is technically feasible, resulting in a sustainable and environmentally friendly source of vitreous material. The effect of PDK on porosity and compressive strength were tested. The internal microstructure, and hydration were investigated by using modern methods such as, Thermo-gravimetric (TGA) and differential thermal analysis (TGA, DTGA), scanning electron microscopy (SEM) and Fourier transform infrared spectroscopy (FTIR). The findings assure the potentiality for the application of PDK as a siliceous material can be used in manufacturing of geopolymer cement.
Keywords: partially de-aluminated metakaolin (PDK), geopolymer, metakaolin, compressive strength, microstructure
Kulcsszavak: részben alumíniummentesített metakaolin (PDK), geopolimer, metakaolin, nyomószilárdság, mikroszerkezet

1. Introduction

Geopolymer is a good binding material which can be used in several construction fabrications, since it can be casted in situ at the ambient temperature like ordinary mortar/concrete but of higher surface quality. Stained geopolymer paste can be fabricated by using metakaolin and various pigments. Geopolymer product has better resistance against acid and heat compared to Ordinary Portland Cement (OPC) concrete or mortar [1-4].

The natural siliceous rocks and OPC can be replaced by geopolymer binder with better physical and chemical properties such as acid and saline water resistance, early development of mechanical strength [5-7].

Geopolymer was patented by using of the highest rank of clay minerals (kaolin), as a source of alumina and silica for preparation of geopolymer through the reaction of the kaolin with alkaline silicate solution [8-10]. It's commonly carried out by the interaction of a fine ground aluminum silicate materials with an alkali metal silicate solution at room temperature forming polymer chain (-Si–O–Al–O-) [11, 12]. Geopolymer is a type of amorphous aluminous-siliceous cementitious material which can be produced by polymerization reaction of aluminum silicates materials with alkali metals solutions. Geopolymeric mortar/concrete can be produced by using of pozzolana, which is a waste material obtained from various activities. The numerous characteristics of inorganic polymer can be determined from civil works in term of the mechanical characteristics such as compressive strength for geopolymeric mortar and concrete, resistance to chemicals attack [13-16] excellent repairing substances for ancient constructions, to the modern applications in aircraft which utilizes the property of anti-fire characteristics of the geopolymer blends [17, 18]. Various geopolymer blends does not ignite, or evolve gases even after extended exposure of heat. Therefore, they are excellent inert materials for aircraft lining cabins, floor panels, sidewalls, and insulators for wires [19, 20].

The inorganic and physical chemistry, with other geological science such as mineralogy, geochemistry and engineering, utilized the unique characteristics of geopolymer. The potential applications of geopolymer includes: refractory, low energy ceramic tiles, tech composites for aircraft interior and automobile decoration artifacts, thermal insulation, thermal shock refractories, concretes, certain blends for construction repairing and supporting, radioactive and toxic waste containment immobilization, archaeological restoration [21-24].

Metakaolinite is a greatly utilized as one of the precursors starting materials for manufacturing of geopolymeric binder, and is produced by calcination of kaolinite clay. The thermal treatment of clay minerals in the range from 550 up to 800 °C causes dehydroxylation of from the internal structure of the clay mineral. The coordinated hydroxyl groups of the octahedral aluminate sheet are lost and the structure becomes disordered meta-phase in which the internal crystalline structure of clay minerals is collapsed. The stable phase of the distorted kaolinite is reactive and is called pozzolanic material [25, 26]. Calcination of kaolinite at higher temperatures causes reorganization of the internal structure and crystallization forming spinel and mullite minerals [27, 28]. Several studies have reported the using of byproduct or waste materials in the manufacturing of geopolymer, such as fly ash and granulated slag as an aluminum silicate materials [29, 30]. This reaction yields water, while in OPC hardening, water is required for startup of hydration reactions. Upon heating of OPC concrete at 300 °C, dehydration takes place yielding dehydrated products causing shrinkage and formation of calcium oxide and carbonation of calcium at 500 °C, further heating up to 800 °C calcium carbonate decomposes forming caustic lime, while, geopolymer become stable up to 1000 °C. Ordinary Portland Cement (OPC) is the primary ingredient in concrete of structure of the buildings, and the roads and bridges. Production of cement releases the major greenhouse gas CO_2. Heating of limestone and fossil fuels result in CO_2. Hence to reduce CO_2 emissions it is required to find an alternative for the traditional cement [31, 32].

PDK is a by-product of aluminum sulphate industry and it derives from acid leaching of MK (e.g. calcined kaolin, $Al_2O_3{\cdot}2SiO_2$). As result of the de-alumination process, the SiO_2/Al_2O_3 ratio and BET values are increased. The increasing of specific surface observed as consequence of acid attack was found due to the increasing of the pore volume [33].

It was found that mixing of PDK and lime and using isothermal calorimetric tests, PDK shows an appreciable pozzolanic activity [34, 35]. The pozzolanic activity of PDK in blended cements was also demonstrated by the same method. They also reported that PDK exhibits higher BET values than silica fume. Other researchers have also shown that the porous structure of calcined kaolin particles does not collapse owing to the acid attack [36].

Zhang et al. [37] investigated the effect of the three key ratios "SiO_2/Al_2O_3, M_2O/Al_2O_3, H_2O/M_2O" on the production of metakaolinite-based geopolymers, where M is alkali metal ions (Na^+ or K^+). Several blends of different mole ratios SiO_2/Al_2O_3, Na_2O/Al_2O_3, H_2O/Na_2O were adopted to examine their impacts on the mechanical strength. The results of all tests that were obtained exhibit that the ratios Na_2O/Al_2O_3 and H_2O/Na_2O had direct impact on the compressive strength. It was found that highest compressive strength (34.9 MPa) was recorded at a ratio SiO_2/Al_2O_3= 5.5, Na_2O/Al_2O_3= 1.0 and H_2O/Na_2O = 7.0. These ratios achieved complete geopolymerisation reaction. Referring to the results of the current paper, it was found that the compressive strength increases with increase in quantity of PDK to reach maximum at SiO_2/Al_2O_3=2.8, Na_2O/Al_2O_3 = 0.9 and H_2O/Na_2O = 13.7. These ratios may differ from the above, this attributed to the raw materials and the preparation of alkaline silicates from DK, and so, the compressive strength of the concrete relies upon the quantity of activated aluminum silicates materials in the precursors, the activating solution type and the curing temperature as reported by [38, 39].

From the above results obtained, it was noted that there is no need for higher temperature curing, whereas activation was preceded properly. Geopolymer concrete produced show higher compressive strength without need to add sodium silicate, as sodium silicate was formed during activation process as a result of the chemical reaction between activated silicate in PDK and the stoichiometry amount of sodium hydroxide. Workability of geopolymer concrete is very low at the nominal blends. So, superplasticizer of any type or little excess water has to be added to facilitate workability.

In this study an experimental work has been done to test the feasibility of using industrial wastes of PDK as a source of uncommon silicates with MK in the production of geopolymer concrete. For this purpose, MK was partially substituted with PDK at ratios of 0, 5, 10, 15, 20, 25, 30, 35, 40, 45, 50, 55, and 60% by weight. The compressive strength was determined by testing standard cubes at 7th and 28th day. The effect of PDK on the specific gravity, porosity and mechanical characteristics were studied. The presence of crystalline components, hydration and the internal structure were tested.

2. Experimental procedure

2.1 Materials

Metakaolin was prepared in ASCE laboratory, kaolin was supplied from south Sinai Quarries. Metakaolin was produced by thermal dehydroxylation at 750 °C for 2 hr. and the PDK were collected from aluminum sulphate Co. of Egypt (ASCE). *Fig. 1(a* and *b)* show the thermogravimetric analysis (TG/DTG) of raw kaolin and MK, displaying the water released and the total mass loss (14.23 wt. %, 0.04% respectively) at the optimum temperature for calcination of kaolin (750 °C).

Aluminum oxide in PDK is significantly lower than corresponding value of MK due to the dealumination process that performed by sulphuric acid for formation of aluminum sulphate product. This lead to an appreciable increase of SiO_2/Al_2O_3 ratio (from 1.94 for average value in MK to 16.95 for average value in PDK). In mortar mixes, sand stone was used with density 2.5. Different conditioning procedures were also adopted for PDK before using it as an additive: PDK was adopted as amorphous silicate source after drying in oven at 100°C for 12 h. The dry source was also used after further grinding; the ground source was also used after further dispersion as water slurry (ground-slurry). BET analysis revealed a high fineness for PDK (43 m^2/g) and the density of 1.36. BET results of MK and PDK are plotted in *Fig. 2 (a* and *b)* which shows that 90% of MK diameter is ~8.6 μm and 10% is ~1.3 μm with an average diameter of ~4.5 μm. and 90% of PDK diameter is ~70.33 μm and 10% is ~4.3 μm with an average diameter of ~9.5 μm. The surface texture of PDK particles characterized by high roughness as already observed by [32]. PDK plays a significant role in simultaneous synthesis of sodium silicate during geopolymerisation process. The

reaction between PDK and NaOH increases the building up of strength of the fabricated geopolymer mortar by inducing the activation and speciation of siliceous aluminous ions of the raw materials, and self-formation of alkaline silicate compensate shortage of silicate in the geopolymerisation medium.

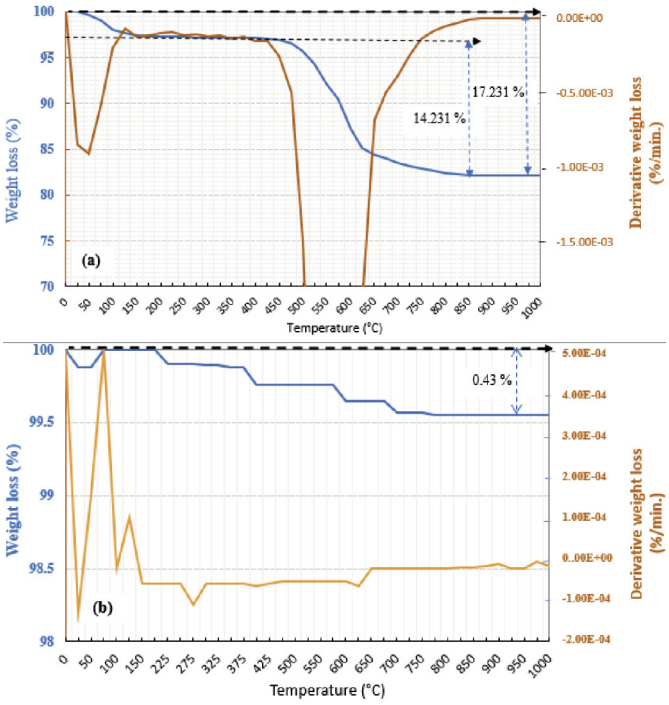

Fig. 1 Thermal gravimetric analysis (TGA / DTGA) of (a) raw kaolin and (b) calcined kaolin at 750 °C for 2 hrs. (MK)
1. ábra A nyers kaolin (a) és a 750 °C-on történő 2 órás hőkezelés után kaolin (b) termogravimetriás analízise (TGA/DTGA)

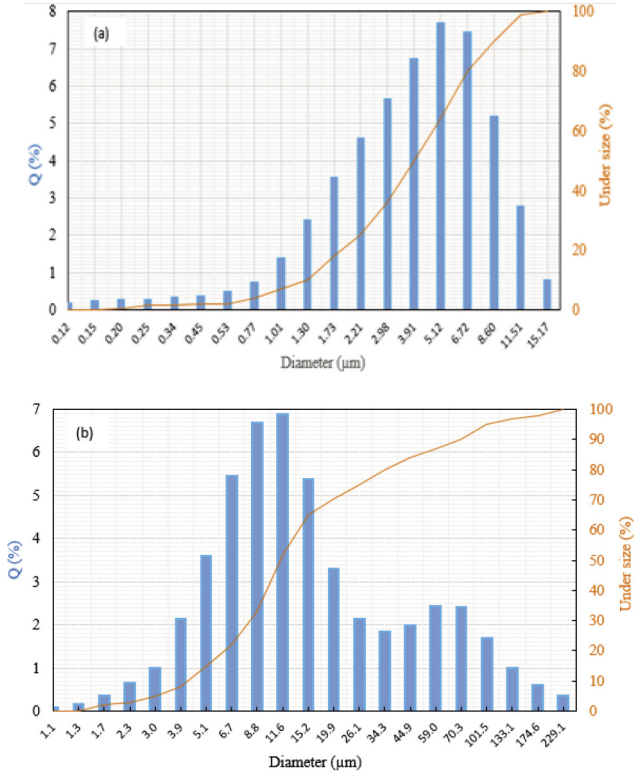

Fig. 2 Particle size distribution [(a) for MK and (b) for PDK
2. ábra Az MK (a) és a PDK (b) szemcseméret-eloszlása

The chemical composition of (MK) and (PDK) are shown in *Table 1*. According to the percentages of SiO_2+Al_2O_3+Fe_2O_3 in DK is about, which fulfill the requirements of IS 3812:2003 this sample can be considered as a pozzolanic material. The mineralogical characteristics of MK and PDK are shown in *Fig. 3 (a* and *b)*. XRD show that there is no mineral in the MK samples prepared, just only mullite resulted during calcination and quartz impurities derived from the source kaolin. XRD pattern of PDK shows quartz, kaolinite montmorillonite peaks and amorphous background.

Compound	Amount (weight %)		EN 450-1 Limits
	PDK	MK	
SiO_2	82.83	52.2	
SiO_2 (active)	60 = 1.0 M	37.43 = 0.62 M	Not less than 25%
Al_2O_3	6.00 = 0.059 M	33 = 0.32 M	-
SiO_2/Al_2O_3	16.95	1.94	
Fe_2O_3	0.50	1.41	-
TiO_2	3.20	2.2	-
MgO	0.09	0.19	Less than 4%
CaO	0.15	0.51	-
Na_2O	0.03	0.16	Less than 5%
K_2O	0.05	0.07	-
SO_3	0.85	0.39	Less than 3%
P_2O_5	0.01	0.12	Less than 5%
SrO	0.046	-	-
Cl-	0.06	0.11	Less than 0.1%
L.O.I	5.84	5.05	Category A: Not greater than 5.0% by mass / Category B: Not greater than: 7.0% by mass / Category C: Not greater than 9.0% by mass

Table 1 Chemical analysis of PDK and MK from ASCE
1. táblázat A PDK és az MK kémiai elemzése az ASCE-től

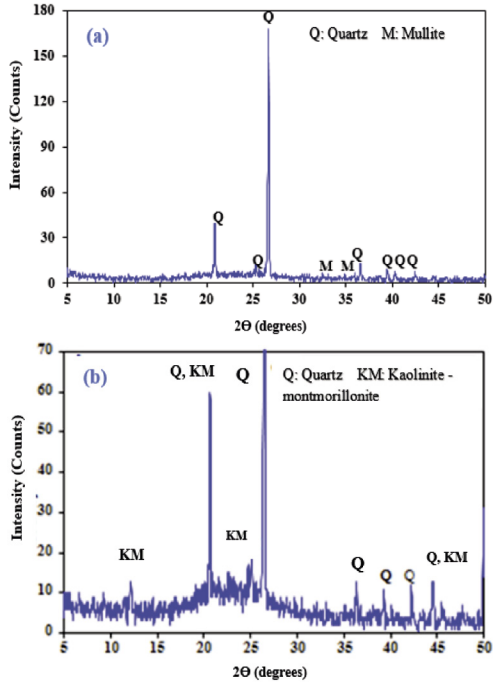

Fig. 3 XRD patterns of (a) MK and (b) PDK
3. ábra Az MK (a) és a PDK (b) XRD mintái

2.2 Geopolymerisation and curing

Geopolymer samples were prepared by added dry materials of PDK to MK in ratio of 0:100, 5:95, 10:90, 15:85, 20:80, 25:75, 30:70, 35:65, 40:60, 45:55, 50:50, 55:45 and 60:40 by weight, and alkali metal activating solutions (alkaline sodium hydroxide) and water in a 70-L pan mixer are given in *Table 2*. These different combinations of PDK and MK were used with two molar concentration of Na_2O (2.32 and 1.94) that have achieved two ranges of Na_2O/Al_2O_3 (0.83–0.96 M) and (0.70 – 0.80 M) respectively. NaOH was applied as an alkali metal activating solution in this research. Sodium hydroxide in platelet form was dissolved in distilled water to produce 12.26 M (Na_2O) sodium hydroxide solution.

Mix No.		Ratios of binder in geopolymer	
Na_2O (2.32 M)	Na_2O (1.94 M)		
Na_2O/Al_2O_3 (0.83- 0.96 M)	Na_2O/Al_2O_3 (0.70 – 0.80 M)	Partially De-aluminated metakaolin (PDK), weight %	Metakaolin (MK), weight %
M1	M14	0	100
M2	M15	5	95
M3	M16	10	90
M4	M17	15	85
M5	M18	20	80
M6	M19	25	75
M7	M20	30	70
M8	M21	35	65
M9	M22	40	60
M10	M23	45	55
M11	M24	50	50
M12	M25	55	45
M13	M26	60	40

Table 2 The mix combinations between PDK and MK
2. táblázat A PDK és az MK keverékösszetételei

For improvement of the workability of geopolymer pastes, the suitable amount of water needed for geopolymer mixing was determined, normal consistency was measured applying Humboldt Vicat's apparatus [40, 41]. The dry components of the precursors were blended firstly and the alkali activating solution were then added into the pan and mixed thoroughly for about 4 min until the mixture became glossy and well blended. The mixture was then poured into 5 cm^3 cubic moulds, vibrated for perfect compaction and insulated with a cover to prevent loss of water as most as possible. All blends were kept undisturbed for curing at the ambient temperature for (24 hrs.), demolded and then subjected to further curing at the room condition 23-25 °C, and then tested for the compressive strengths. The resulted fragments were then immersed in acetone for 24 h before being dried at 60 °C, and pulverized for analysis [42].

2.3 Methods of investigation

The total-porosity was done for the relatively higher compressive strength specimens (M1 – M13). It was measured by the same equation applied previously in [44, 45] as in Eq. (1):

$$\text{The total porosity (\%)} = \frac{W1 - W3}{W1 - W2} \times 100, \quad (1)$$

Whilst the percentage of absorbed water was recorded by:

$$\text{Water-absorption (\%)} = [(W1-W3)/W3] \times 100. \quad (2)$$

Where: W1: saturated-weight, W2: suspended-weight and W3: dried-weight at 105 ± 2 °C. FTIR used for illustration of the crystalline and the amorphous constituents of geopolymer structure using Jasco-6100 with the aid of KBr binder in the range from 400 to 4000 cm^{-1} [46, 47].

The morphology and microstructure of hardened geopolymer composites was examined by SEM [Inspect S-FEI Company, Netherlands] equipped with EDX. Thermogravimetry conducted using DT-50 Thermal Analyzer (Shimadzu Co-Kyoto, Japan), where the samples were crushed, transferred immediately to an alumina crucible, held under isothermal conditions for 60 min at 40 °C to equilibrate in a nitrogen environment (N_2 flowing at 200 ml/min), and then heated to1000 °C at 10 °C/min in the same gas environment.

3. Results and discussion

3.1 Total-porosity and water-absorption

Fig. 4 illustrates the total-porosity of the investigated specimens at 28 days. Generally, the total-porosity decreases with the older hydration age. This is related to the continuous hydration and accumulation of hydration-products that occupies the available micro-pores within the binder matrix causing a pore size decreasing and reducing the total-porosity as well. As it can be noticed from *Fig. 4*, the presence of 25 weight % PDK (M6) marginally decreases the total-porosity at 28 days as compared to the reference. This reduction refers to the filling and pozzolanic impact of the fine PDK particles. These fine-particulates and hydration products that precipitate in the pores of the solidified geopolymer blend and consequent increase in the bulk density. However, the presence more than 25 weight % PDK causes relative increase of the total-porosity. This result are expected, because if the amount of the finest particles is higher than the optimum packing arrangement, the packing density reduces due to the clustering, leaving fin holes in between the clusters.

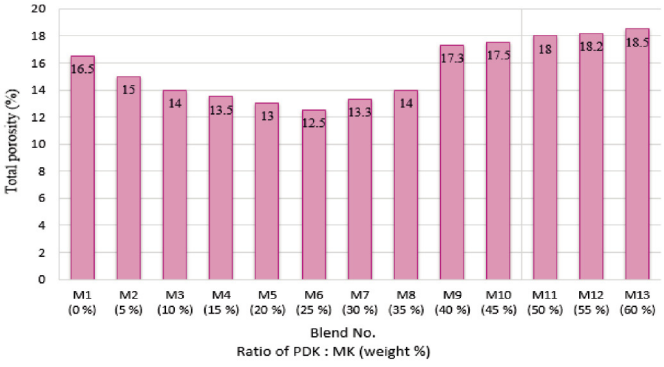

Fig. 4 Total porosity of the different combination of SiO_2 and Al_2O_3 at curing time of 28 days using constant Na_2O and the Na_2O/Al_2O_3 of 0.83 - 0.96
4. ábra A SiO_2 és Al_2O_3 különböző kombinációinak teljes porozitása 28 napos kikeményedési idő, állandó Na_2O és 0,83-0,96 Na_2O/Al_2O_3 értékek alkalmazásával

Fig. 5 illustrates the percentage of water-absorption for the tested specimens at 28 days. As expected, the trend of the water absorption is directly proportion with those of total-porosity.

The presence of 25 weight % PDK (M6) reduces the percentage of water-absorption at 28 days, whilst the presence more than or lower than 25 weight % increases it in a relative manner. So, it can be concluded that the preferred range of PDK is from 20 to 30 weight % and optimized at 25 weight %.

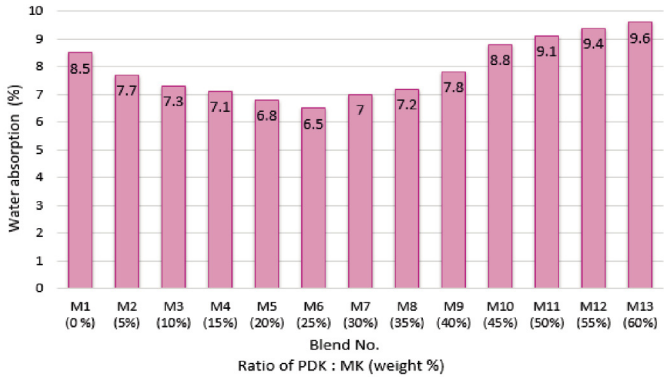

Fig. 5 Water absorption of the different combination of SiO_2 and Al_2O_3 at curing time of 28 days using constant Na_2O and the Na_2O/Al_2O_3 of 0.83 - 0.96
5. ábra A SiO_2 és az Al_2O_3 különböző kombinációinak vízfelvétele 28 napos kikeményedési idő, állandó Na_2O és 0,83-0,96 Na_2O/Al_2O_3 arány alkalmazásával

3.2 Compressive strength

Variation of compressive strength with different combinations of SiO_2 and Al_2O_3 and different ratios of Na_2O are given in *Tables 3, 4* and the results are also graphically illustrated as a function of curing period in *Figs. 6* and *7*. The results reveal that the compressive strength increases with increasing hydration time (7 and 28 days) for all curing conditions due to continuous geopolymerisation and hydration reactions, also the compressive strength maximize at 25 weight % (M6) and then decreased with further addition up to 60 weight % (M13). It was found that the addition of PDK increase the compressive strength, it reach to a maximum value of 64 MPa at a percentage of 25 weight % PDK (M 6). It was found also that addition of PDK up to 55 weight % provide satisfactory compressive strengths at 7th and 28th days.

PDK was used as a source of active silica in the form of silicate of de-aluminated kaolinite along with metakaolin for manufacturing of geopolymer mortar. The effect of the three key ratios "SiO_2/Al_2O_3, M_2O/Al_2O_3, H_2O/M_2O" on the production of metakaolinite-based geopolymers, where M express the alkali metal ions (Na or K ion) was investigated. A total of 26 geopolymer pastes with different mole ratios SiO_2/Al_2O_3, Na_2O/Al_2O_3, H_2O/Na_2O were prepared to examine their effects on the compressive strength. The gradation analysis of experimental results that were obtained revealed that Na_2O/Al_2O_3 and H_2O/Na_2O had significant impact on the compressive strength. The compressive strength increases up to 64 MPa with increasing in the quantity of PDK to reach maximum at SiO_2/Al_2O_3=2.8, Na_2O/Al_2O_3 = 0.9 and H_2O/Na_2O = 13.7 these ratios were considered as fully reacted geopolymer mortar (*Table 3, Fig. 6*). Satisfactory results have been achieved at SiO_2/Al_2O_3=2.8, Na_2O/Al_2O_3 = 0.75 and H_2O/Na_2O = 13.7 (*Table 4, Fig. 7*), but of lower compressive strength, so it is very important to optimize the Na_2O/Al_2O_3 ratio to be in the range of 0.83-0.96 to get better mechanical characteristics of the geopolymer binder.

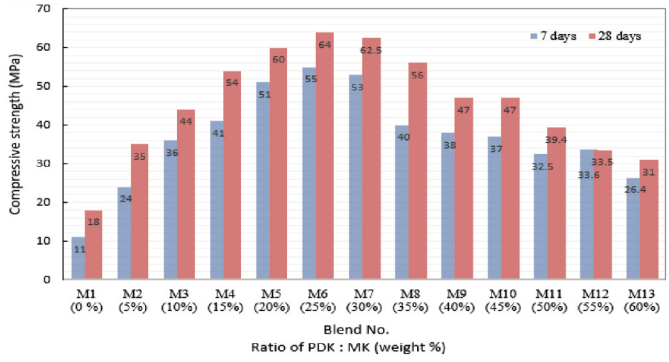

Fig. 6 Compressive strength of the different combination of SiO_2 and Al_2O_3 at curing time of 7 and 28 days using constant Na_2O that made the Na_2O/Al_2O_3 to be 0.83 - 0.96
6. ábra A SiO_2 és az Al_2O_3 különböző kombinációinak nyomószilárdsága 7 és 28 napos kikeményedési idő, állandó Na_2O és 0,83-0,96 Na_2O/Al_2O_3 arány alkalmazásával

No.	PDK		H_2O	NaOH Na_2O	H_2O Total	MK Molar ratio		SiO_2/Al_2O_3 Molar ratio	Na_2O/Al_2O_3 Molar ratio	H_2O/Na_2O Molar ratio	Compressive strength, (MPa)	
	SiO_2 Moles	Al_2O_3 Moles	Moles	Moles	Moles	SiO_2 Moles	Al_2O_3 Moles				7 days	28 days
M1	0	0						1.90	0.96		11	18
M2	0.5	0.029						2.0	0.94		24	35
M3	1.0	0.058						2.28	0.93		36	44
M4	1.5	0.087						2.45	0.92		41	54
M5	2.0	0.116						2.60	0.91		51	60
M6	2.5	0.145						2.80	0.90		55	64
M7	3.0	0.174	23	2.32	31.8	4.68	2.43	2.95	0.89	13.7	53	62.5
M8	3.5	0.203						3.10	0.88		40	56
M9	4.0	0.232						3.26	0.87		38	47
M10	4.5	0.261						3.41	0.86		37	47
M11	5.0	0.290						3.56	0.85		32.5	39.4
M12	5.5	0.319						3.70	0.84		33.8	33.5
M13	6.0	0.348						3.84	0.835		26.4	31

Table 3 Compressive strength at the 28 day for a molar ratio of Na_2O/Al_2O_3 between 0.83-0.96
3. táblázat 28 napos nyomószilárdság a Na_2O/Al_2O_3 0,83-0,96 közötti moláris aránya esetén

No.	PDK		H_2O Moles	NaOH Na_2O Moles	H_2O Total Moles	MK		SiO_2/Al_2O_3 Molar ratio	Na_2O/Al_2O_3 Molar ratio	H_2O/Na_2O Molar ratio	Compressive strength, (MPa)	
	SiO_2 Moles	Al_2O_3 Moles				SiO_2 Moles	Al_2O_3 Moles				7 days	28 days
M14	0	0						1.90	0.80		8	12
M15	0.5	0.029						2.0	0.799		17	25
M16	1.0	0.058						2.28	0.78		32	44
M17	1.5	0.087						2.2.45	0.77		39	51
M18	2.0	0.116						2.60	0.76		41	52
M19	2.5	0.145						2.80	0.75		45	54
M20	3.0	0.174	22	1.94	26.7	4.68	2.43	2.95	0.74	13.7	33	44
M21	3.5	0.203						3.10	0.73		30	43
M22	4.0	0.232						3.26	0.73		30	40
M23	4.5	0.261						3.41	0.72		33	40
M24	5.0	0.290						3.56	0.71		28	35
M25	5.5	0.319						3.70	0.705		22	30
M26	6.0	0.348						3.84	0.70		16	22

Table 4 Compressive strength at the 28 day for a molar ratio of Na_2O/Al_2O_3 between 0.70-0.8
4 táblázat 28 napos nyomószilárdság a Na_2O/Al_2O_3 0,83-0,96 közötti moláris aránya esetén

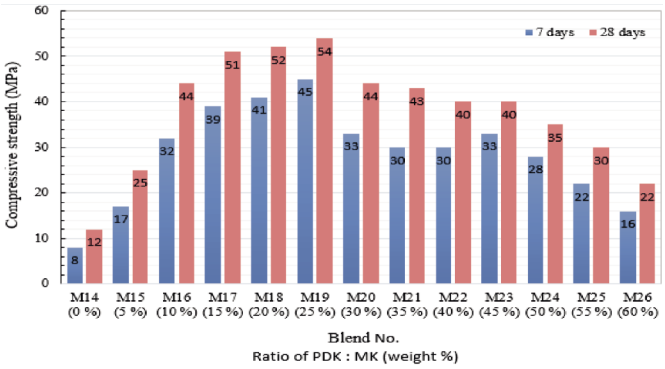

Fig. 7 Compressive strength of the different combination of SiO_2 and Al_2O_3 at curing time of 7 and 28 days using constant Na_2O that made the Na_2O/Al_2O_3 to be 0.70 – 0.80
7. ábra A SiO_2 és az Al_2O_3 különböző kombinációinak nyomószilárdsága 7 és 28 napos kikeményedési idő, állandó Na_2O és 0,70-0,80 Na_2O/Al_2O_3 arány alkalmazásával

3.3 Thermal analysis (TGA and DGA)

Figures 8, 9 show the differential thermogravimetric/thermogravimetric analysis (DTG/TG) for geopolymer composites with various ratio of PDK. *Figure 8* shows the main endothermic peaks at about 80, 170, 450, and 700 °C whereas the first peak of the characteristic endotherm represents the free water released from the polymerization reactions, coined in macro pores of the geopolymer binder [48, 49], the second peak represents the dehydroxylation step of the strongly bound water in zeolite, as well as the dehydroxylation of strongly bound water in a calcium silicate hydrate (C-S-H gel) binder [50]. There are another endothermic peak at about 700 °C representative for calcium carbonate [51] resulting from the natural processes on the PDK after sample preparation. The figure illustrates the growth in the strength of endothermic peak at about 80 °C with curing time in mix M6 at 28 days as a results of continuous hydration and development of geopolymer reactions with aging, while there is a significant shifting in this endotherm to higher temperature informing the presence of aluminum silicate gel with strongly bound water within the geopolymeric chains in M6 rather than the other samples (*Fig. 8*). Through the examination of the effect of the added PDK, the endothermic peak for free water, increased with PDK addition to about 25 weight % indicating the growth of amorphous geopolymer content with weakly bound free water. It can witnessed that here is a clear endothermic peak for water escaped of C-S-H gel and aluminum silicate gel at 170 °C for which increased in strength with PDK addition up to 25 weight % (M6) as a results of the building up in geopolymerisation reactions which used the free silica in geopolymer production than in CSH alumino- silicate gel. A weak peak for M6 appeared at 700 °C, which refers to the destruction of carbonate salt into carbon dioxide [52]. There is wide peak in the carbonate endotherm at 650 - 700 °C, whereas the excess free alkali metal hydroxide that is not consumed in geopolymer formation as a result of early synthesis of Faujasite zeolite mineral formation which partially hinders geopolymerisation and this may cause efflorescence M1 and M5. *Fig. 9* shows the weight loss of PDK based geopolymer mixes M1, M5, M6 and M7 at 28 days were 3.43, 4.5, 5.1 and 3.5%, respectively. It can be seen the total weight loss increases with PDK increase up to 25 weight % (M6) as an indication for relatively higher rate of geopolymerisation. The high water loss for M1 at a temperature greater than 800 °C displays that the early formed Faujasite zeolite beside geopolymer is destructed releasing the chemical bonded water.

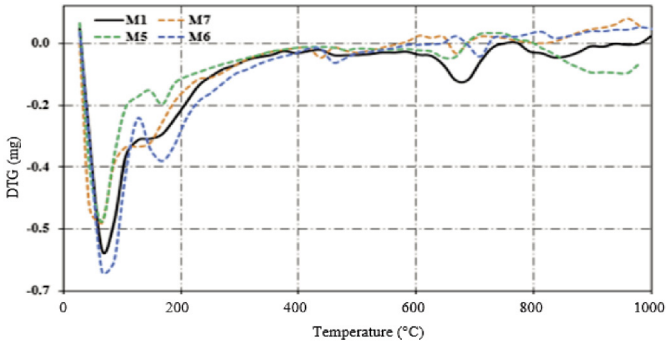

Fig. 8 Differential thermo-gravimetric analysis (DTGA) of the different combination of SiO_2 and Al_2O_3 at curing time of 28 days using constant Na_2O that made the Na_2O/Al_2O_3 to be 0.83-0.96
8. ábra A SiO_2 és az Al_2O_3 különböző kombinációinak differenciális termogravimetriás analízise (DTGA) 28 napos kikeményedési idő és állandó Na_2O alkalmazásával, a Na_2O/Al_2O_3 arány 0,83-0,96

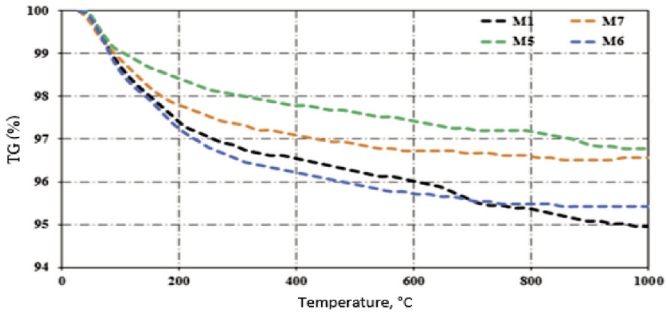

Fig. 9 Thermo-gravimetric analysis (TGA) curves of the different combination of SiO_2 and Al_2O_3 at curing time of 28 days using constant Na_2O that made the Na_2O/Al_2O_3 to be 0.83 - 0.96

9. ábra A SiO_2 és az Al_2O_3 különböző kombinációinak termogravimetriás (TGA) görbéi 28 napos kikeményedési idő és állandó Na_2O alkalmazásával, a Na_2O/Al_2O_3 arány 0,83-0,96

3.4 Fourier transforms infrared spectroscopy (FTIR)

FTIR spectra of the solidified geopolymer pastes which having different ratio of PDK are shown in *Fig. 10*. As can be seen, there are main wide bands of O-H stretching and bending located in the range of 3430-3460 cm^{-1} and 1650 cm^{-1} that characterize the water of crystallization of the hydrated compounds such as calcium silicate hydrate (C–S–H) and calcium alumino-silicate hydrate (C–A–S–H) [53]. The band intensities of the sample M6 is relatively bigger than the other blends. These confirm the higher strength of the M6 sample. The bands located between 1420-1460 cm^{-1} representative to stretching vibrations of O–C–O bond of carbonate compounds, which resulted from the reaction of carbon dioxide with the leached out alkali hydroxide [54]. The strongest band located at 950–1100 cm^{-1} is essentially resulted from the asymmetric stretching vibration of (T-O-Si), where T is tetrahedral silicon or aluminum. As seen, the bands featured for asymmetric stretching vibration of Si–O-T located at approximately 980 cm^{-1} are displaced to a lower frequency for M6 sample. This displacement is an evidence for the formation of amorphous aluminum silicate phases, indicating to new highly cross-linked geopolymer network [55]. The intensity of the band of M6 sample is higher than the other samples. The higher intensity of the band is an indication of increasing the mean chain length of aluminum silicate polymers [56]. Furthermore, the symmetric stretching vibration (Si-O-Si) in the region of 770 cm^{-1} and 690 cm^{-1} and bending vibration (Si–O– Si) and (O-Si-O) in the region of 500 cm^{-1} band intensities of M6 sample are relatively higher than other samples.

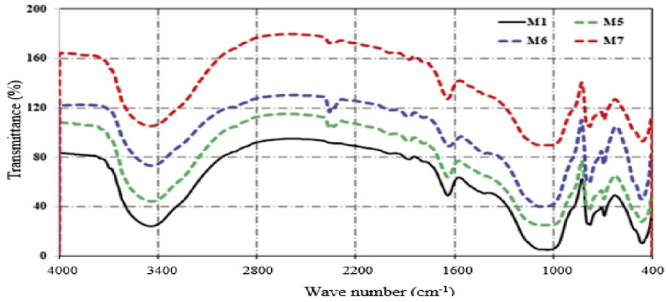

Fig. 10. FTIR spectra of the geopolymer pastes of different ratio of SiO_2 and Al_2O_3 at curing time of 28 days using constant Na_2O that made the Na_2O/Al_2O_3 to be 0.83 - 0.96

10. ábra A SiO_2 és Al_2O_3 különböző arányú geopolimer paszták FTIR spektrumai 28 napos kikeményedési időnél, állandó Na_2O alkalmazásával, a Na_2O/Al_2O_3 arány 0,83-0,96

3.5 Microstructure analyses

The micrographs of electron scanning microscope for geopolymer pastes at the 28th day which have having different ratio of DK are shown in *Fig. 11*. The micrograph for control blend M1 show micro-porous matrix formation with the distribution of both CSH and geopolymer within the matrix (*Fig. 11a*), while applying more DK up to 25% (M6) results in the generation of intensified homogenized geopolymer structure with growth of the amorphous (N-A-S-H) gel and the binding gels (C–A–S–H) that has advanced impact on the micro-structural characteristics forming compacted three-dimensional network from geopolymer strains (*Fig. 11b*). Adding more DK results in an increased dissimilarity with large spaces between its components causing reduction of the effectiveness of the reactions (*Fig. 11c*) as interpreted from the FTIR and DTG.

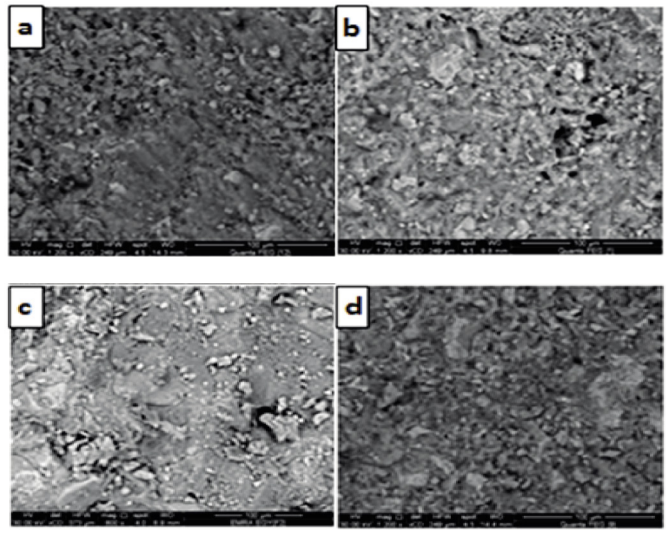

Fig. 11 SEM micrographs of the geopolymer pastes of different ratio of SiO_2 and Al_2O_3 at curing time of 28 days using constant Na_2O that made the Na_2O/Al_2O_3 to be 0.83 - 0.96 for the blends M1 (a), M5 (b), M6(c) and M7 (d).

11. ábra A SiO_2 és Al_2O_3 különböző arányú geopolimer paszták SEM mikroszkópos felvételei 28 napos kikeményedési idő és állandó Na2O alkalmazásával, a Na_2O/Al_2O_3 arány 0,83-0,96 volt az M1 (a), M5 (b), M6(c) és M7 (d) keverékek esetében

4. Conclusions

The following items were concluded from the study the potentiality for using PDK as a siliceous material for manufacturing of geopolymer cement.

1. The geopolymer cement produced with different combination of MK and PDK are able to produce geopolymer cement (mortar) of high compressive strength (64 MPa) by self-curing mechanisms.
2. The influences of PDK on strength of geopolymer paste mixes were studied. It has been observed that the increasing the quantity of PDK increases the compressive strength of geopolymer to a certain limit of SiO_2/Al_2O_3.
3. The measured compressive strengths of geopolymer mixes are in the range from 18 MPa to 64 MPa and maximum of 64 MPa for SiO_2/Al_2O_3 ratio of 2.8 and Na_2O/Al_2O_3 ratio of 0.9 and H_2O/Na_2O_3 ratio of 13.7.

4. Sodium silicate has been prepared simultaneously during geopolymers synthesis by the reaction between PDK and NaOH that increased the building up strength of the fabricated geopolymeric mortar by inducing the activation and speciation of the siliceous and aluminum ions of the raw materials, and the self-preparation of silicates compensates shortage of silicate in the raw materials at the same time.
5. Apart from less energy intensiveness, the geopolymer concrete utilizes the industrial wastes for producing the binding system in concrete. There are both environmental and economic benefits of using MK and PDK.

References

[1] Astutiningsih, S. and Liu, Y. 2005. "Geopolymerisation of Australian Slag with effective dissolution by the Alkali", Proc. of the World Congress Geopolymer 2005, Geopolymer Institute, Saint Quentin, France June 29th, 69-73.

[2] Rashad, A. M., Khafaga, S A. and Gharieb, M., "Valorization of fly ash as an additive for electric arc furnace slag geopolymer cement", Constr. Build. Mater. 294 (2021). https://doi.org/10.1016/J.CONBUILDMAT.2021.123570.

[3] Rashad, A. M. and Gharieb, M., "Solving the perpetual problem of imperative use heat curing for fly ash geopolymer cement by using sugar beet waste", Constr. Build. Mater. 307 (2021). https://doi.org/10.1016/J.CONBUILDMAT.2021.124902.

[4] Gharieb, M., Mosleh, Y. A. and Rashad, A. M., "Properties and corrosion behaviour of applicable binary and ternary geopolymer blends", Int. J. Sustain. Eng. 14 (2021) 1068–1080. https://doi.org/10.1080/19397038.2021.1913532.

[5] Palomo, A., Blanco-Varela, M.Y., Ranizo, M. L., Puertas, F., Vazques, T. and Grutzeck, M. W. 1999. "Chemical stability of cementitious materials based on metakaolin", Cement and Concrete Research, 29, 997-1004.

[6] Davidovits, J. 2002. "Technical talk: Geopolymer Applications", Curtin University, Western Australia, October 25th.

[7] Davidovits,J. 1982. US Patent no. 4, 399,386.

[8] Rahier, H., Van Mele, B. and Wastiels, J. 1996. "Low-temperature synthesized aluminosilicate glasses. Part II Rheological transformation during low-temperature cure and high-temperature properties of a model compound", Journal of Materials Science, 31, 80-85.

[9] Rahier, H., Van Mele, B., Wastiels, J. and Wu, X. 1996. "Low-temperature synthesized aluminosilicate glasses. Part I Low-temperature reaction stoichiometry and structure of a model compound", Journal of Materials Science, 22, 71-79.

[10] Rahier, H., Simons, W., and Van Mele, B. 1997. "Low-temperature synthesized aluminosilicate glasses. Part III Influence of the composition of the silicate solution on production, structure and properties, Journal of Materials Science, 32, 2237-2247.

[11] Chindraprasirt, P., Chareerat, T., and Sirivivatnanon, V. 2007. "Workability and strength of coarse high calcium fly ash geopolymer", Cement and Concrete Composites, 29, 224-229.

[12] Yip, C. K., Lukey, G. C., Provis, J. L., van deventer, J. S. J. 2008. "Effect of calcium silicate sources on geopolymerization", Cement and Concrete Research, 38, 554-564.

[13] Sathia, R., Babu, K. G. and Santhanam, M. 2008. "Durability study of low calcium fly ash geopolymer concrete", the 3rd. ACF International Conference –ACF/VCA.

[14] Thokchom, S., Ghosh, P. and Ghosh, S. 2010. "Performance of Fly ash Based Geopolymer Mortars in Sulphate Solution", J. Eng. Tech. Rev., 3, 1, 36-40.

[15] Rashad, A. M. and Gharieb, M. 2021. "An investigation on the effect of sea sand on the properties of fly ash geopolymer mortars", Innovative Infrastructure Solutions. 6:53. https://doi.org/10.1007/s41062-020-00421-9.

[16] Ouda, A. S. and Gharieb, M. 2020. "Development the properties of brick geopolymer pastes using concrete waste incorporating dolomite aggregate", Journal of Building Engineering, 27, 100919.

[17] Barsoum, M. W. and Ganguly, A. 2006. "Microstructural Evidence of Reconstituted Limestone Blocks in the Great Pyramids of Egypt." Journal of the American Ceramic Society, 89.

[18] Khater, H. M. and Gharieb, M. 2020. "Optimization of geopolymer mortar incorporating heavy metals in producing dense hybrid composites", Journal of Building Engineering 32, 101684. https://doi.org/10.1016/j.jobe.2020.101684.

[19] Kong, D. L. Y. and Sanjayan, J. G. 2010. "Effect of elevated temperatures geopolymer paste, mortar and concrete", Cement Concrete Res., 40, 334-339.

[20] Silva, P. D., Sagoe-Crenstil, K. and Sirivivatnanon, V. 2007. "Kinetics of geopolymerisation: Role of Al_2O_3 and SiO_2." Cement Concrete Res 37, 512-518.

[21] Davidovits, J. 1976. "Solid phase synthesis of a mineral block polymer by low temperature polycondensation of alumino-silicate polymers", IUPAC International Symposium on Macromolecules Stockholm; Sept. Topic III, New Polymers of high stability.

[22] Khater, H. M., & Ghareib, M. (2020). Utilization of alkaline Aluminosilicate activation in heavy metals immobilization and producing dense hybrid composites. Arabian Journal for Science and Engineering, 1-16.

[23] Gharieb, M., Mosleh, Y. A., & Rashad, A. M. (2021). Properties and corrosion behaviour of applicable binary and ternary geopolymer blends. International Journal of Sustainable Engineering, 1-13.

[24] Davidovits, J. 2008. "Geopolymer Chemistry and Applications. Institute Geopolymer, Saint-Quentin: France, 2nd Ed, 32.

[25] Dieter, G.E. 1987. "Mechanical metallurgy", Mc-Graw Hill, 326-327.

[26] Astutiningsih, S. 2005. "Alkali activation and curing of aluminosilicate based-geopolymers", PhD Theses, The University of Western Australia, 98.

[27] Mendelovici, E. 1997. "Comparative study of the effects of thermal and mechanical treatments on the structures of clay minerals", Journal of Thermal Analysis 49,3, 1385–1397.

[28] McManus, J., Ashbrock, S. E. and MacKenzie, K. J. D. 2001. "Wimperis S. 27Al multiple- Quantum MAS and 27Al (1H) CPMAS NMR study of amorphous aluminosilicates". Journal of Non-Crystalline, 282, 278–290.

[29] Buchwald, A. 2006. "What are geopolymers? Current state of research and technology, the opportunities they offer, and their significance for the precast industry", Concrete Precasting Plant and Technology, 72, 7, 42–49.

[30] Duxson, P., Fernndez-Jiménez, A., Provis, J., Lukey, G., Palomo, A. and van Deventer, J. 2007. "Geopolymer technology: the current state of the art", Journal of Materials Science, 42, 9, 2917–2933.

[31] Praveen Kumar T.R., Sudheesh, C, and Sasi Kumar, S. 2015. "Strength Characteristics of Saw Dust Ash Based Geopolymer Concrete", International Journal for Chem. Tech. Research, Vol. 8(2), 738-785.

[32] Gharieb, M., and Rashad, A.M. 2020. "An initial study of using sugar-beet waste as a cementitious material", Construction and Building Materials 250, 118843.

[33] Vollet, D. R., Macedo, J. C. D. and Mascarenhas Y. P. 1994. "Pore structure characterization of kaolin, metakaolin and their acid-treated products using small angle X-ray scattering", Appl. Clay Sci. 8 (6), 397-404.

[34] Mostafa, N. Y., El-Hemaly, S. A. S., Al-Wakeel, E. I., El-Korashy, S. A. and Brown, P.W. 2001."Characterization and evaluation of the pozzolanic activity of Egyptian industrial by-products I: Silica fume and de-aluminated kaolin" Cem. Conc. Res. 31, 467-474.

[35] Mostafa, N. Y. and Brown, S. A. 2005. "Heat of Hydration of high reactive pozzolana in blended cements: Isothermal conduction calorimetry" Termochimica Acta, 435, 162-167.

[36] Macedo, J. C. D., Mota, C. J. A., Menezes, S. M. C. and Camorin, V. 1994. "NMR and acidity studies of de-aluminated metakaolin and their correlation with cumin cracking", Appl. Clay Sci., 8 (5), 321-330.

[37] Zhang, Y., Sun, W. and Li, Z. 2010. "Composition design and microstructural characterization of calcined kaolin-based geopolymer cement", Applied Clay Science, 47, 271– 275.

[38] Ferone, C., Colangelo, F., Roviello, G., Asprone, D., Menna, C., Balsamo, A., Prota, A., Cioffiand, R. and Manfredi, G. 2013. "Application-oriented chemical optimization of a metakaolin based geopolymer", Materials, 6, 1920-1939.

[39] Andrea, V. K. and Harald, H. 2004. "Investigation of geopolymer binders with respect to their application for building materials". Ceramics– Silicaty, 48, 3, 117-120.

[40] Ouda, A. S. and Gharieb, M. 2021. "Behavior of alkali-activated pozzocrete-fly ash paste modified with ceramic tile waste against elevated

temperatures and seawater attacks", Construction and Building Materials, 285, 122866. https://doi.org/10.1016/j.conbuildmat.2021.122866.

[41] Suwan, T. and Fan, M. 2014. "Influence of OPC replacement and manufacturing procedures on the properties of self-cured geopolymer", Constr. Build. Mater., 73, 551-61. https://dx.doi.org/10.1016/j.conbuildmat.2014.09.065.

[42] Ke, X., Bernal, S. A., Ye, N., Provis, J. L. and Yang, J. 2014. "One-Part Geopolymers Based on Thermally Treated Red Mud/NaOH Blends", J. Am. Ceram. Soc., 1-7.

[43] ASTM C109M, 2016. "Standard Test Method for Compressive Strength of Hydraulic Cement Mortars", Annual Book of ASTM Standards; ASTM International: West Conshohocken, PA, USA.

[44] Ugheoke, B. I., Onche, E. O., Namessan, O. N. and Asikpo, G. A. 2006. "Property Optimization of Kaolin - Rice Husk Insulating Fire - Bricks", Leonardo Electronic Journal of Practices and Technologies, 9, 167-178.

[45] Abo-El-Enein, S. A., El-kady, G., El-Sokkary, T. M. and Gharieb, M. 2015. "Physico-mechanical properties of composite cement pastes containing silica fume and fly ash" HBRC, Journal, 11, 7–15.

[46] Alexandre Silva de Vargas, Denise. C. C., Dal Molin, Ângela, B., Masuero, Antônio, C. F., Vilela, Joao Castro-Gomes, Ruby, M. and Gutierrez. 2014. "Strength development of alkali-activated fly ash produced with combined NAOH and $CA(OH)_2$ activators", cement and concrete composites, 53, 341-349.

[47] Panias, D., Giannopoulou, I. P. and Perraki, T. 2007. "Effect of synthesis parameters on the mechanical properties of fly ash-based geopolymers", Colloids and Surfaces A: Physico-chem. Eng. Aspects, 301, 246–254.

[48] Weitzel, B., Hansen, M. R., Kowald, T. L., Müller, T., Spiess, H. W. and Trettin, H. F. R. 2011. "Influence of Multi walled Carbon Nanotubes on the Microstructure of CSH-Phases" , In proceeding of 13th congress on the Chemistry of Cement, 3-8 july 2011, Madrid, Spain.

[49] Alarcon-Ruiz, L., Platret, G., Massieu, E. and Ehrlacher, A. 2005. "The use of thermal analysis in assessing the effect of temperature on a cement paste", Cem. Concr. Res., 35(3), 609–613.

[50] Buchwald, A., Tatarin, R. and Stephan, D. 2009. "Reaction progress of alkaline-activated metakaolin-ground granulated blast furnace slag blends", J. Mater. Sci., 44, 5609–5617.

[51] Bernal, S. A., Provis, J. L., Rose, V. and Mejía de Gutiérrez, R. 2011. "Evolution of binder structure in sodium silicate-activated lag metakaolin blends", Cem. Concr. Compos., 33(1), 46–54.

[52] Bernal, S. A., Rodríguez. E. D., de Gutiérrez, R. M., Gordillo, M. and Provis, J. L. 2011. "Mechanical and thermal characterisation of geopolymers based on silicate-activated metakaolin/slag blends", J. Mater. Sci., 46(16), 5477–86.

[53] Duxson, P., Provis, J. L. and van Deventer, J. S. J. 2009. "Geopolymers: Structures, Processing, Properties and Industrial Applications", Wood head Publishing, Abingdon UK.

[54] Puligilla, S. and Mondal, P. 2013. "Role of slag in microstructural development and hardening of fly ash-slag geopolymer", Cement Concr. Res., 43, 70-80.

[55] Autef, A., Joussein, E., Poulesquen, A., Gasgnier, G., Pronier, S., Sobrados, I., Sanz, J. and Rossignol, S. 2013. "Influence of metakaolin purities on potassium geopolymer for- mulation: the existence of several networks", J. Colloid Interface Sci., 408, 43–53.

[56] Rees, C. A., Provis, J. L., Lukey, G. C. and van Deventer, J. S. J. 2007. "Attenuated total reflectance fourier transform infrared analysis of fly ash geopolymer gel aging", Langmuir, 23, 8170–8179.

Ref.:
Abdullah, Nabil Ahmed– **El-Sokkary**, T. M. – **Gharieb**, Mahmoud: *Synthesis of geopolymer binder from the partially de-aluminated metakaolinite by-product resulted from alum industry*
Építőanyag – Journal of Silicate Based and Composite Materials, Vol. 74, No. 5 (2022), 166–174. p.
https://doi.org/10.14382/epitoanyag-jsbcm.2022.25

Effect of waste limestone powder on properties and sulphate-carbonate corrosion of autoclaved silicate materials

Zdzisław PYTEL ▪ AGH University of Science and Technology, Faculty of Materials Science and Ceramics, Department of Building Materials Technology, Poland ▪ pytel@agh.edu.pl

Érkezett: 2022. 05. 22. ▪ Received: 22. 05. 2022. ▪ https://doi.org/10.14382/epitoanyag-jsbcm.2022.26

Abstract

This paper summarises the results of laboratory testing of potential applications of waste limestone powder as an additive to sand-lime bricks. This mineral component is added to improve their mechanical properties. It is anticipated that chemical reactions between calcium and silica ions in the presence of carbonate ions and under specific conditions will yield a separate mineral scawtite. Due to its chemical composition and internal structure, scawtite has inferior chemical resistance when compared to calcium silicate hydrates such as C-S-H gel. At lower temperatures, materials containing this mineral phase may succumb to corrosion due to the presence of sulphates and carbonates, this process is also referred to as thaumasite corrosion.

During the tests the samples were made with various amounts of waste limestone powder. The influence of amount of waste limestone powder on the quality of resultant materials was evaluated based on the functional testing data. The results indicate that the presence of waste limestone powder in the proportion 10-25% by weight in the component mix ensures the products' compliance to the normative standards relating to absorbability, at the same time their compressive strength is improved. In order to verify the potential occurrence of the sulphate-carbonate corrosion, selected samples of the so obtained autoclaved products were exposed to water solutions of salts containing CO_3^{2-} or SO_4^{2-} ions or their mixtures, at reduced temperatures. Potential effects of changes of phase composition and microstructure of sand-lime materials in simulated conditions prompting the thaumasite formation were registered by the XRD, DTA, IR and SEM+EDAX methods.

Keywords: sand-lime bricks, hydrothermal conditions, waste limestone powder, C-S-H gel, tobermorite, scawtite formation, thaumasite corrosion, sulphate attack

Kulcsszavak: mészhomoktégla, hidrotermikus körülmények, hulladék mészkőpor, C-S-H gél, tobermorit, scawtite képződés, taumasit korrózió, szulfáttámadás

Zdzisław PYTEL

is an employee of the Department of Building Materials Technology at the Faculty of Materials Science and Ceramics at the AGH University of Science and Technology in Krakow. He works as an academic teacher and conducts scientific research on the technology of obtaining both ceramic building materials and building materials obtained on the basis of mineral binders such as cement and/or lime. A special area of his interest is the technology of obtaining autoclaved building materials such as sand-lime bricks and aerated concrete. In this regard, he conducts systematic research on the use of non-traditional raw materials for the production of this type of building materials.

1. Introduction

Sand-lime bricks are conventionally manufactured from mineral components, i.e. a specially prepared mixture of burnt lime and quartz sand, and the manufactured bricks have the strength parameters of bricks categorised as class 20 or 25 [1–5]. There is, however, a strong demand for construction materials with the strength parameters exhibited by the class 35 or higher. Functional parameters (compressive strength) of sand-lime bricks depend on a number of factors [6–9]. The improvement can be achieved in several ways, the most efficient method involves the modification of chemical processes involved in the manufacture and processing of these bricks in the autoclave [10, 11]. The structure and microstructure of sand-lime bricks are finally determined during the final stage of bricks processing in the autoclave. Those properties determine the functional parameters of the ready bricks, associated with their strength and durability which are of key importance for customers and potential users. Modification of the manufacturing process involves the change of conditions of synthesis: time and temperature hydrothermal processing [12–14] and introduction of mineral additives to the mixture, which has a good effect on structure and microstructure of bricks [15, 16]. When mineral additives are introduced to the traditional mixture, new ions appear in the reaction environment that might lead to qualitative and quantitative changes of the final products of synthesis proceeding in hydrothermal conditions [17]. These ions might either speed up the transition of amorphous C-S-H gel into crystalline products (such as tobermorite $C_5S_6H_5$ or xonotlite C_6S_6H) or stabilize the C-S-H gel and by so doing prevent its further transformations into phases that do not produce the required strength parameters of autoclaved bricks [18, 19]. When those reaction systems are chemically activated by sulphate or alkali ions, the rate of the substrate reaction might be enhanced and the quantity of the synthesis product shall be larger, which directly affects the strength parameters of autoclaved materials [20].

Finally, the composition of the process mixture might be modified to generate additional phases, which leads to an improvement of mechanical parameters of the final products. Laboratory tests revealed that waste limestone powder is an excellent additive [21, 22]. In the course of limestone reactions with calcium and silica in controlled conditions we get a separate mineral phase, referred to as scawtite [23-25]. Scawtite is a calcium carbonate-silicate: $Ca_7[Si_6O_{18}](CO_3)\cdot 2H_2O$. It has a layered structure in which a layer of octahedrons CaO_6

interfaces with layers composed of CO_3^{2-} groups and Si_6O_{18} rings [26]. Research has revealed [23, 27] that scawtite is formed during the autoclaving of the mixture of quartz, calcium carbonate and calcium hydroxide. It is reasonable to expect that it shall be formed when waste limestone powder is introduced to the mixture used typically in the manufacture of sand-lime bricks. Apart from the classical components: quartz sand and burnt lime, the mixture shall also contain waste limestone powder. As regards the cost-efficiency of the proposed solution it is advisable to use waste limestone powder, a by-product in plants manufacturing burnt lime or carbonate sorbents to be used in desulphurization installations. Accordingly, it seems justified to add waste limestone powder as the component of a mixture to make sand-lime bricks with the required mechanical properties [28].

On account of the presence of carbonate ions in the structure of scawtite, the durability of sand-lime bricks containing waste limestone powder may deteriorate because of the potential occurrence of thaumasite form of sulphate attack [29]. This form of corrosion is caused by interactions between materials containing mineral binders such as cement or lime and SO_4^{2-} and CO_3^{2-} ions in the conditions of high humidity and, in extreme cases, under the action of water and at reduced temperatures. The corrosion process results in thaumasite formation $Ca_3[Si(OH)_6]\cdot CO_3\cdot SO_4\cdot 12H_2O$ [10, 30, 31]. Even though thaumasite may be formed by several ways (direct or indirect), in the case of sand-lime materials thaumasite emerges as a product of a direct reaction between the C-S-H gel and calcium sulphate or carbonate [32]. Consequently, the C-S-H gel will gradually lose its basic function, i.e. that of the substance binding the silica sand grains, as a result the sand-lime bricks, which at first exhibit the desired structural parameters and functional features, will slowly yet inevitably deteriorate in quality, changing into a shapeless and amorphous mass, which in the long-run will prove unable to carry all the typical loads due to the operation and maintenance of the engineering structures. Thus, susceptibility of sand-lime bricks to this form of corrosion may be due to their being manufactured from modified component mixes. In the case of autoclaved sand-lime products containing waste limestone powder [33], this additive becomes the source of CO_3^{2-} ions and in the presence of adverse environmental conditions: high humidity and reduced temperatures, the process of thaumasite formation may be triggered.

Considering the above considerations, it should be stated that the purpose of the research related to the use of waste limestone powder in the production process of sand-lime products was primarily to confirm its positive impact on most of the functional characteristics of the type of building materials indicated and to demonstrate no negative impact in relation to the durability of these products in terms of the potential for thaumasite corrosion.

In conclusion, it can be concluded that the proposed technological solution primarily leads to the improvement of the quality of sand-lime products, but it also has an economic and ecological aspect. Considering the scale of silicate industry production, the reduction in the consumption of quicklime for the production of sand-lime products will certainly affect its clearly lower demand. This, in turn, will reduce the process CO_2 emissions generated during its production, and thus indirectly improve environmental protection.

2. Experimental investigation

2.1 Design of the research program

In considerations of the cognitive aspects of the research program, the experiments were designed involving the fabrication of sand-lime products containing varied amounts of powdered limestone. The mineral additive in the form of waste limestone powder was added to the standard component mix: burnt lime and quartz sand in the molar ratio CaO/SiO_2 (C/S) equal to 0.09. Testing was done on ground limestone rocks from various limestone deposits in Poland and having a similar grain size distribution, the maximal grain size being 60-80 μm. The actual amounts of mineral additives were equal to 5-30% (% mass fraction) the total amount of the two basic components in the dry mixture.

The influence of the presence of a mineral additive on the final product quality: sand-lime bricks were assessed by analysing the changes in their functional parameters and on the basis of structural and microstructure testing data. In the first place tests were performed to check the durability of sand-lime bricks and the potential of thaumasite corrosion. Taking into account the conditions required for thaumasite formation, the sand-lime brick samples were kept in various corrosion-prone environments. The comparative analysis used the reference material made of the two component mix only (quartz sand plus burnt lime), with no mineral additives.

2.2 Materials

Three types of mineral products were used in the tests. Natural quartz sand from the deposit "Łysa Góra" (QS-LG) was used as an aggregate, the binder material is the highly-reactive burnt lime obtained from an industrial process (LB-HR). Ground limestone from several Polish limestone plants using limestone from various deposits of different geological ages, acted as mineral additive and the following types of waste limestone powders were used:

- limestone powder "Czatkowice" - LS-CZ
- limestone powder "Bukowa" - LS-B
- limestone powder "Tarnów Opolski" - LS-TO
- limestone powder "Kujawy" - LS-K
- limestone powder "Mielnik" - LS-M
- limestone powder "Trzuskawica" - LS-T

The grain size compositions of quartz sand were found by the screening method utilizing a Hosokawa Alpine screen. Results are compiled in *Fig. 1*.

The specifications of the burnt lime LB-HR: chemical composition, grain size distribution, chemical reactivity, and moisture, are given in *Table 1*. It also provides the characteristics of waste limestone powders LS-B, LS-TO used as a benchmark for showing the properties of the remaining carbonate materials.

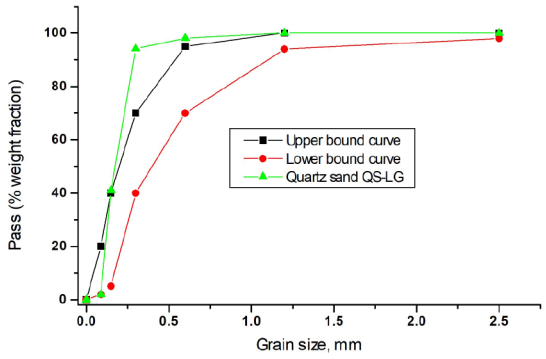

Fig. 1 Grain size distribution curve of quartz sand QS-LG
1. ábra QS-LG kvarchomok szemcseméret-eloszlási görbéje

Control parameter	Types of raw materials		
	LB-HR	LS-B	LS-T0
CaO, %	97.9	96.2 ($CaCO_3$)	95.7 ($CaCO_3$)
MgO, %	0.5	0.4 ($MgCO_3$)	1.8 ($MgCO_3$)
$(CaO+MgO)_{ac}$, %	96.6	-	-
Al_2O_3, %	0.1	0.4	0.1
Fe_2O_3, %	0.04	0.2	0.4
SiO_2, %	0.5	2.1	1.7
CO_2, %	0.8	-	-
SO_3, %	0.1	-	-
***t*60, min.**	0.6	-	-
T_{max}, °C	79.8	-	-
Moisture, %	-	0.4	0.3
$R_{0.09}$, mm	5.2	7.2	8.1
$R_{0.2}$, mm	0.2	0.2	0.5

Table 1 Specification of the burnt lime and selected ground limestone
1. táblázat Az égetett mész és a kiválasztott őrölt mészkő jellemzői

The grain size distribution of the natural carbonates used in the tests is shown in *Fig. 2* and *Table 2*. Grain size measurements were taken with a SediGraph 5100 analyzer (Micromeritrics), the specific density was measured with a helium pycnometer AccuPyc (Micromeritics) and specific surface area measurements S_{BET} were taken by the BET method (Micromeritics).

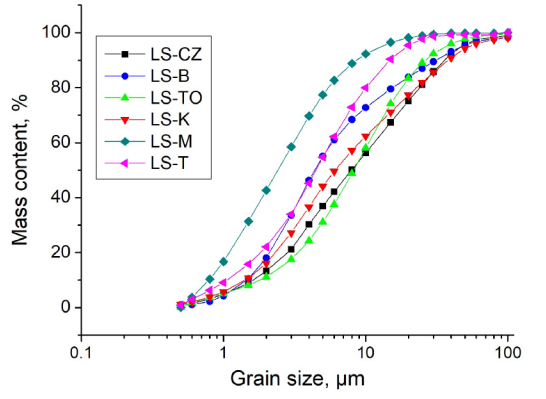

Fig. 2 Grain size distribution curves of carbonate raw materials
2. ábra Karbonát alapanyagok szemcseméret-eloszlási görbéi

Control parameter	Waste limestone powder types					
	LS-CZ	LS-B	LS-T0	LS-K	LS-M	LS-T
Median, mm	7.9	4.4	8.2	6.1	2.4	4.5
Mode, mm	4.5	3.3	9.4	4.0	1.7	4.5
Specific density, g/cm³	2.79	2.76	2.77	2.77	2.77	2.79
BET specific surface area, m²/g	2.18	1.77	1.63	2.38	3.12	2.14

Table 2 Characteristics features related to grain size of carbonate raw materials
2. táblázat A karbonát alapanyagok szemcseméretével kapcsolatos jellemzők

2.3 Sample preparation

Samples of autoclaved sand-lime bricks were obtained from mixtures of quartz sand QS-LG, burnt lime LB-HR and waste limestone powder. The main components, i.e. quartz sand and burnt lime were in the proportion 92% and 8% (% by weight). This composition of raw mixture used in manufacturing of the reference materials (LS-0) was then modified by adding specified amounts of waste limestone powder. The added waste limestone powder would account for 5-30% (% by weight) of the total sand and burnt lime in the dry mixture. To ensure the adequate rheological properties, homogenized mixtures of the two components were mixed with water to achieve the forming humidity of 6%, so that the bricks could be press-formed. Components of all process mixtures used at this stage of research to prepare the samples of autoclaved bricks are summarized in *Table 3*.

Type of component	Content of waste limestone powder, wt. %					
	0	5	10	15	20	30
	Content of component in the mixture, wt. %					
QS-LG	86.0	82.0	78.2	74.9	71.8	66.2
LB-HR (CaO) [1]	7.8 (7.5)	7.4 (7.1)	7.1 (6.8)	6.8 (6.2)	6.5 (6.2)	6.0 (5.8)
LS-X [2]	0.0	4.5	8.5	12.2	15.6	21.7
Water [3]	6.2 (2.4+3.8)	6.1 (2.3+3.8)	6.2 (2.2+4.0)	6.1 (2.1+4.0)	6.1 (2.0+4.1)	6.1 (1.8+4.3)

[1] - lime content in the mixture with specification of the amount of active (CaO + MgO)
[2] - X - designation of waste limestone powder
[3] - total amount of water, with specification of the amount of water required for slacking of CaO contained in the given amount of binder and the amount of water required to achieve the predetermined mixture humidity forming

Table 3 Compositions of mixtures used to obtain the autoclaved materials
3. táblázat Az autoklávozott anyagok előállításához használt keverékek összetétele

The sample preparation procedure was always the same. The precisely controlled amounts of mixture components were carefully weighted and homogenized in a dry process (mixed in a mortar), followed by a wet process (mixing in a mortar after adding the required amount of water). The mixture was then placed inside an air-tight glass container for the purpose of mixture slacking at the temperature 70 °C using a dryer. The slacking process lasted for 1 h and afterwards the obtained mass was homogenized again.

Samples were formed and shaped like cylinders with the height and diameter 25 mm. They were formed in a process of axial, two-sided and double-stage pressing, with inter-stage deaeration.

The initial and final pressures of pressing were 10 and 20 MPa, respectively. As soon as samples are formed, they were subjected to hydrothermal treatment, with the use of steel pressure cylinders. The conditions of the synthesis reproduced the conditions of sand-lime materials treatment in industrial autoclaves:

- pressure of saturated water vapour – 1.002 MPa
- temperature of vapour – 180 °C
- autoclaving time – 9.5 h

The hydrothermal treatment was carried out in accordance with the approved regime: 1.5 h reaching the predetermined steam temperature and pressure level; 8 h isobaric–isothermal treatment of products; free cooling to the ambient temperature.

3. Experimental results

3.1 Physical properties of obtained autoclaved materials

Selected physical parameters of thus obtained autoclaved samples were tested in accordance with the procedure set forth in the standard [34] and research procedures specified in sections of the standard PN-EN 772. Accordingly, the following parameters were determined:

- compressive strength f_B [35],
- bulk density $\rho_{n,u}$ [36].

Thus obtained functional parameters expressed as averaged values are summarized in *Table 4*.

3.2 Porosity

Porosity of thus obtained silicate materials was determined by mercury porosimetry method, using a Carlo Erba Instruments porosimeter (model PO-225). The measurements were taken in a pressure range 0.1-200 MPa, enabling us to determine the volumetric fraction of macro- and micropores. Selected results in the form of pore size curves are graphed in *Fig. 3* and *4*. For comparison, curves obtained for samples with variable waste limestone powder LS-CZ contents are contrasted with the reference sample curve LS-0 (*Fig. 3*), obtained for a two-component mixture, without waste limestone powder. *Fig. 4* shows the contrasted curves of volumetric fractions of pores obtained for the mixtures with the same amount (15 wt.%) of various types of limestone powders.

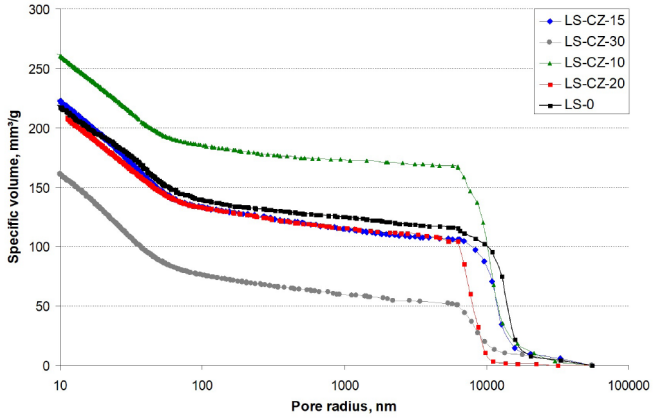

Fig. 3 Pore size distribution in samples containing different amounts of waste limestone powder LS-CZ
3. ábra Pórusméret-eloszlás különböző mennyiségű LS-CZ hulladék mészkőport tartalmazó mintákban

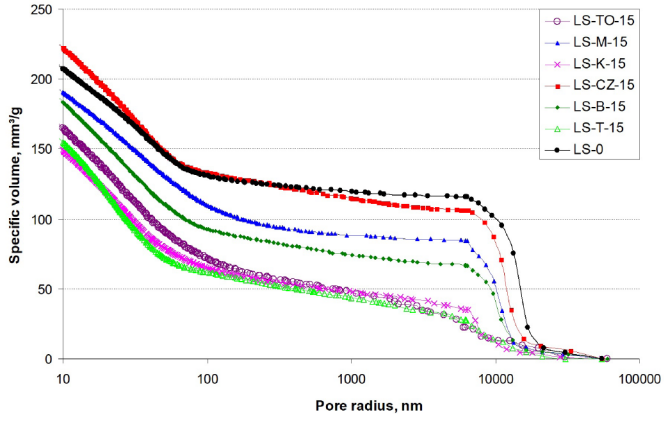

Fig. 4 Pore size distribution in samples containing 15% of added waste limestone powder
4. ábra Pórusméret-eloszlás 15% hozzáadott hulladék mészkőport tartalmazó mintákban

3.3 Mineral composition

Mineral composition of autoclaved samples was established by the XRD method. X-ray images were registered using a Phillips X'Pert PW 3020 X-ray diffractometer, the parameters in the measurement procedure: radiation level CuK_a, reflective graphite monochromator, lamp voltage 35 kV, current in the lamp 30 mA, step recording - $\Delta 2\theta = 0.05°$, t=1 s.

Property	Reference material LS-0	Limestone content (wt. %)	Limestone powder type					
			LS-CZ	LS-B	LS-TO	LS-K	LS-M	LS-T
Compressive strength f_B, MPa	19.2	5	-	24.5	20.2	24.3	20.2	-
		10	22.1	28.6	19.8	28.1	19.9	27.1
		15	23.1	28.7	22.3	27.7	22.1	-
		20	24.7	27.5	28.6	27.0	-	34.5
		30	27.3	-	-	-	-	-
Bulk density $\rho_{n,u}$, g/cm³	1.66	5	-	1.74	1.74	1.73	1.71	-
		10	1.70	1.79	1.75	1.76	1.75	1.8
		15	1.73	1.81	1.80	1.79	1.77	-
		20	1.77	1.84	1.85	1.83	-	1.88
		30	1.81	-	-	-	-	-

Table 4 Properties of autoclaved materials containing waste limestone powder coming from various sources
4. táblázat Különböző forrásokból származó hulladék mészkőport tartalmazó autoklávozott anyagok tulajdonságai

Interplanar distances obtained from X-ray pattern images were utilized in identification of mineral phases making up the tested samples, supported by the data from the ICPDS-ICDD catalogue (version of 2005) and the computer program XRAYAN. Selected results are shown in *Fig. 5*.

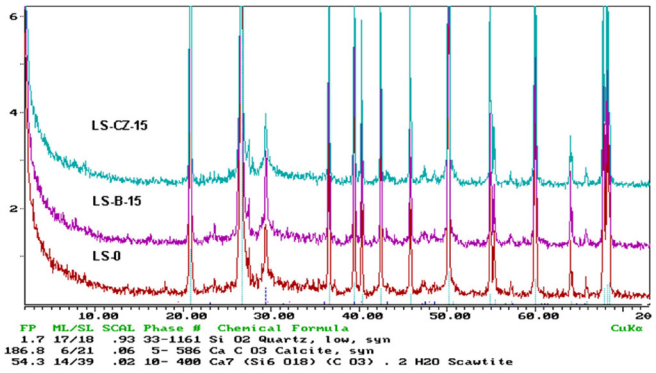

Fig. 5 Compiled X-ray images for selected samples
5. ábra Összeállított röntgenfelvételek a kiválasztott mintákról

3.4 Studies of thaumasite corrosion of sand-lime products

Autoclaved products are kept in conditions most favourable for the thaumasite corrosion attack. Depending on the modifications of the mix composition, the analyzed materials are kept in precisely controlled conditions. In the case of products containing waste limestone powder as a mineral additive being an internal source of CO_3^{2-} ions, the samples are kept at lower temperatures (+5 °C) immersed in the solution of Na_2SO_4 (sample symbol NS) or $MgSO_4$ (sample symbol MS), with the concentration of SO_4^{2-} ions equal to 16.0 g/dm^3. Samples are kept in a chamber originally designed for running the tests required to investigate the process of carbonization of concrete and mortars, too. They are kept under lower temperatures as well (+5 °C), air relative humidity being 30% and concentration of CO_2 - 1 vol.%. Furthermore, in order to vary the humidity conditions within the chamber, the proofed samples are kept in air with humidity 50% (positioned over the solid $AgNO_3$), or 90% (over the distilled water) or immersed in distilled water, thus ensuring the 100% humidity. The samples are kept under those conditions for a sufficiently long period of time to observe the occurring changes. The longest period (950 days) of exposure to simulated corrosion-prone conditions (aqueous solutions of sulphate salts) ensues in the case of samples containing different amounts of waste limestone powder. In the case of those samples, the symptoms of disintegration are evident, so they are subjected to rigorous quality analyses by several methods and the results are given in the form of XRD, DTA, TG and IR graphs, supported by microstructure test data obtained by the SEM method in conjunction with the EDAX studies. For the sake of comparison, the samples made of the reference material (LS-0) and those containing waste limestone powder (LS-B-20) are subjected to the tests, too.

The analysis of the phase composition of thus obtained materials is based on X-ray test data. X-ray tests are performed using an X-ray diffractometer (Philips PW 1040). X-ray patterns are registered in the angle range CuK_α 5-60° 2θ and the presence of mineral phases is established on the basis of ICPDS-ICDD database (version of 2005). The results in the form of graphs of X-ray patterns for the selected samples are shown in *Fig. 6*.

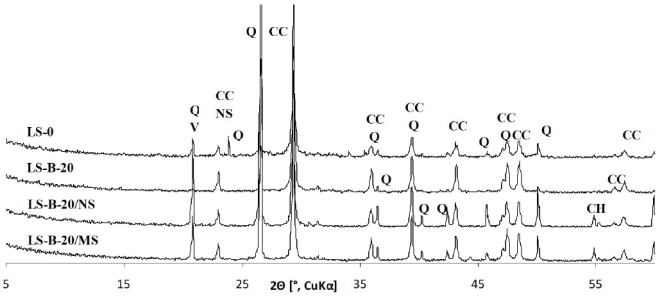

Fig. 6 Phase composition of analysed samples established by the XRD method Designations meaning: Q - quartz, CC – calcite, V – vaterite, NS – sodium sulphate, CH – calcium hydroxide
6. ábra A vizsgált minták XRD-módszerrel megállapított fázisösszetétele Jelölések jelentése: Q - kvarc, CC - kalcit, V - vaterit, NS - nátrium-szulfát, CH - kalcium-hidroxid

The thermal methods use a thermo-balance STA 449 F3 Jupiter (NETZSCH). Measurements are taken on the carried DTA-TG in the temperature range 20-1000 °C, the heating rate 10 °C/min in the atmosphere of air in the Al_2O_3 crucible. Test results in the form of DTA and TG curves are shown in *Fig. 7*.

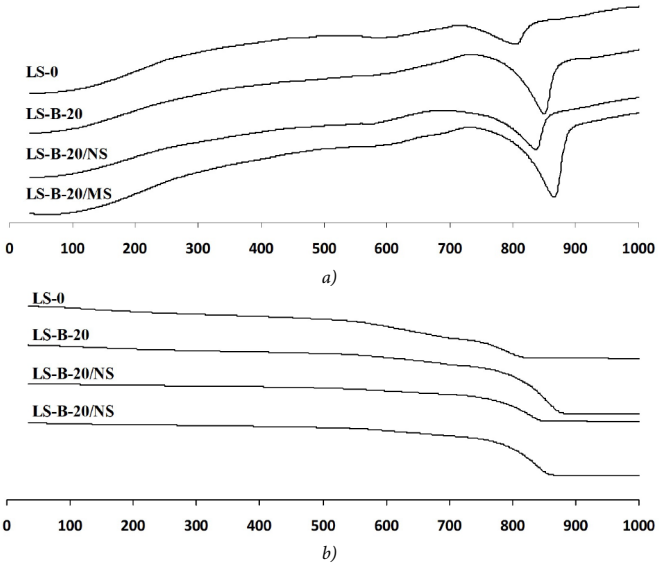

Fig. 7 Thermal test data: a) DTA curves, b) TG curves
7. ábra Termikus vizsgálati adatok: a) DTA-görbék, b) TG-görbék

Middle-range IR spectra (400-400 cm^{-1}) are registered by the standard method using KBr pills. Measurements are taken with a Fourier spectrometer Bruker VERTEX 70v with 4 cm^{-1} resolution, with 128 repetitions. The results in the form of IR spectra of the investigated samples are shown in *Fig. 8*.

The microstructure of materials obtained under hydrothermal conditions is investigated by the scanning microscopy technique, using a scanning microscope $NOVA_{NAMO}$ SEM 2000 (FEI Company) equipped with a micro-analyzer EDAX. Prior to the tests, the samples were sputtered with gold. The most characteristic images of microstructure of the samples' profiles are shown in *Fig. 9*.

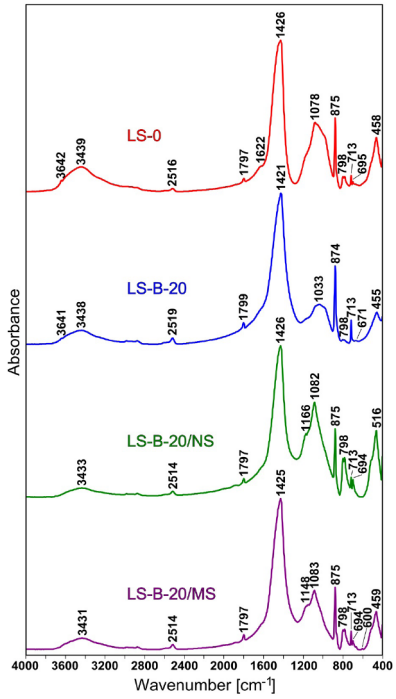

Fig. 8 IR spectra of investigated samples
8. ábra A vizsgált minták IR-spektrumai

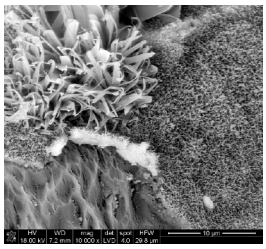

9a) Sample LS-0

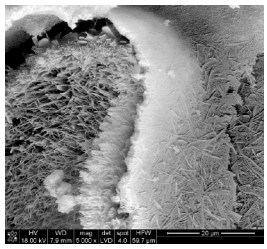

9b) Sample LS-B-20

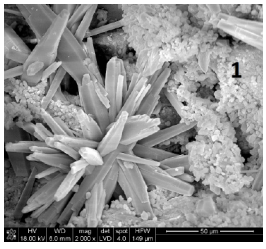

9c) Sample LS-B-20/NS

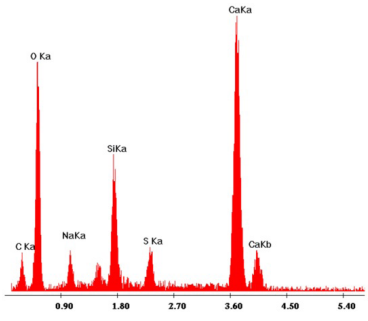

9d) EDAX analysis in point 1

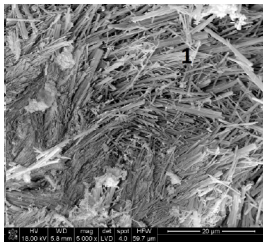

9e) Sample LS-B-20/MS

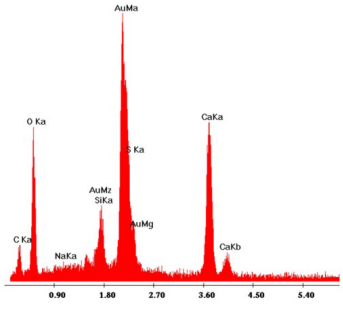

9f) EDAX analysis in point 1

Fig. 9 Microstructure of the analysed samples
9. ábra A vizsgált minták mikroszerkezete

4. Discussion

The actual position of the grain size distribution curve for sand QS-LG (see *Fig. 1*) with respect to boundary curves suggests this sand does not meet the requirements posed by manufacturers of sand-lime bricks production. Investigated sand contains too much fine fractions (0.0-0.5 mm) and lacks in coarser fractions (0.5 - 2.0 mm).

It is readily apparent (see *Table 4*) that regardless of the type of added waste limestone powder, the compressive strength of manufactured samples is improved. Besides, there is an evident correlation between the amount of added waste limestone powder and the samples' compressive strength.

Porosity data suggest that regardless of the type and amount of added limestone powder, the obtained products have similar porosity in the range of capillary and gel pores. Qualitative and quantitative changes are evident in the domain of macropores about 10 mm in diameter. As the waste limestone powder contents increases, the proportion of these pores tends to decrease, which affects the overall porosity of the samples. The presence of these pores is associated with the applied sample forming method and the grain size distribution in the process mixture, which in turn depends on the size of crushed sand grains. It is reasonable to suppose, therefore, that added minerals: waste limestone powder with the maximal grain size 60-80 mm, act as micro-aggregate, leading to the most desirable modifications the resultant grain size distribution curve and the manufactured press-formed materials will become more compact (*Fig. 9*).

Of major interest are X-ray images of the reference sample (LS-0) and samples made with the addition of waste limestone powder "Bukowa" (sample designation LS-B-15) and waste limestone powder "Czatkowice" (sample designation LS-CZ-15), with clearly indicated diffraction peaks of identified phases. It is readily apparent that mineral compositions of analyzed materials are vastly similar. Crystalline phases include not reacted reagents in the shape of quartz sand, $Ca(OH)_2$ and calcite as well as products of synthesis, such as scawtite as the lines evidencing its presence are of low intensity. The presence of the C-S-H gel cannot be confirmed by the XRD methods, though it becomes evident in the scanning microscope images. It is reasonable to suppose that this phase occurs mostly in the amorphous form or, though less probable, that its quantity is too small to be detected by the applied method.

To investigate the carbonate-sulphate corrosion processes, testing was done on autoclaved sand-lime products obtained from mix compositions modified by adding the precisely controlled amounts of mineral additives in the form of raw carbonate materials. The effects of this mineral additive on properties and parameters of thus obtained sand-lime products are very positive (*Table 4*). The analyzed sand-lime products were then subjected to the sulphate-carbonate corrosion processes and the results are evaluated basing on phase composition data obtained by several methods. It is worthwhile to mention that experiments conducted so far indicate that the corrosion process at the fastest rate in samples containing waste limestone powder in different proportions and kept at the temperature +5 °C immersed in aqueous solutions of Na_2SO_4 or $MgSO_4$ in which the concentration of SO_4^{2-} ions was 16.0 g/dm^3.

The phase composition data obtained by the XRD method (*Fig. 6*) for samples kept under such conditions for 950 days reveal that the main product of corrosion is calcium carbonate in the form of vaterite, which co-occurs with calcite being the key component of waste limestone powder. Even though the effects are similar for the two types of corrosion solutions, yet in the case of $MgSO_4$ the samples (LS-B-20/MS) after the exposure period will totally disintegrate whilst the samples LS-B-20/NS kept in the solution of Na_2SO_4 still retain their shape.

These results are corroborated by those obtained by thermal methods. When comparing DTA and TG graphs (*Fig. 7*), we clearly see that they are similar and the only distinctive endothermic effect is revealed on the DTA graph, with its maximum in the temperature range 820-860 °C and accompanied by the reduction of mass revealed on the TG graphs, associated with thermal dissociation of calcite or vaterite, which is a further evidence of the presence of these compounds in the analyzed sand-lime bricks.

More data about the altered phase composition of analyzed samples will be available after observations of IR absorption spectra (*Fig. 8*) [37]. The reference spectrum is that registered for the reference material (LS-0) made of the traditional mix of ingredients. The reference spectrum reveals several lines, which can be divided in three groups. High-intensity spectral lines at about 1426 cm^{-1} can be ascribed to vibrations stretching the C-O bonds. The occurrence of other spectral lines at 875 and 713 cm^{-1}, also ascribed to carbonate groups, evidences the presence of calcite in the samples. The other group includes lower-intensity spectral lines, associated with vibrations of silica-oxygen groups. In the range of wave numbers 1100-900 cm^{-1} we get asymmetric vibrations stretching the Si-O(Si) bonds and in the range 490-460 cm^{-1} there are vibrations bending the O-Si-O. A doublet of spectral lines is revealed at 798 and 778 cm^{-1}, evidencing the presence of quartz in the analyzed sample. It is worthwhile to mention that all spectral bands in this range feature a large FWHM value (full width at half minimum), which may be attributable to an amorphous or unordered structure of silicate phases. The third category of spectral lines is associated with vibrations of the OH^- groups. In the range of wave numbers 3300-3700 cm^{-1} there are spectral bands associated with tensile vibrations of hydroxyl groups. There is a band at 3641 cm^{-1} in this range which can be associated with the presence of portlandite ($Ca(OH)_2$). A broad band at about 3440 cm^{-1} may be associated with OH^- groups located in an unordered manner in the structure of the material (for instance associated with C-S-H gel) or with the presence of molecular water. Spectral bands associated with vibrations that bend H_2O are revealed at about 1620 cm^{-1}.

When compared to the reference spectrum, the spectrum registered for the sample containing 20% of waste limestone powder (LS-B-20) displays a higher integral intensity of spectral bands associated with vibrations of carbonate groups in relation to spectral bands associated with the presence of silico-oxygen tetrahedrons in the analyzed sample. This is caused by the admixture of waste limestone powder, leading to a higher content of CaO. Comparison of the two spectra reveals that the ratio of quartz actually expended in the reaction to the total amount of quartz in the sample containing waste limestone powder is higher, which is evidenced by a reduced intensity of the doublet of spectral lines in the range 800-780 cm^{-1}. The higher intensity of the spectral band at 960 cm^{-1} compared to the remaining bands associated with vibrations stretching Si-O(SiO) implies the presence of significant amounts of the C-S-H gel.

The further two spectra are those of samples subjected to sulphate-carbonate attack. These spectra reveal an additional spectral band at 1082 cm^{-1}, which is associated with the disappearance of the C-S-H gel and formation of thaumasite. The occurrence of this phase is evidenced by the presence of low-intensity spectral bands associated with the vibrations of the octahedron quartz for the wave number 760 and 500 cm^{-1} [37]. Comparing the two spectra, we clearly see that in sand-lime products exposed to magnesium sulphate (LS-B-20/MS) silicate phases get disintegrated in a larger degree than when exposed to sodium sulphate (LS-B-20/NS). It is worthwhile to mention that the spectrum of a sample exposed to magnesium sulphate reveals two new bands in the spectral range: at 661 and 660 cm^{-1}. Their presence is probably associated with the phase whose structure features the presence of silica-oxygen rings, such as those encountered in the scawtite structure [38].

The analysis of microstructure of the tested samples (*Fig. 9*) reveals in reference silicate material (LS-0) the zones occupied by typical products of synthesis under hydrothermal conditions, represented by both the C-S-H gel and crystalline tobermorite with elongated crystals. These products are always present on the surface of quartz sand grains, they tend to interpenetrate and hence act the grain binders. An entirely different microstructure is revealed for samples kept in solutions containing sulphate ions. In both cases we observe areas dominated by calcium carbonate, though the zones of fiber-structured crystals are revealed too. In the light of the EDAX data, it is reasonable to suppose that this can well be thaumasite [39].

5. Conclusions

Results of the experimental investigations lead us to the following conclusions:

1. No matter how the actual composition of process mixtures containing waste limestone powders should vary both in qualitative and quantitative terms, manufactured sand-lime bricks display higher compressive strength in comparison to the reference sample made from the process mixture without the added mineral components.
2. The evident improvement of the mechanical features is attributable to the synergy effect involving physical and chemical interactions between the waste limestone powder and the remaining mixture components.
3. Powdered limestone plays a triple role:
   - it acts as a micro-aggregate so the semi-finished products are more compacted during the formation process,
   - similar to lime, it plays the role of a plasticizer improving the rheological properties of pressed mixtures,
   - as a chemically active substance it acts as a mineral additive, the product of the reaction being a separate mineral phase known as scawtite.
4. Extensive testing of structure and microstructure of sand-lime materials suggests that an addition of limestone powder favourably impacts on the parameters of sand-lime bricks.
5. On account of a relatively short time of exposure to corrosion-prone environments, it is difficult to finally conclude whether sand-lime bricks containing waste limestone powder are subjected to sulphate-carbonate corrosion, involving the formation of thaumasite.

6. Test results might be utilized to implement the new solution in the industrial practice, whereby sand-lime bricks should be manufactured from the prepared mixed binder obtained from grinding or mixing of burnt lime and fine-grained limestone.
7. Application of a new formula of the mixed binder might help reduce the unit consumption of lime whilst the quality of obtained silicate materials should not deteriorate, or, when the lime consumption remains the same we get products with more favourable strength parameters.

Acknowledgements

This work was supported from the subsidy of the Ministry of Education and Science for the AGH University of Science and Technology in Krakow (Project No 16.16.160.557).

References

[1] Michaëlis, W. (1880) Verfahren zur Erzeugung von kunstsandstein, German Patent (Patentschrift) No. 14195.
[2] Van DerBurgh, G.E. (1866), Britisch Patent No. 2470.
[3] Van DerBurgh, G.E. (1865) Improved solution for saturating natural and artificial stone, U.S. Patent No. 175788.
[4] Kwiatkowski, L.F. (1904) Process of making artificial brick or stone, U.S. Patent No. 55595.
[5] Bolkvadze, L.S., Karumidze, Z.I., Kvaratskheliya, R.N., Sokhadze, G.V., Khoperiya, Sh.P. (1983) Study of the strength of silicate brick made from Kemperi sands with chemical admixtures, USSR Patent No. 220830.
[6] Crennan, J.M., El-Hemaly, S.A.S., Taylor, H.F.W. (1977) Autoclaved Lime-Quartz Materials. I. Some Factors Influencing Strength, Cem. Concr. Res., Vol. 7, No 5, pp. 493-502.
[7] Jambor, J. (1963) Relation between phase composition, overall porosity, and strength of hardened lime-pozzolana pastes, Mag. Concr. Res. Vol. 15, No 45, pp. 131-142.
[8] Rademaker, P.D., Reiman, V. (1994) Autoclaving calcium silicate bricks, Zement-Kalk-Gips Vol. 47, No 11, pp. 636-642.
[9] Chenzhi Li, Linhua Jiang, Ning Xu, Shaobo Jiang (2018) Pore structure and permeability of concrete with high volume of limestone powder addition, Powder Technol. No 338, pp. 416-424
[10] Taylor, H.F.W. (1964) The calcium silicate hydrates, Chapter 5 of The Chemistry of Cements, Press, London and New York, Vol. 1, pp. 168-227.
[11] Pytel Z. (2014) Modification of the phase composition and microstructure of autoclaved sand-lime bricks, Papers of the Commission on Ceramic Science, Polish Ceramic Bulletin, Ceramics, Vol. 116 (in Polish)
[12] Quincke, J.E. (1960) Effect of lime and silica, grain-size distribution and structure in calcareous sandstone, Tonidustrie Zeitung und Keramische Rundschau Vol. 84, pp. 198–200.
[13] Chan, C., Sakiyama, M., Mitsuda, M.T. (1978) Kinetics of calcium oxide-quartz-water reaction at 120° to 180°C in suspension, Cem. Concr. Res., Vol. 8, No 1, pp. 1–5.
[14] Sakiyama, M., Oshio, Y., Mitsuda, T. (2000) Influence of quartz particle size and lime/quartz ratios on the strength of autoclaved calcium silicate board, Proceedings of the 6th Inter. Congr. on Applied Mineralogy, Gettingen, Germany, Vol. 2, pp. 903–906.
[15] Pytel, Z., Małolepszy, J. (2000) Effect of mineral admixtures on the properties of sand-lime bricks, Proceedings of the International Conference on the Science and Engineering of Recycling for Environmental Protection - Waste Materials in Construction "WASCON 2000" Edited by: G.R. Woolley, J.J.J.M. Goumans, P.J. Wainwright Harrogate, England, 31 May - 2 June, Pergamon, Waste Management Series Vol. I, pp. 371-372.
[16] Pytel, Z., Małolepszy, J. (2003) The structure and microstructure of autoclaved materials modified by pozzolanic mineral admixtures, Proceedings of the 11th ICCC, Durban, South Africa, pp. 1640-1649.
[17] Crennon, J.M., Dyczek, J.R.L., Taylor, H.F.W. (1972) Quantitative phase compositions of autoclaved cement-quartz cubes, Cem. Concr. Res. Vol. 2, No 3, pp. 277-289.
[18] Jauberthie, R., Temimi, M., Laquerbe, M. (1996) Hydrothermal Transformation of Tobermorite Gel to 10 Å Tobermorite, Cem. Concr. Res. Vol. 26, No 9, pp. 1335-1339.
[19] Taylor, H.F.W. (1959) The transformation of tobermorite into xonotlite, Mineral. Mag. Vol. 32, pp. 110-116.
[20] Dyczek, J.R.L. (1979) The calcium oxide-silicon dioxide-water system as a base of technology of autoclaved building materials, Zeszyty Naukowe Akademii Górniczo-Hutniczej im. Stanisława Staszica, Ceramika Vol. 42, Kraków (in Polish).
[21] Pytel, Z. (2006) Investigation and physical properties of sand-lime bricks produced with addition of ground limestone, Proceedings of the 6th International Conference on the Environmental and Technical Implications of Construction with Alternative Materials Science and Engineering of Recycling for Environmental Protection, Belgrade, Serbia & Montenegro, May 30 – June 2, Edited by: Ilic, M., Goumans, J.J.J.M., Miletic, S., Heynen, J.J.M., Senden, G.J., pp. 497-505.
[22] Turgut, P. (2010) Masonry composite material made of limestone powder and fly ash, Powder Technol. No 204, pp. 42-47.
[23] Števula, L., Petrovič, J. (1981) Formation of scawtite from mixtures of calcium oxide, magnesite and quartz under hydrothermal conditions, Cem. Concr. Res. Vol. 11, No 4, pp. 549-557.
[24] Kurdowski, W. (1992) On the mechanism of scawtite formation, Proceedings of the 9th ICCC, New Delhi, Vol. IV, pp. 170-174.
[25] Kapralik, I., Števula, L., Petrovič, J., Hanic, F. (1984) Study of the system calcium oxide-silicon dioxide-carbon dioxide-water in relation to scawtite under hydrothermal conditions, Cem. Concr. Res. Vol. 14. No 6, pp. 866–872.
[26] Pluth, J.J., Smith, J.V. (1973) Crystal structure of scawtite, $Ca_7(Si_6O_{18})(CO_3)\cdot 2H_2O$, Acta Crystalographica, Section B: Structural Crystallography and Crystal Chemistry, Vol. B29, No 1, pp. 73–80.
[27] Diederich, P., Mouret, M., De Ryck, A., Ponchon, F., Escadeillas, G. (2012) The nature of limestone filler and self-consolidating feasibility-Relationships between physical, chemical and mineralogical properties of fillers and the flow at different states, from powder to cement-based suspension, Powder Technol., No 218, pp. 90-101.
[28] Pytel, Z. (2006) Formation of scawtite and its influence on the properties of sand-lime bricks, Proceedings of the 16th International Conference on Building Materials "IBAUSIL 2006", Weimar, Germany, Vol. 2, pp. 2-0849–2-0858.
[29] Bensted, J. (2000) Mechanism of thaumasite sulphate attack in cements, mortars and concretes, ZKG Interantional Vol. 53 No 12, pp. 704–708
[30] Skalny, J., Marchand, J.M., Odler, I. (2002) Sulfate attack on concrete, Modern Concrete Technology 10, London and New York.
[31] Van Aardt, J.H.P., Visser, S. (1975) Thaumasite formation: A cause of deterioration of Portland cement and related substances in the presence of sulphates, Cem. Concr. Res. Vol. 5 No 3 pp. 225–232.
[32] Bensted, J. (2003) Thaumasite-direct, woodfordite and other possible formation routes, Cem. Concr. Compos. Vol. 25 No 8 pp. 873-877.
[33] Pytel, Z. (2012) Study of the possibility of thaumasite corrosion in sand-lime products obtained with selected mineral admixtures, Proceedings of the 18th International Conference on Building Materials "IBAUSIL 2012", Weimar, Germany, Vol. 2 pp. 2-1236–2-1247.
[34] EN-771-2 (2011) Specification for masonry units - Part 2: Calcium silicate masonry units.
[35] EN-772-1:2011+A1 (2015) Methods of test for masonry units - Part 1: Determination of compressive strength.
[36] EN-772-13 (2000) Methods of test for masonry units - Part 13: Determination of net and gross dry density of masonry units (except for natural stone).
[37] Blanco-Varela, M.T., Carmona-Quiroga, P.M., Sáez del Bosque, I.F., Martínez-Ramírez, S. (2012) Role of organic admixtures on thaumasite precipitation, Cem. Concr. Res. Vol. 42 No 7 pp. 994–1000.
[38] Farmer, V.C. (1974) The Infrared Spectra of Minerals, Mineralogical Society, London.
[39] Pytel, Z. (2015) Properties and durability of sand-lime bricks containing ground limestone, Proceedings of the 13th International Conference on Resent Advances in Concrete Technology and Sustainability Issues, CANMET/ACI, July 14 - 17, Ottawa, Canada Vol. Supplementary Papers pp. 219-238.

Ref.:
Pytel, Zdzisław: *Effect of waste limestone powder on properties and sulphate-carbonate corrosion of autoclaved silicate materials*
Építőanyag – Journal of Silicate Based and Composite Materials, Vol. 74, No. 5 (2022), 175–182. p.
https://doi.org/10.14382/epitoanyag-jsbcm.2022.26

3D concrete printing: review

Salem NEHME ▪ associate professor ▪ salem.nehme@emk.bme.hu
Ayman ABEIDI ▪ Ph.D. candidate ▪ aymanabeidi@edu.bme.hu.
Érkezett: 2022. 05. 30. ▪ Received: 30. 05. 2022. ▪ https://doi.org/10.14382/epitoanyag-jsbcm.2022.27

Abstract
3D printing technology is an exciting young method that can change the construction industry as we know it. But as with any new change, people are hesitant and worried about it; this paper aims to give a general review of the 3D printing technology concerning the construction industry. The current construction approach requires many expensive labours and formwork that can be dispensed with the 3D printing technology. It is also more harmful to the ecological system and more time-consuming. The 3D printing technology allows the modification of the materials used for printing, which opens the door for trying new mixtures and reduces the impact of construction on the ecological system. The technology is a developing one that you can see different approaches to the way to do it and the missing regulations for testing and designing. The most commonly used material is concrete. However, 3D printed concrete must be pumpable and extrudable while it's still fresh and suitable for building into layers as it reaches the hardening stage.
Keywords: 3D printing technology, 3D concrete printing, extrusion, concrete composition, layer thickness, gap time, pumpability, extrudability
Kulcsszavak: 3D nyomtatási technológia, 3D betonnyomtatás, extrudálás, betonösszetétel, rétegvastagság, hézagidő, szivattyúzhatóság, extrudálhatóság

Salem NEHME
Assoc. Prof., BME, Department of Construction Materials and Technologies. MSc Civil Engineer. Member of the Technical Committee of Concrete Working Group (MSZT/ MB 107) of Hungarian Standardization Institute; Hungarian Group of fib; Hungarian engineer chamber (MMK: 01-9159). Fields of interest: concrete technology, mass concrete, self-compacting concrete, fibre reinforced concrete, quality control of building materials, non-destructive testing, reinforced concrete structures, recycling of building materials.

Abeidi AYMAN
Civil engineer (MSc, University of BME), PhD candidate at the Construction Materials and Technologies Department. Main fields of interest: Concrete technology, Self-compacting concrete, durability properties, non-destructive testing, high-performance concrete, fibre reinforced concrete.

1. Introduction

With the global understanding of our planet, the reduction in the carbon footprint has become a common factor in evaluating anything we do. The conventional construction industry has proven a solid and reliable way to construct a great range of structures. With the more knowledge we have, the more complex designs we can do, new technologies have been added to the industry, but the technique of construction has not significantly changed; it remained with a high environmental impact while depending on high labour during labours shortage time, and needs a lot of time and money which lead to higher costs of residential houses to a raising population.

Cutting waste, reducing time on site, and addressing labour shortages. Those are the three main goals that 3D printing technology can try to achieve. 3D printing is a modern technology that can build everything from small structures to whole houses and even varied structures like wind turbines. It is an exciting new way of making buildings, and it has the potential to solve many of the problems we face when trying to find affordable housing.

The 3D printing technology is done by providing a cad file into the system and providing how fast and how much of the material should be extruded. It works in the same way as the brick system; after the completion of the first line of bricks, the second line starts as well does the 3D printing it extrudes a layer of the mixture and repeats the process with a spaced time between the layers called the gap time.

The technology can construct a vast range of structures, but the load bearing of these structures remains not equivalent to what the conventional way can provide. But it allows the creation of a new, more environmental mixture to be used for the new constructions using local materials and with a lower carbon footprint. The mixture has some requirements to keep as it has to go through the pumping phase to the layer phase, thermal performance, and durability.

2. Conventional construction industry

The construction industry is a traditionally conservative industry that had seen no significant modifications in the daily practice at the time that most of the industries have implemented modern technologies to improve the overall method. The traditional building method can be described as expensive, laborious, and time-consuming. Moreover, the construction sector is responsible for high environmental impacts worldwide [1, 2].

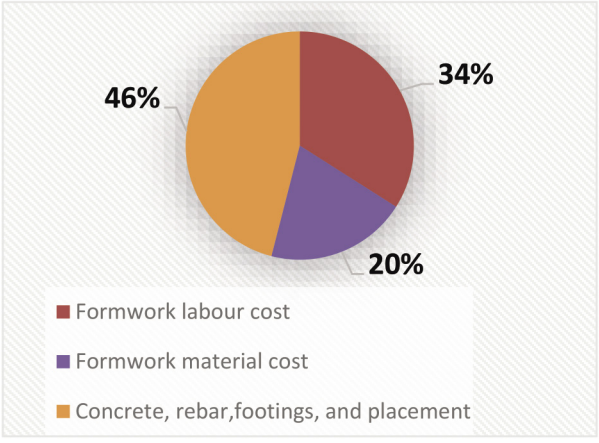

Fig. 1 Cost distribution of a typically constructed project
1. ábra Egy tipikusan épített projekt költségeloszlása

The construction of structural elements in the conventional way is a limiting process that has disadvantages that can be overcome or reduced by the modification of the process itself or by introducing a new way to construct. In the conventional way, the concrete is poured into the formwork and then compacted. The formwork will shape the structural element constructed; this can be a very limiting method for architects as the shapes are confined to the formwork requirements. Moreover, the conventional way has disadvantages such as time and money consumption,

dependency on high manual labour, and a high ecological impact. *Fig. 1* shows the cost distribution and how much formwork affect the cost, from the cost of formwork materials and the part of the labour performing the formwork [3].

The world's population is the main factor that affects the demand for housing and the climate change issues we have. The United Nations (UN) predicts that there will be 10.9 billion people by the end of the century [4]. More recent research from the Institute for Health Metrics and Evaluation (IHME) shows that we would reach a peak in 2064 (9.7B). A total of 8.8 at the end of the century [5], International Institute for Applied Systems Analysis (IIASA) also predicts a lower population than both have expected; the reason for the significant differences between the predictions is in the fertility evaluation in the Sub-Sahara Africa as *Fig. 2* shows [6].

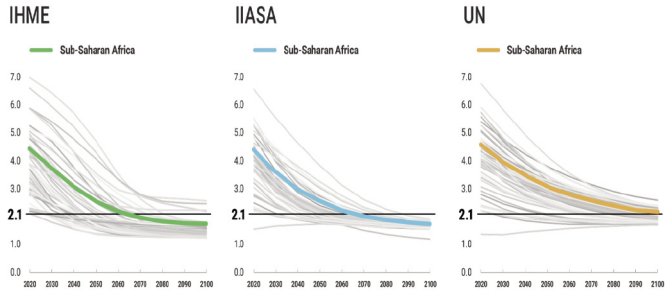

Fig. 2 Fertility rates in the Sub-Sahara Africa for (IHEM, IIASA, and UN) ertility rates in the Sub-Sahara Africa for (IHEM, IIASA, and UN)
2. ábra A szubszaharai Afrika termékenységi rátái (IHEM, IIASA és ENSZ) a szubszaharai Afrikában (IHEM, IIASA és ENSZ)

The larger the population, the worse the issue of housing and climate change (the greenhouse effect of CO_2 emissions). Globally there has been a rise in the cost of constructing residential buildings for the rising world population. With the increasing awareness of the environmental effect we are causing on the ecological system, carbon footprint reduction is becoming a primary concern for evaluating the methods used.

The current construction industry method is highly dependent on manual labour, which is in increasing quantitative shortage caused by significant excess demand with insufficient workers, which caused the rise of unskilled labour's salaries, thus the overall cost of the structure. Moreover, slow supply for the development requirement and a dependency on foreign labour. An example is the EU increasing international and cross-border mobility as a solution while avoiding brain drain [7]. With the reliance on manual labour, human error stays a significant factor in the waste of materials and time among projects.

All the mentioned raised the necessitates for the minimisation of the quantities used, the total cost, and the time needed, which has made it the task of researchers to find, develop and apply modern technologies.

3. 3D printing technology

There have been uses for technology implementation in the industry, but 3D printing has redefined the way we do things, the properties needed for the material used, and even the overall material used, as we can reduce the use of concrete for other mixtures suitable for the case. The technology is vast and new and thus lacks tests, and a clear perspectives chapter is going to lay out some aspects of the technology of 3D printing concerning the construction industry.

3D printing can construct a building in just a few days. 3D printing also offers a significant amount of design freedom, allowing architects to experiment with shapes and styles that would have been impossible using traditional building methods. Errors on site have been almost completely eradicated, saving time, and wasted material and money. While deceiving for a single building might be modest. It adds up when looking at it on a larger scale for development and the housing industry. 3D printing can be built in any location with a different elevation, as well the printing can be operated in harsh climate conditions with full-day printing without additional costs.

As the technology is relatively young, educating people about 3D printing is a barrier that prevents the technology from moving forward to becoming a widely used method in construction. It is a modern technology for contractors, engineers, and the skilled and unskilled labourers themselves, which causes hesitation in using the technology. So, there are still some mean fears about using this technology. Educating people and securing building certification and permits is a huge step for 3D printing to be treated as a valid replacement method for the conventional way. It will teach us how to cope with this technology and adapt to it rather than be threatened by it. The more people are comfortable using 3D printing, the more it becomes widespread and creates a driving force in the research fields to cover the needed knowledge [8].

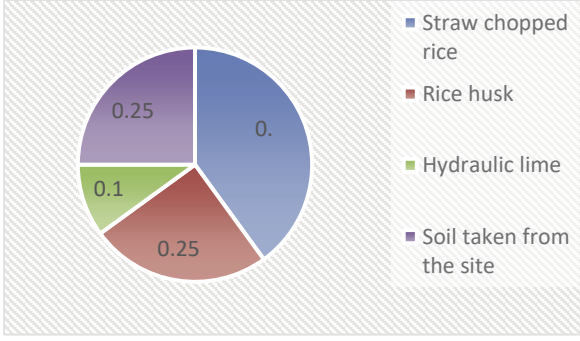

Fig. 3 WASP and RiceHouse mixture components
3. ábra WASP és RiceHouse keverék összetevői

Using 3D printing technology will play a vital role as it allows the possibility of using a good range of materials that can be analysed and assessed to reduce environmental impact. One of the fitting examples can be seen in the Gaia project by the WASP company on using natural materials from the surrounding area, which will be done with a much lower history, footprint, and overall cost. WASP with RiceHouse provided a homogeneous and workable mixture for printing which uses straw chopped rice along with rice husk and hydraulic lime, *Fig. 3* shows the ratios for the components, the soil was made of (30% clay, 30% sand and 40% silt) [9]. Nevertheless, more testing (structural and thermal) must be done [10].

3D printed houses are the current most favourable option mathematically speaking, as they can provide opportunities with much lower costs, which come from lower material consumption than conventional designs use, waste of materials on-site from the human errors and the complexity of cutting the waste and following up with everything going with each aspect in the conventional process, reduction of the labour costs needed as the digital system can use as low as 2-3 people to do almost half of the construction (the printing part of the house), and of course the reduction of time needed which is a considerable cost reduction, it only takes around 48 hours to set up the machine, the building speed (250-1000 mm/s) vary based on the layout, number of robotic arms, type of the robotic arm used and the material used that controls the time gap, the exact numbers vary from place to another on how much the actual reduction of the overall cost is as the materials availability plays a factor, Nevertheless, reduction of some of the issues is being observed.

3D printing construction companies are riding the wave of 3D printing technology. Houses with even three levels using a 3D printed base are getting permitted. Other companies are using multiple printing robotic arms to facilitate and speed up the process even more for spacious structures. Not all companies print on-site; fixed printers can be used to build the pieces. They will then be transported to the building site, such as Mighty buildings, where their printers use a thermoset composite material called light stone materials; it will harden under exposure to UV light [11].

The hopes of becoming a multi-planet species have been surfacing again. The 3D printing technology is being tested to be used to build the first home for humans on another planet. ICON company is working on two technologies with NASA, including the Olympus project, where the focus is to find a suitable construction system to support future exploration of the moon [12], and the Mars Dune Alpha where a simulation for the mars habitat has been done to prepare for a long-duration human mission to Mars [13].

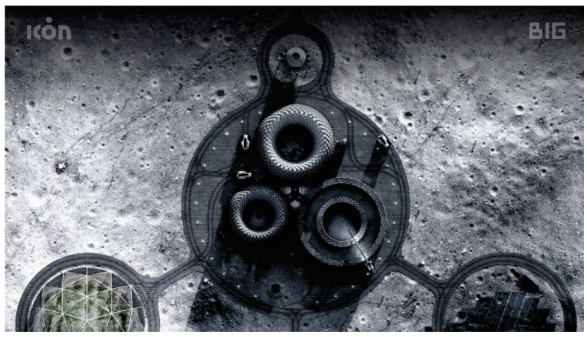

Fig. 4 Olympus project a futuristic vision
4. ábra Az Olympus futurisztikus jövőképet vetít előre

The printing technology have factors must be considered when thinking of specific project with known printing robotics.

- Arm movement (the printing speed of the robotic technology used, gap time between two consecutive layers).
- Tube capacity and nozzle used (diameter and nature of end), printing continuity, and constant layer thickness.
- Reinforcement of the structure (deferent approaches exist on how to reinforce the 3D printed structure. This is still under early studies and needs more data on whether the reinforcing of the concrete will be done manually or by robotics technology.
- Material used: the mixture of the material chosen have the mechanical properties needed.

The technology itself is moving with the research as well. BOD2, a second-generation, was released; BOD2 can print with speeds of up to 100 cm/second – the fastest printer yet, the company COBOD claims [14]. There is a need to systemise and regulate tests to check and adapt to the study and analysis of the mixture and more studies on the effect of the composition of the mix.

The robotics field has advanced the process in many sectors, and 3D printing was the construction industry's share. The current system is expensive, time-consuming, requires sizeable manual labour and environmentally has a more significant impact. The technology is still young but promising.

The leading candidate to be used for the 3D printing technology is concrete. Thus, we will narrow the paper to the concrete and discuss what to consider while dealing with concrete as the material to be printed.

4. Concrete as the printing material

3D concrete printing technology has made a significant impact by introducing a revolutionary way to build. The contradicting properties needed for the mixture in the printing stage and after printing opened the door to many questions, basically how to follow the technology's needs and adapt within these needs to provide the engineering requirements needed for the structure.

When choosing the material to used attention must be given to the mechanical properties of the final mixture. As the mechanical properties represent the material ability to be built using this technology. The material that will be printed has to have good rheological behaviour that is, the mixture is easy to mix and extruded through the printing arm's nozzle and to be able to keep a shape without deformation till the material starts to gain strength.

The 3D printed concrete goes through two stages; in the first stage (fresh concrete), when it is still mixable and easy to be handled, we can generalise the required properties for fresh concrete into two main properties [15, 16]:

- Pumpability: the ability of the mixture to be easily mixed and remain stable while it is being pumped and without losing the fresh mixed properties as the pressure needed to pump the concrete will tend to segregate the mixture.
- Extrudability: as the mixture reaches the end of the pump and approaches the nozzle, it will be extruded into layers without formwork or temporary supports; thus, there is a need to make sure that the mixture will be able to withstand the yield stresses at that stage and remains in the wanted shape without any deformations.

It is worth mentioning that the workability and shelf life of fresh concrete are essential considerations in 3D concrete printing, and the consistency and compactness of fresh

concrete (uncompressed body density and air content) affect the compressive strength and durability of concrete [17].

The durability of the concrete depends on how the fresh concrete can be applied, the consistency, and the air content, so in the case of compaction or shotcrete, the shot has a crucial role in achieving the lowest possible air content. During 3D printing, the correct air content can be ensured by the right consistency and the pressure in the tube. This is usually higher than compacted concrete, so it is important to compensate with a lower w/c ratio.

After the mixture has retained its shape and as time passing, the hardening process starts and speeding up the hardening of the mix after being extruded is a very desirable property of the hardened mixture. The hardened concrete properties can also be generalised into two main properties [18]:

- Buildability: with each layer added, the higher the stresses on the first layer placed (Based layer), and as it is the oldest layer, it had the most time to reach a higher bearing load. The failure in the base layer can be used as failure criteria for the structure [19].
- Interlayer bonding: This part is the most critical part of the process. After adding a layer, if there were no interface bonding between the layers, it would be a poorly printed structure with a high probability of failure as the layers are not acting together as they should.

The composition of concrete also affects the strength, ductility, and durability of concrete, which is mainly influenced by the adhesives of the raw materials and their mixing ratios, as well as between the cement paste, the admixture, and the layers. In addition, the pore content, size, and distribution of the cement paste influence the strength and durability.

For a better 3D printing of concrete, the general approaches for creating a good concrete composition should be easily checked and adapted based on the design needs and robotic printing technology used, considering the following aspects [19-21]:

- Production of suitable base concrete composition and the study of its modifications depending on local raw materials available and the required properties.
- Optimal consistency (appropriate standards and guidelines for testing concrete are not yet available).
- Method of accelerating setting (with cement type and setting accelerator additives) as the cement as a sole binder is highly affected by the time gap between layers.
- Maximum shelf life.
- Adequate stability, ensuring cohesion, proper adhesion, and bonding interface between layers.
- Sufficient compressive strength, ductility, and durability.

When designing the 3D printing concrete, the fresh concrete and hardened concrete properties should be kept in mind for each concrete composition and better identification of the effects of:

- Binder: The binder plays a vital part in the strength of the concrete, the sensitivity to the gap time between layers, intermediate setting time, and adhesion. The effect of the type of the binder.
- Fine sand aggregates: When it comes to the fine sand aggregates, the maximum grain size, grain distribution curve, and the fineness modulus.
- Water: The water-binder factor, water volume, strength, and durability issues
- Additives: The usage of additives is going to improve the concrete as we get to satisfy some of the required properties for the printing concrete, like the use of viscosity modifier (VMA) to achieve the suitable dough-like rheology, the use of stabilisers, the setting accelerator, the shrinkage reduction factors as concrete will shrink due to lack of compaction, the use of sealants, adhesive bridge, hydrophilising agent, and the type and amount of additives effects.
- Fibres: The use of fibres as reinforcement for the 3D printing concrete, the effect of fibres on the workability, viscosity, yield stress, and flexural strength.

The technology of 3D concrete printing is a complex task and attention should be paid to more than the modelling and the recipe, but also a proper operation and execution should be taken into consideration.

- The type of the 3D printing technology used, the nozzle size, the allowed time gap, and tests for the used materials should be developed to ensure the wanted properties were fulfilled.
- Mixing machine type and whether it will be mixed on-site or the mix will be transported to the site of which the compositions are primarily designed for mobile mixing and tests suggested for checking the transported concrete.
- Alignment of the pump machine and the robotics arm to consider the layout, nozzle control speed, discharge rate, wanted layer size and the time gap between layers.
- The operator should be well-trained and have some expertise in dealing with concrete technology problems to notice any issues during the process.

5. Conclusions

The conventional construction is not going anywhere anytime soon, with all the additional costs and ecological impact it is still the known and verified way to design and construct structures under considerable imposed load. On the other hand, 3D printing technology opens a new way for limited types of structures but eliminates some limits on those structures. 3D printing does it faster, more accurate, less labour needed, cheaper, and less ecological impact.

3D printing has requirements for the material to be used, the first part of the materials life is while it is being pumped so the mixture needs to be pumpable and after it is extruded it needs to withstand a shape without formwork, the second part for the material is as it starts to harden, how will the layers are boning, the load bearing, and other properties.

The technology is still developing and there are a lot to be studied, new tests are also needed as the material is needed to have properties for it to be suitable.

Acknowledgments

The authors of the article would like to thank VKE for the research support received through the 2018-1-3-1_0003 "Materials Science Development of Modern Concrete Elements" tender.

References

[1] Alhumayani, H. – Gomaa, M. – Soebarto, V. – Jabi, W. "Environmental assessment of large-scale 3D printing in construction: A comparative study between cob and concrete," J. Clean. Prod., vol. 270, 2020, https://doi.org/10.1016/j.jclepro.2020.122463.

[2] De Schutter, G. – Lesage, K. – Mechtcherine, V. – Nerella, V. N. – Habert, G. – Agusti-Juan, I. "Vision of 3D printing with concrete — Technical, economic and environmental potentials," Cem. Concr. Res., vol. 112, no. August, pp. 25–36, 2018, https://doi.org/10.1016/j.cemconres.2018.06.001.

[3] Jha, K. N. "FORMWORK FOR CONCRETE STRUCTURES," Tata McGraw Hill Educ. Priv. Ltd. New Delhi, 2012.

[4] UN, "World Population Prospects 2019: Data booklet," 2019.

[5] Vollset, S. E. et al. "Fertility, mortality, migration, and population scenarios for 195 countries and territories from 2017 to 2100: a forecasting analysis for the Global Burden of Disease Study," Lancet, vol. 396, no. 10258, pp. 1285–1306, Oct. 2020, https://doi.org/10.1016/S0140-6736(20)30677-2.

[6] Kaneda, T. "Understanding and Comparing Population Projections in Sub-Sahara Africa," 2021. https://www.prb.org/resources/understanding-and-comparing-population-projections-in-sub-saharan-africa/

[7] Smajda, L. "Labour Market Shortages in the European Union. Policy Department A: Economic and Scientific Policy," p. 170, 2015, [Online]. Available: http://www.europarl.europa.eu/RegData/etudes/STUD/2015/542202/IPOL_STU(2015)542202_EN.pdf

[8] Buswell, R. A. – Leal de Silva, W. R. – Jones, S. Z. – Dirrenberger, J. "3D printing using concrete extrusion: A roadmap for research," Cem. Concr. Res., vol. 112, no. June, pp. 37–49, 2018, https://doi.org/10.1016/j.cemconres.2018.05.006.

[9] WASP, "The first 3D printed House with earth | Gaia," 2018. https://www.3dwasp.com/en/3d-printed-house-gaia/

[10] Bester, F. "3D Printing of Concrete within the South African Building and Construction Industry," Greenovate Award., no. December, 2018, [Online]. Available: https://www.researchgate.net/publication/329365708%0A3D

[11] "Mighty buildings." https://mightybuildings.com/mks

[12] "'PROJECT OLYMPUS,' ICON".

[13] "'MARS DUNE ALPHA,' ICON." https://www.iconbuild.com/technology/mars-dune-alpha.

[14] "'COBOD,' COBOD." https://cobod.com/.

[15] Malaeb, Z. – AlSakka, F. – Hamzeh, F. "3D Concrete Printing." Elsevier Inc., 2019. https://doi.org/10.1016/b978-0-12-815481-6.00006-3.

[16] Sanjayan, J. G. – Nematollahi, B. "3D Concrete Printing for Construction Applications." Elsevier Inc., 2019. https://doi.org/10.1016/b978-0-12-815481-6.00001-4.

[17] Papachristoforou, M. – Mitsopoulos, V. – Stefanidou, M. "Evaluation of workability parameters in 3D printing concrete," Procedia Struct. Integr., vol. 10, pp. 155–162, 2018, https://doi.org/10.1016/j.prostr.2018.09.023.

[18] Khan, M. A. "Mix suitable for concrete 3D printing: A review," Mater. Today Proc., vol. 32, pp. 831–837, 2020, https://doi.org/10.1016/j.matpr.2020.03.825.

[19] Wangler, T. – Roussel, N. – Bos, F. P. – Salet, T. A. M. – Flatt, R. J. "Cement and Concrete Research Digital Concrete : A Review," vol. 123, no. June, 2019.

[20] Lowke, D. – Dini, E. – Perrot, A. – Weger, D. – Gehlen, C. – Dillenburger, B. "Particle-bed 3D printing in concrete construction – Possibilities and challenges," Cem. Concr. Res., vol. 112, no. November 2017, pp. 50–65, 2018, https://doi.org/10.1016/j.cemconres.2018.05.018.

[21] Paul, S. C. – van Zijl, G. P. A. G. – Gibson, I. "A review of 3D concrete printing systems and materials properties: current status and future research prospects," Rapid Prototyp. J., vol. 24, no. 4, pp. 784–798, 2018, https://doi.org/10.1108/RPJ-09-2016-0154.

Ref.:
Nehme, Salem – **Abeidi**, Ayman: *3D concrete printing: review*
Építőanyag – Journal of Silicate Based and Composite Materials, Vol. 74, No. 5 (2022), 183–187. p.
https://doi.org/10.14382/epitoanyag-jsbcm.2022.27

A novel conceptional approach for calculating the stability time related to converting the anticipated degradation from the curve of conductivity for flexible poly (vinyl chloride)

Ali I. AL-MOSAWI
PhD in polymers Engineering at Institute of Ceramic and Polymer Engineering, Faculty of Materials Science and Engineering, University of Miskolc, Hungary. Research Interests: Polymers, Composite Materials, Rubber Technology, Flame Retardants, Materials Testing, Materials Processing.

Ali I. AL-MOSAWI ▪ Institute of Ceramic and Polymer Engineering, University of Miskolc, Hungary ▪ alialmosawi76@gmail.com

Érkezett: 2022. 07. 04. ▪ Received: 04. 07. 2022. ▪ https://doi.org/10.14382/epitoanyag-jsbcm.2022.28

Abstract

The current study introduces a novel method for calculating the stability time by a new approach based on the conversion of degradation from the conductivity curve results obtained by the conventional method. The stability time calculated by the novel method is shorter than the time measured by the conventional method. The stability time in the novel method can be calculated by the endpoint of the tangency of the conversion curve with the tangent line. This point of tangency represents the stability time, as will be explained in detail. Still, it gives a clear and accurate envisage of the dehydrochlorination behavior and can be generalized to all types of polyvinyl chloride compared to the stability time measured by conventional ones based on measuring the conductivity which cannot be used to compare different compounds because PVC-based compounds may include varying amounts of PVC. As a result, the conventional method is inapplicable in all cases. For example, specific conductivity of 60 µS/cm indicates the same quantity of HCl but a different degradation grade. If this conventional approach is used alone, the results obtained will be inaccurate. Therefore, the novel method possesses greater sensitivity and accuracy for these differences in PVC-based compounds.

Keywords: stability time, thermal dehydrochlorination, novel evaluation, flexible poly (vinyl chloride)
Kulcsszavak: stabilitási idő, termikus dehidroklórozás, új értékelés, lágyított poli (vinil-klorid)

1. Introduction

The unique characteristics of polymers in general, including poly (vinyl chloride) (PVC), have made them a real competitor to the rest of the materials in various applications that require high performance and quality such as aerospace, automotive, medical and electronics applications [1-4]. However, like everything in this universe, there is nothing entirely perfect, and polymers, despite their distinctive characteristics, suffer from a significant deterioration in their thermal resistance at high temperatures. This is the primary determinant of their choice in such applications that require high thermal resistance. In addition, the type of polymer will determine the decomposition behavior at high temperatures and the resulting compounds [5-8]. In the case of poly (vinyl chloride), when the temperature rises from 170 °C and above, the chlorine and hydrogen will be removed from the poly (vinyl chloride) molecules. This released chlorine and hydrogen will react to create hydrogen chloride (HCl), which also will be released as a product of degradation as shown in *Fig. 1* [5]. This removal process of HCl is called dehydrochlorination, which will be activated and stimulated by high temperatures. The degradation of the PVC structure is randomly generated through the lattice defects created during the polymerization process, and these defects are allylic chlorine atoms and tertiary chlorine atoms [5, 9-12]. During the polymerization process, tertiary chlorine and allylic chlorine atoms are produced due to branch formation and polymerization termination. Poly (vinyl chloride) degradation is initiated at the defects created by these atoms [13,14]. During the process, new defects caused by hydrogen chloride are generated, which add to the existing defects resulting from polymerization. When there is no interference from the stabilizer, whether due to incompetence or lack thereof, stops the release of HCl, the zipper-like continuation will continue.

A light yellow color will develop when six to seven conjugated double bonds are formed after the formation of HCl and conjugated double bonds, i.e., polyene sequences. With increasing conjugation length, this light yellow appearance can darken to red, brown, and black [15-20]. When the temperature is not reduced, this cycle of dehydrochlorination will be repeated and restored rapidly and significantly. At this stage, the decomposition becomes permanent and will cause structural and apparent deformation of the material [21, 22]. Due to the fact that poly (vinyl chloride) is heated to soften phase during processing, such as extrusion or rolling, minimizing HCl release is a priority. This can only be accomplished by halting or minimizing decomposition. Numerous studies have established HCl's autocatalytic activity on poly (vinyl chloride) degradation

[10, 23]. As we know, the conventional method used to evaluate the thermal degradation of poly(vinyl chloride) depends on exposing a sample of poly (vinyl chloride) placed in the device cylinder to high temperatures in order to measure the stability time, which represents the time at which the polymer begins to release HCl, i.e., starting of degradation [24-31].

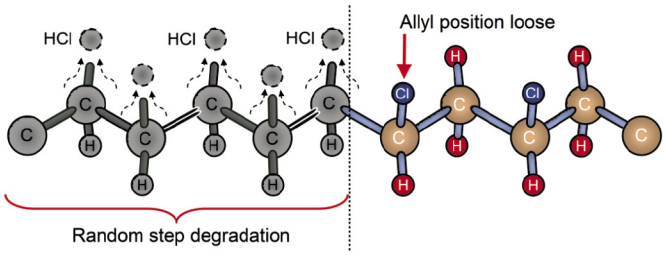

Fig. 1 Mechanism of poly(vinyl chloride) thermal degradation
1. ábra A poli(vinil-klorid) termikus lebomlásának mechanizmusa

As a result, the dehydrochlorination conversion rate is approximately 0.9% at 60 µs/cm conductivity. At these measuring conditions, there will be errors in the measurement and consequently a glitch in the obtained results and their accuracy in giving the correct concept and a clear and non-misleading vision of the degradation [32]. The reason for this state lies in the fact that not all poly (vinyl chloride) based compounds contain the same amount of poly (vinyl chloride). Therefore, it becomes difficult to compare the degradation behavior of these different compounds. So, another method of measurement must be relied upon to be more adapted to these compounds and provide a high level of accuracy and not be affected by the different amounts of poly (vinyl chloride), but rather on the principle of measuring them on other parameters that can give the same degradation behavior but more precisely as we have mentioned even if it was in a shorter time. The novel developed method is based on determining the level i.e. the conversion of degradation from the conductivity curve, which is obtained through the dehydrochlorination test performed by the conventional method [5]. In practice, this developed method is considered more accurate in measuring the level of decomposition of poly (vinyl chloride) because it depends on the measurement of a stable parameter, which is the conductivity, which gives sufficiently precise results in the measurement as mentioned for all types of poly (vinyl chloride). The advantage of the novel method is that the measured stability time is shorter than in the case of the conventional method. Despite this, it clearly describes the degradation behavior of poly (vinyl chloride).

2. Methodology

2.1 Materials

The poly (vinyl chloride) mixture or blend generally consists of primary powder of PVC and additives that give it its distinctive characteristics, as shown in *Fig. 2*.

1. Primary powder: 100 phr of PVC suspension type S-507070 (Ongrovil®).
2. Additives: two groups of additives were used, which included:
   a. Essential additives are necessary to give the basic characteristics of PVC synthesis. These additives are 70 phr DOP Bis (2-ethylhexyl-phthalate) as a plasticizer; 1.5 phr of Ca-Zn based (Newstab-50®) stabilizer; and finally 0.3 phr of Wax E (Licowax®E) as an external lubricant. The suppliers of these materials are BorsodChemZrt., DEZA, a. s. CO., Betaquímica CO., and Clariant International Ltd, respectively.
   b. Additional additives and the aim of adding them are to improve the initial properties and give new properties to the possibility of using poly (vinyl chloride) in more comprehensive applications with outstanding performance. This study added 1-5 wt.% of Oxydtron as a flame retarding-stabilizing agent was added. Oxydtron is a unique mineral nanocement additive applied to improve the workability and durability of concrete. Oxydtron is composed of several chemical compounds and copolymers. The supplier of Oxydtron is Bioekotech.

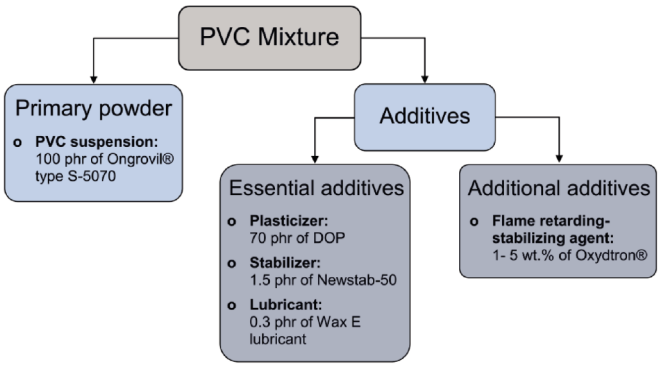

Fig. 2 Components of flexible poly(vinyl chloride) mixture
2. ábra lágyított poli(vinil-klorid) keverék összetevői

2.2 Mixing process

The mixing process includes two main stages, preparatory and definitive mixing, as shown in *Fig. 3*, with specific processing conditions listed in *Table 1*.

1. **Preparatory mixing:** It can also be called primary mixing. This mixing aims to configure poly (vinyl chloride) basic formulation mixture. In this stage, all the basic components of the poly (vinyl chloride) mixture (primary powder and essential additives) are mixed using a mechanical mixer type MTI-Mischtechnik to produce poly (vinyl chloride) basic formulation mixture. This stage takes place with a specific time of 40 minutes divided into three steps, each step having a particular speed, temperature, and time. The three steps of preparatory mixing are:
   i. **Initiatory mixing:** In this step, all the solid ingredients are mixed first, where the PVC suspension, stabilizer, and wax lubricant are put together in the mixer and started to rotate at 600 rpm speed and 30 °C temperature for two minutes. Then, during the rotation, the liquid plasticizer is gradually poured over the solid mixture, and the ingredients are left to mix well for three minutes at the same speed of rotation.

ii. **High speed-temperature mixing:** The mixing speed will be increased to 2700 rpm at this step. As a result of the high rotational speed, the shearing of particles between the mixture's components will increase, leading to rises steadily from room temperature to 150 °C. This step takes 15 minutes. The plasticizer will reach deeper into the PVC particles with speed stability, resulting in a homogeneous structure with better manufacturing properties.

iii. **Cooling:** The PVC mixture will be cooled by reducing the mixing speed to 600 rpm and pumping cooling water between the walls of the mixer. At this step, the mixture remains for 20 minutes, during which its temperature drops 150 °C to below 45 °C. At this step's end, the PVC mixture's temperature will reach 30 °C.

2. **Definitive mixing:** It can be called metaphorically secondary mixing. In this stage, the Oxydtron will be added in various weight ratios (1, 3, and 5 wt.%) to the poly (vinyl chloride) basic formulation mixture produced by the preparatory mixing stage. Then, the final mix will be mixed by a laboratory blender type Snijders scientific-LB20E at room temperature with 500 rpm speed for 1 minute.

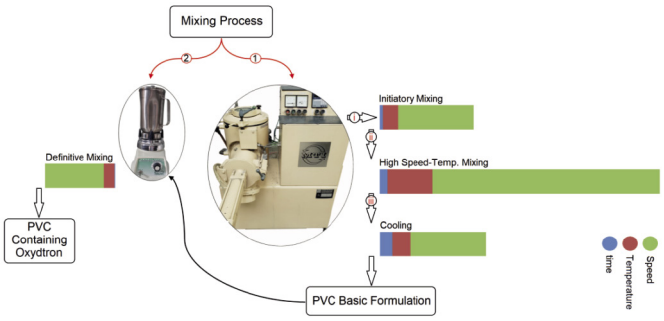

Fig. 3 The procedure of mixing process
3. ábra A keverési folyamat eljárása

Parameter	Preparatory mixing			Definitive mixing
	Initiatory mixing	High speed-temp. mixing	Cooling	
Time, min	5	15	20	1
Temperature, °C	30 °C	From 30 °C increased to 150 °C	From 150 °C dropped to 45 °C and reached to 30 °C at the end	Room temp.
Speed, rpm	600	2700	600	500

Table 1 Processing conditions of preparatory mixing
1. táblázat Az előkészítő keverés feldolgozási feltételei

2.3 Samples preparation and testing

The samples of dehydrochlorination test were prepared using twin-screw extrusion machine type Schloemann BT-50 as pellets with 3 mm diameter and 2 mm thickness. The dehydrochlorination behavior of flexible poly (vinyl chloride) containing Oxydtron has been measured by conventional method using Metrohm 763 Thermomat found at BorsodChem Zrt., Hungary. This test was completed according to ISO 182-3:1993 standard [33] with temperature 200 °C.

3. The procedure of calculating stability time

The procedure for calculating the stability time includes the following steps:

1. **Data collection:** the data of dehydrochlorination results obtained by the conventional method have been stored as a Notepad file, as shown in *Fig. 4. a*. These stored data represent time in seconds (s) and measured values of conductivity (μS/cm).

2. **Data analysis:** A data conversion program developed specifically to extract the concentrations of HCl from the stored data of dehydrochlorination has been used to analyze those data. The conversion program requires entering the quantity of poly(vinyl chloride) alone without other components. This program converted conductivity to HCl concentration using the conversion function depending on the Foxboro data table, which represents the conductivity vs. concentration for common solutions [34]. The HCl concentration is illustrated by the following equation [32]:

$$\lg(c) = -1.05788 + 0.9882 \times \lg(k) + 0.003988 \times (\lg(k))^2 \quad (1)$$

Where:
(c) the HCl concentration measured in mg/l,
(k) the specific conductivity measured in μS/cm.

Since the Metrohm 763 Thermomat device in the conventional method usually utilizes a quantity of water of 50 ml, the absorbed HCl can be measured, which will be c/20. In addition, if the exact mass of PVC in the testing sample can be determined, then the conversion of degradation can be estimated by converting the dehydrochlorination curve using the following equation [32]:

$$k = m_{HCl}/0.584 \times m_{PVC} \quad (2)$$

This is because 58.4% of HCl is produced during the whole degradation of poly (vinyl chloride)'s basic formulation.

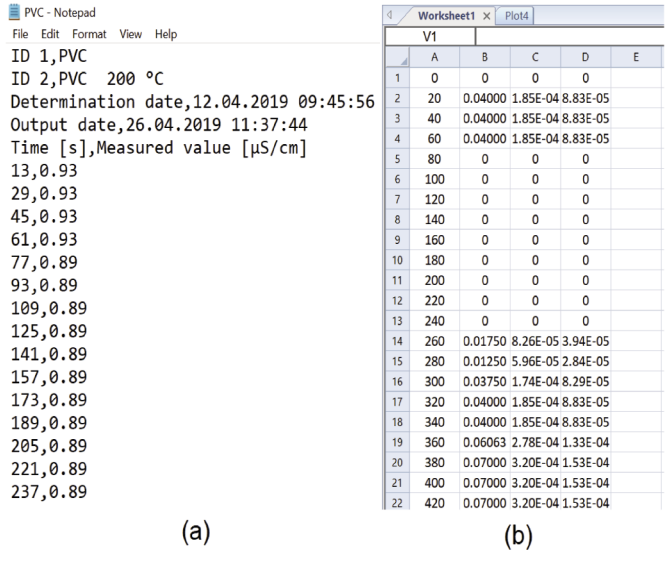

Fig. 4 (a) The stored results as notepad file in Metrohm 763 Thermomat database, and (b) Columns of the result files obtained by data conversion program
4. ábra (a) A metrohm 763 Thermomat adatbázisban jegyzettömbfájlként tárolt eredmények, és (b) Az adatkonverziós program által kapott eredményfájlok oszlopai

3. **Organizing output data:** When the data from the analysis step is imported, four reorganized data types will appear, distributed over four columns, as shown in *Fig. 4b*. These four reorganized data represent:
   i. Time in seconds in steps given by the program (20 or 30 s) (Column A).
   ii. Interpolated conductivity in µS/cm (Column B).
   iii. HCl evolved in mg, not the concentration but in the 50ml water (Column C).
   iv. Conversion in percent (after inputting the PVC in mg for the program) (Column D).

4. **Calculation of stability time:** Here, we get the stability time by locating the endpoint of the tangency between the conversion curve and the tangent line, where this point of tangency represents the stability time, as shown in *Fig. 5*.

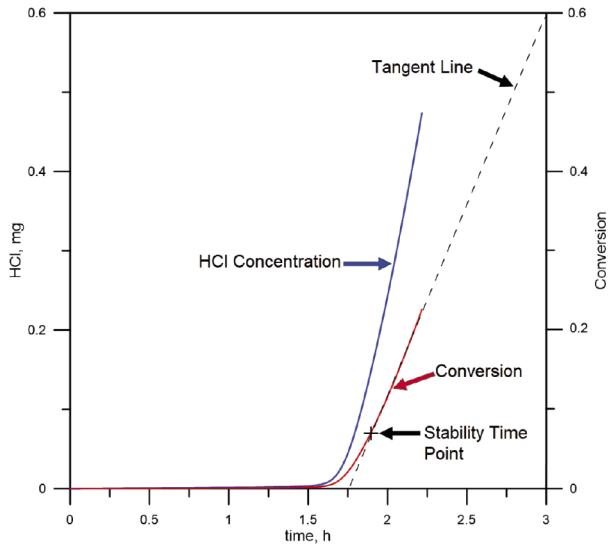

Fig. 5 Calculating the stability time by the novel method
5. ábra A stabilitási idő kiszámítása az új módszerrel

4. Results and discussion

4.1 Dehydrochlorination

As the temperature rises, the structure of poly (vinyl chloride) becomes unstable, which results in a significant release of hydrogen chloride (HCl) by the dehydrochlorination process and accompanied by a decrease in the resistance of poly (vinyl chloride). As a result, the conjugated polyene sequences are formed during the dehydrochlorination process of poly (vinyl chloride), leading to degradation. The poly (vinyl chloride) goes through three significant stages of degradation, namely initiation, propagation, and termination. The entry of the polymer into any of these stages depends on its thermal resistance, the temperature to which it is exposed, the period of exposure, and the percentage of plasticizer. These exceptional circumstances will determine the extent of deformation and damage to the poly (vinyl chloride) [35, 36]. The degradation behavior of flexible poly (vinyl chloride) has been shown in *Fig. 6*, which represents the dehydrochlorination test for flexible poly (vinyl chloride) not containing additional additives at 200 °C analyzed by the conventional standard and novel methods. As we can note from this figure, the dehydrochlorination results are represented by the relationship between conductivity and time for poly (vinyl chloride) measured by the conventional method (a). In contrast, the results obtained by the novel method are related to HCl concentration time and conversion parameters (b). From the two methods we can see that the poly (vinyl chloride) undergoes severe degradation when exposed to such a high temperature, and the thermal stability is greatly decreased, as explained above [37-40].

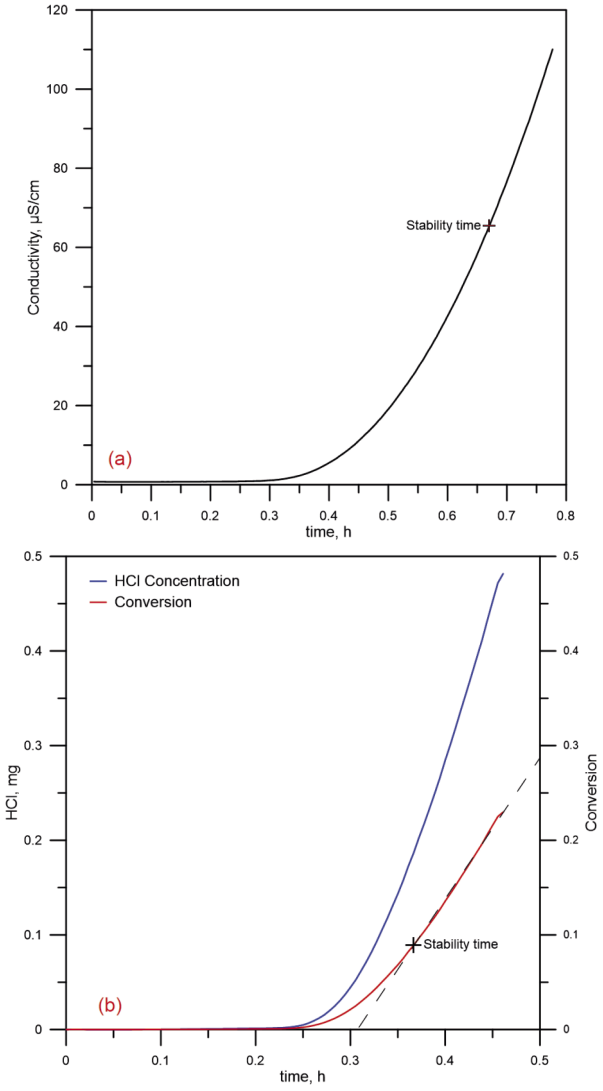

Fig. 6 Analysis of the degradation behavior of pure flexible poly(vinyl chloride) by (a) conventional and (b) novel methods during the dehydrochlorination process at 200 °C
6. ábra Tiszta, hajlékony poli (vinil-klorid) lebomlási viselkedésének elemzése a) hagyományos és b) új módszerekkel a 200 °C-on történő dehidroklórozási folyamat során

From *Fig 6.b.* we can see how quickly and sharply HCl loss occurs, where the slope of the curve is extremely steep (414×10^{-6} %s^{-1}). Poly (vinyl chloride) has this characteristic due to its limited thermal resistance at elevated temperatures. When HCl is released into the poly (vinyl chloride) structure, this heat resistance lowers more and more as the structure of poly (vinyl chloride) is significantly distorted [35]. Activation energy plays an essential role in the degradation process. The

low activation energy of poly (vinyl chloride) compared to other polymers such as polyethylene, polystyrene, or polypropylene causes it to enter the initiation stage of degradation at relatively low temperatures of about 100 °C. Under temperatures above 100 °C, unstable and reactive allylic and tertiary chlorines will produce chloride ions or chlorine radicals. The removal of chlorine from the poly (vinyl chloride) structure will also stimulate the release of hydrogen, leading to the formation of a double bond. Finally, the HCl will be created and released as a degradation product. The allylic group will be introduced when HCl is released from the poly (vinyl chloride)'s structure. This process will act as a self-stimulant or catalyzed to remove more HCl. Thus, poly (vinyl chloride) quickly enters the second degradation stage (propagation), followed by complete burning, representing the termination's third stage [41-47].

The important thing that can be deduced from *Fig. 5* is the difference between the stability time measured by the novel method and the conventional method one, where the stability time measured by the novel method is considerably shorter than that measured by the conventional method by 8.25%, at relatively low conductivity rates (less than 60 µS/cm), as listed in the *Table 2* which represents the stability time of flexible poly (vinyl chloride) containing Oxydtron as measured by the novel method and compares the results with the measurements obtained by the conventional method. Noting that the actual value of the conductivity in the case of the conventional method, based on which the stability time was calculated, is not exactly 60 µS/cm, but somewhat higher than it, which is what found when analyzing the conductivity values in the original notepad files.

Material	Stability time measured by novel method, h	Stability time measured by conventional method standard, h	time difference between the two methods, %
PVC	0.367	0.400	8.25
PVC+1wt.% of Oxydtron	0.622	0.670	07.16
PVC+3wt.% of Oxydtron	0.772	0.850	10.10
PVC+5wt.% of Oxydtron	0.783	0.860	09.83

Table 2 Stability time of flexible poly(vinyl chloride) containing Oxydtron measured by novel method and conventional method at 200 °C
2. táblázat Az Oxidtront tartalmazó hajlékony poli (vinil-klorid) stabilitási ideje új módszerrel és hagyományos módszerrel mérve 200 °C-on

The best way to increase the thermal resistance of polymers in general and poly (vinyl chloride) in particular is to use additional additives with the essential additives that make up the polymer. This new, improved behavior can be clearly seen from *Fig. 7*, representing the dehydrochlorination test for flexible poly (vinyl chloride) containing 1 wt.% of Oxydtron measured at 200 °C and analyzed by the novel and conventional methods. Looking at this figure, it will be apparent that reducing the value of the slope to 335×10^{-6} %s^{-1} and extending the time to complete degradation from (0.46 h) to (0.78 h) are indications of an increase in the thermal resistance of the flexible poly (vinyl chloride) after adding Oxydtron. Therefore, from the point of view of the analytical meaning, it can be said that the poly (vinyl chloride) has a more stable structure at elevated temperatures. The Oxydtron will act as an inhibitor for polyenes synthesis by reducing the tendency for allylic chloride groups production. This will prevent the poly (vinyl chloride) from entering the propagation stage, thereby extinguishing the fire. As observed previously in the novel method plot, the conventional method also shows the improvement in the degradation behavior of flexible poly (vinyl chloride) after adding 1 wt.% of Oxydtron.

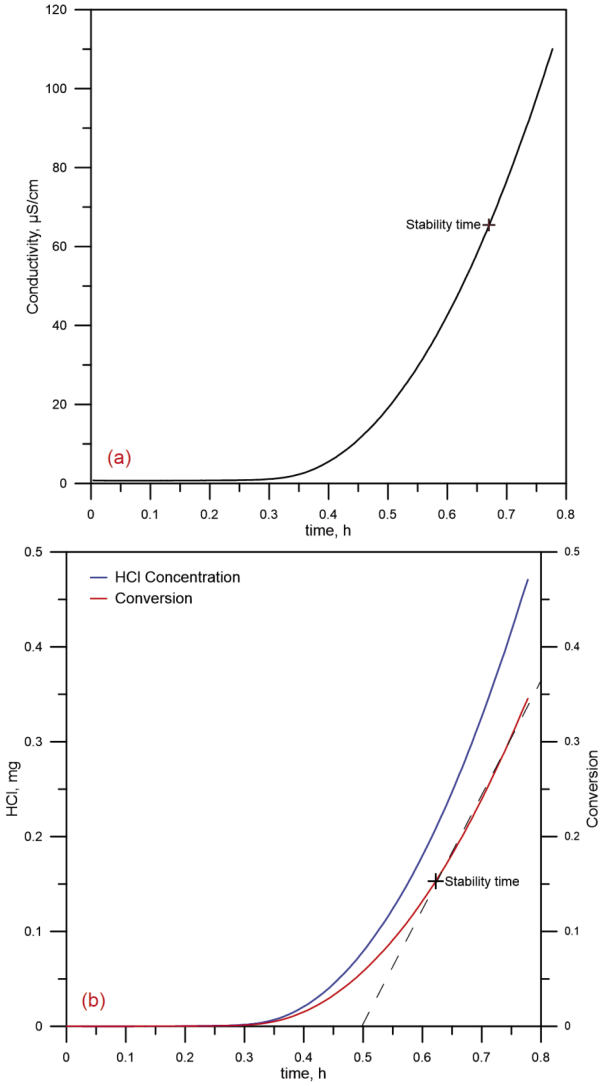

Fig. 7 Degradation behavior of flexible poly(vinyl chloride) containing 1wt.% of Oxydtron during dehydrochlorination process at 200 °C analyzed by (a) conventional and (b) novel methods
7. ábra Az 1wt.% Oxydtront tartalmazó rugalmas poli (vinil-klorid) lebomlási viselkedése a 200 °C-on végzett dehidroklórozási folyamat során, a) hagyományos és b) új módszerekkel elemezve

After the Oxydtron has been added, we notice that the stability time measured by the novel method remained shorter than that of the conventional method by 7.16%, as shown in *Table 2*. Adopting the HCl concentration criterion instead of conductivity in determining the stability time will be better and more accurate in determining the actual degradation time. As we know, the stability time in the conventional method is recorded after releasing a sufficient amount of HCl capable of generating an increase in conductivity at the range of 60 µS/cm

[37, 48, 49]. At the novel method, the short stability time is also accompanied by a low value of the conductivity, at which time value will be recorded. The sharp increase in conductivity with a long time interval because the addition of Oxydtron increased the thermal stability of poly (vinyl chloride) by creating a synergistic stabilizing effect with the original stabilizer. This synergistic stabilizing behavior is due to the composition of Oxydtron, which consists of numerous compounds such as oxides and carbonates, which function as synergistic agents with the original stabilizer, improving the thermal stability of poly (vinyl chloride).

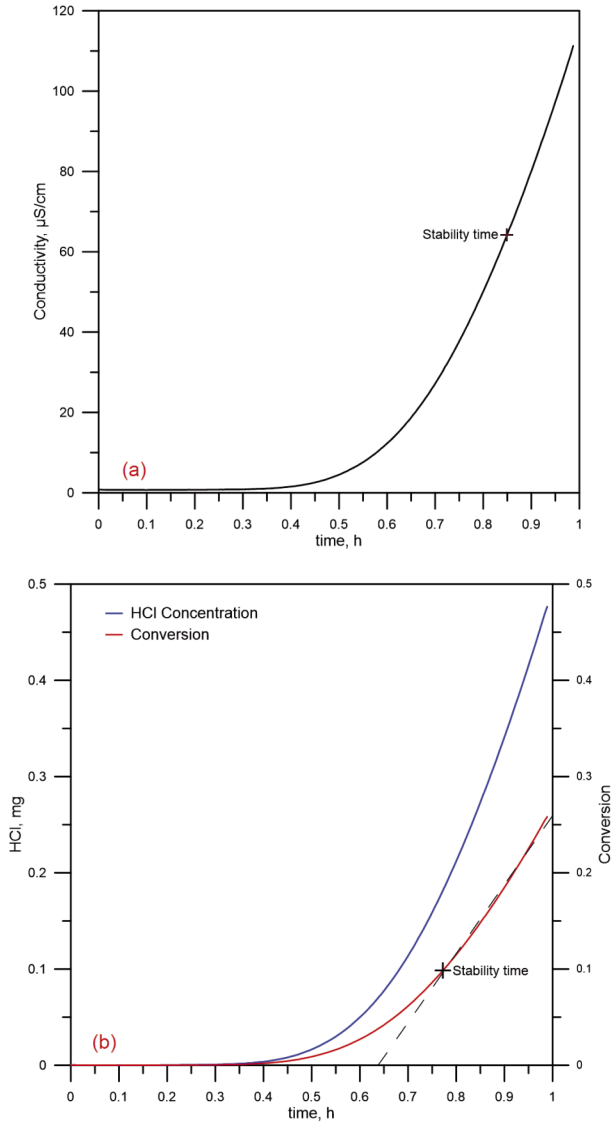

Fig. 8 Degradation behavior during dehydrochlorination process at 200 °C analyzed by (a) conventional and (b) novel methods for flexible poly(vinyl chloride) containing 3 wt.% of Oxydtron

8. ábra Lebomlási viselkedés a 200 °C-on történő dehidroklórozási folyamat során a) a 3 wt.% Oxydtront tartalmazó rugalmas poli (vinil-klorid) hagyományos és b) új módszereivel elemezve

Increasing the proportions of Oxydtron to 3 wt.% and 5 wt.% will further improve the thermal stability of flexible poly (vinyl chloride), which positively reflects its resistance to thermal degradation. The improvement in the degradation behavior of the flexible poly (vinyl chloride) after adding 3 %wt. and 5 %wt. of Oxydtron nanocement is shown in *Fig. 8* and *Fig. 9* respectively. At 3 wt.% addition, the slope of the conversion rate dropped to 199×10^{-6} $\%s^{-1}$, and at 5 wt.% addition kept going down to 165×10^{-6} $\%s^{-1}$, indicating that the degradation resistance has been enhanced, with an increase in the overall degradation time to 0.99 h and 1.02 h, respectively. On the other hand, for the conventional method, the conductivity also increases with the increased of the proportion of artificial silica added. As a result of the improvement in degradation resistance of poly (vinyl chloride) after adding Oxydtron with weight fractions of 3 wt.% and 5 wt.%, the stability time will also increase after these additions. The stability time rises from 0.772 h in the case of 3 wt.% of Oxydtron to 0.783 h in the case of adding 5 wt.% of Oxydtron. However, this rise in the stability time is still shorter than the measured by the conventional method by 10.10% and 09.83% at Oxydtron ratios of 3 wt.% and 5 wt.%, respectively, as is evident from *Table 2*.

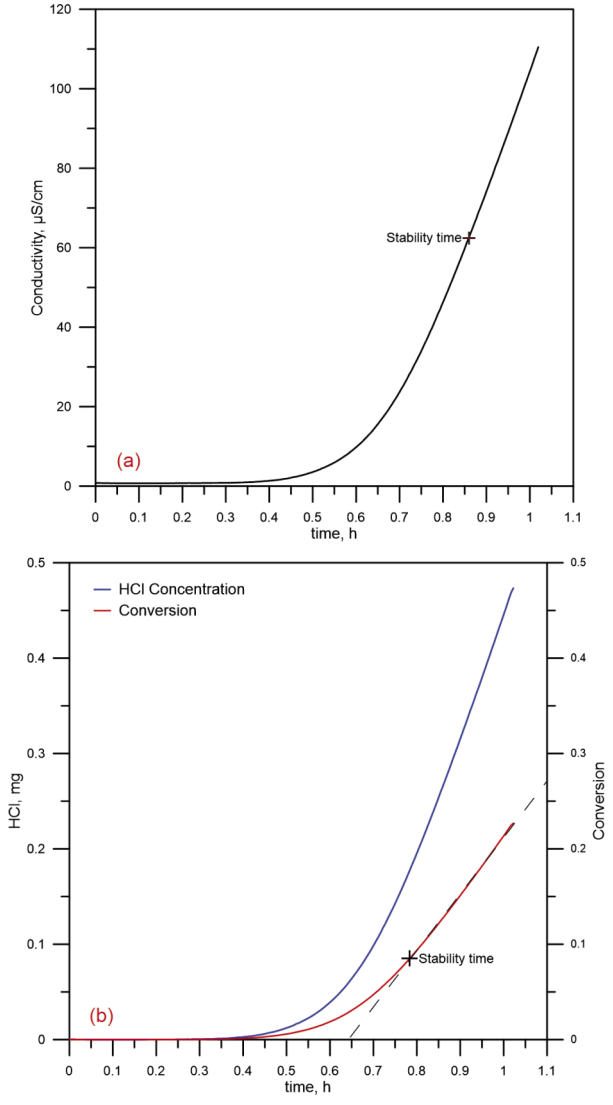

Fig. 9 Degradation behavior of flexible poly (vinyl chloride) containing 5 wt.% of Oxydtron during dehydrochlorination process at 200 °C and analyzed by (a) conventional and (b) novel methods

9. ábra Az 5 wt.% Oxydtront tartalmazó rugalmas poli (vinil-klorid) lebomlási viselkedése 200 °C-on történő dehidroklórozási eljárás során, amelyet a) hagyományos és b) új módszerekkel elemeznek

5. Conclusions

Through the results of the stability time obtained from the novel method and compared with the conventional method, it will become apparent that the entry of poly (vinyl chloride) to the initiation stage of degradation is faster than we expected. So the degradation entry to the next stage, which is propagation down to the stage termination stage, will be shorter. Therefore, more care must be taken when poly (vinyl chloride) is exposed to high temperatures while providing maximum protection through appropriate additives. In contrast to the conventional method, the novel developed method describes better the process in particular in case of PVC compounds. It shows a good agreement with the discoloration and initial color changes.

References

[1] Brinson H., Brinson L., Characteristics, applications and properties of polymers, In Brinson, H.F., Brinson, L. (eds.) Polymer engineering science and viscoelasticity: an introduction, 1st edition, Springer, Boston, MA, pp. 55-97, (2008). https://doi.org/10.1007/978-0-387-73861-1_3

[2] Sharifzadeh E., Cheraghi K., Temperature-affected mechanical properties of polymer nanocomposites from glassy-state to glass transition temperature, Mechanics of Materials, Vol. 160, pp.103990, (2021). https://doi.org/10.1016/j.mechmat.2021.103990

[3] Krevelen D.W., Nijenhuis K., Polymers properties, In Krevelen, D., Nijenhuis, K. (auths.) Properties of polymers: their correlation with chemical structure; their numerical estimation and prediction from additive group contributions, 4th edition, Elsevier B.V., pp.3-5 (2009). https://doi.org/10.1016/B978-0-08-054819-7.00001-7

[4] Rusli A., Othman MB., Marsilla K., Plastics in High Heat Resistant Applications, In: Hashmi, M.S.J. (ed.) Encyclopedia of Materials: Plastics and Polymers, Vol.4, pp.200-215, (2022). https://doi.org/10.1016/B978-0-12-820352-1.00073-0

[5] Moslem A. I., Flame Retarding-Stabilizing Behavior of Flexible Poly(vinyl chloride) Containing Novel Heavy Metal Free Modifier, PhD Dissertation, University of Miskolc, Hungary, (2021). https://doi.org/10.14750/ME.2021.039

[6] Lodhi R., Kumar P., Achuthanunni A., Rahaman M., Das P., Mechanical properties of polymer/graphene composites, In M. Rahaman, L. Nayak, I.A. Hussein, and N.Ch. Das (eds.) Polymer Nanocomposites Containing Graphene: preparation, properties, and applications, Woodhead Publishing, USA, pp.75-105, (2022). https://doi.org/10.1016/B978-0-12-821639-2.00019-7

[7] Al-Maamori M.H, Abd Alradha R., Al-Mosawi A.I., Mechanical properties for unsaturated polyester reinforcement by glass fiber using ultrasonic technique, International Journal of Multidisciplinary and Current Research (IJMCR), Vol.1, pp. 1-7, (2013). http://ijmcr.com/wp-content/uploads/2013/07/Paper11-41.pdf

[8] Moldoveanu S., Thermal decomposition of polymers, In: Moldoveanu, S.C. (ed.) Analytical pyrolysis of synthetic organic polymers, Vol.25, Elsevier B.V., pp.31-107, (2005). https://doi.org/10.1016/S0167-9244(05)80003-4

[9] Stabilisers, The European council of vinyl manufacturers (ECVM), Brussels, Belgium, (2020). https://pvc.org/about-pvc/pvc-additives/stabilisers/

[10] Wypych G., Principles of thermal degradation, In: Wypych, G (auth.) PVC degradation and stabilization, 3rd edition, ChemTec Publishing, Canada, pp.79-165, (2015). https://doi.org/10.1016/B978-1-927885-61-1.50007-4

[11] Fisch M.H., Bacaloglu R., Mechanism of poly(vinyl chloride) stabilization, Plastics, Rubber and Composites , Vol.28, Issue.3, pp.119-124, (1999). https://doi.org/10.1179/146580199101540213

[12] Marongiu A., Faravelli T., Bozzano G., Dente M., Ranzi E., Thermal degradation of poly(vinyl chloride), Journal of Analytical and Applied Pyrolysis, Vol.70, Issue.2, pp.519-553, (2003). https://doi.org/10.1016/S0165-2370(03)00024-X

[13] Hjertberg T., Sörvik E.M., Formation of anomalous structures in PVC and their influence on the thermal stability:1. endgroup structures and labile chlorine substituted by phenol, Journal of Macromolecular Science: Part A- Chemistry, Vol. 17, Issue 6, pp. 983-1004 (1982). https://doi.org/10.1080/00222338208056497

[14] Hjertberg T., Sörvik E.M., Formation of anomalous structures in PVC and their influence on the thermal stability: 2. Branch structures and tertiary chlorine, Polymer, Vol.24, Issue.6, pp.673-684, (1983). https://doi.org/10.1016/0032-3861(83)90003-4

[15] Michael Schiller, PVC Additives: Performance, Chemistry, Developments, and Sustainability, 1st Edition, Hanser Publications, 2015. ISBN: 978-1-56990-543-2

[16] Hjertberg T., Sörvik E.M., Formation of anomalous structures in PVC and their influence on the thermal stability: 3. Internal chloroallylic groups, Polymer, Vol.24, Issue.6, pp.685-692, (1983). https://doi.org/10.1016/0032-3861(83)90004-6

[17] Jurriaan C., Heuvel M., Weber A.J.M., End groups in poly(vinyl chloride) and their influence on the thermal stability, Macromolecular Chemistry and Physics, Vol.184, Issue.11, pp.2261-2273, (1983). https://doi.org/10.1002/macp.1983.021841108

[18] Michel A., PVC thermal stability assessment using tests in the presence of stabilizers, Journal of Vinyl and Additive Technology, Vol.7, Issue.2, pp.77-91, (1985). https://doi.org/10.1002/vnl.730070208

[19] Guyot A., Working party on defects in the molecular structure of polyvinylchloride and their relation to thermal stability: general conclusions, Journal of Vinyl and Additive Technology, Vol.7, Issue.2, pp.92-94, (1985). https://doi.org/10.1002/vnl.730070209

[20] Michel A., Working party on defects in the molecular structure of polyvinylchloride and their relation to thermal stability: general introduction, Journal of Vinyl and Additive Technology, Vol.7, Issue.2, pp.46-52, (1985). https://doi.org/10.1002/vnl.730070203

[21] Lu Y-h., Wang B., Xue M-y., Lu Y-w., Kinetics of thermal oxidative degradation of poly (vinyl chloride) containing Ca and Sn at low temperature, Waste Management, Vol.121, pp.52-58, (2021). https://doi.org/10.1016/j.wasman.2020.11.019

[22] Zhao D., Liu W., Yue G., Song Q., Chen J., Pan L., Determination of thermal degradation for high-performance thermoplastic composites manufactured by laser-assisted automated fibre placement, High Performance Polymers, Vol. 34, Issue. 2, pp. 149-161, (2021). https://doi.org/10.1177/09540083211044677

[23] Stromberg R.R., Straus S., Achhammer B.G., Infrared spectra of thermally degraded poly(vinyl chloride), Journal of Research of the National Bureau of Standards, Vol. 60, No. 2, pp.147-152, (1958). https://nvlpubs.nist.gov/nistpubs/jres/60/jresv60n2p147_A1b.pdf

[24] Metrohm, PVC Thermomat, Metrohm Magyarország Kft., Hungary, (2018).

[25] Yu J., Sun L., Ma Ch., Qiao Y., Yao H., Thermal degradation of PVC: a review, Waste Management, Vol.48, pp.300-314, (2016). https://doi.org/10.1016/j.wasman.2015.11.041

[26] Metrohm, Thermostability of PVC and related chlorinated polymers, Technical Report, Application Bulletin 205/2 e, (2016). https://www.metrohm.com/content/dam/metrohm/shared/application-files/AB-205.pdf

[27] Erdoğdu C.A., Atakul S., Devrim Balköse, Semra Ülkü, Development of synergistic heat stabilizers for PVC from zinc borate-zinc phosphate, Chemical Engineering Communications, Vol.196, Issue.1-2, pp. 148-160, (2008). https://doi.org/10.1080/00986440802293148

[28] Bai X-y., Wang Q-w., Sui Sh-j., Zhang Ch-sh., The effects of wood-flour on combustion and thermal degradation behaviors of PVC in wood-flour/poly(vinyl chloride) composites, Journal of Analytical and Applied Pyrolysis, Vol.91, Issue.1, pp.34-39, (2011). https://doi.org/10.1016/j.jaap.2011.02.009

[29] Vatani Z., Eisazadeh H., Fabrication and thermal degradation behavior of poly(vinyl chloride) particle coated with polythiophene and polyaniline, Synthetic Metals, Vol.162, Issues.17-18, pp.1508-1512, (2012). https://doi.org/10.1016/j.synthmet.2012.06.023

[30] Simões P.N., Coelho J., Gonçalves P., Gil M.H., Comparative non-isothermal kinetic analysis of thermal degradation of poly(vinyl chloride)

prepared by living and conventional free radical polymerization methods, European Polymer Journal, Vol.45, Issue.7, pp.1949-1959, (2009). https://doi.org/10.1016/j.eurpolymj.2009.04.021

[31] Puyou Jia, Meng Zhang, Lihong Hu, Caiying Bo, Yonghong Zhou, Thermal degradation and flame retardant mechanism of poly(vinyl chloride) flexible with a novel chlorinated phosphate based on soybean oil, Thermochimica Acta, Vol.613, August 2015, pp.113-120. https://doi.org/10.1016/j.tca.2015.05.011

[32] Al-Mosawi A.I., A novel evaluation method for dehydrochlorination of flexible poly(vinyl chloride) containing heavy metal free thermal stabilizing synergistic agent, Polymers for Advanced Technologies, Vol.32, Issue.8, pp. 3278-3286, (2021). https://doi.org/10.1002/pat.5339

[33] ISO 182-3, Plastics-determination of the tendency of compounds and products based on vinyl chloride homopolymers and copolymers to evolve hydrogen chloride and any other acidic products at elevated temperatures-part 3: conductometric method, International Organization for Standardization, (1993).

[34] Table of conductivity vs. concentration for common solutions, Invensys/ Foxboro, Foxboro, Massachusetts, USA, (1999).

[35] Starnes W., Ge X., Mechanism of autocatalysis in the thermal dehydrochlorination of poly(vinyl chloride), Macromolecules, Vol.37, Issue.2, pp.352-359, (2004). https://doi.org/10.1021/ma0352835

[36] Huang J., Li X., Zeng G., Cheng X., Tong H., Wang D., Thermal decomposition mechanisms of poly(vinyl chloride): a computational study, Waste Management, Vol.76, pp.483-496, (2018). https://doi.org/10.1016/j.wasman.2018.03.033

[37] Taubinger R.P., Allsopp M.W., Vander H.J.M., Mooij L.J.J., Measuring the heat stability of PVC by dehydrochlorination, Polymer Testing, Vol.6, Issue.5, pp.337-350, (1986). https://doi.org/10.1016/0142-9418(86)90039-5

[38] Han W, Zhang M., Li D., Dong T., Ai B., Dou J., Sun H., Design and synthesis of a new mannitol stearate ester-based aluminum alkoxide as a novel tri-functional additive for poly(vinyl chloride) and its synergistic effect with zinc stearate, Polymers, Vol.11, Issue.6, pp.1031, (2019). https://doi.org/10.3390/polym11061031

[39] Chamy P.G., The formation and thermal stability of polyvinyl chloride, PhD Dissertation, University of Glasgow, Glasgow, (1976). http://theses.gla.ac.uk/id/eprint/78729

[40] Wang Z., Xie T., Ning X., Liu Y., Wang J., Thermal degradation kinetics study of polyvinyl chloride (PVC) sheath for new and aged cables, Waste Management, Vol.99, pp.146-153, (2019). https://doi.org/10.1016/j.wasman.2019.08.042

[41] Wang Q., Wu W., Tang Y., Bian J., Zhu S., Thermal degradation kinetics of flexible poly (vinyl chloride) with six different plasticizers, Journal of Macromolecular Science, Part B, Vol.56, Issue.6, pp.420-434, (2017). https://doi.org/10.1080/00222348.2017.1316659

[42] Marcilla A., Beltrán M., Dynamic TG studies on the thermal decomposition of PVC plastisols, Journal of Vinyl and Additive Technology, Vol.1, Issue.1, pp.15-20, (1995). https://doi.org/10.1002/vnl.730010106.n

[43] Sánchez-Jiménez P.E., Perejón A., Criado J.M., Diánez M.J., Pérez-Maqueda L.A., Kinetic model for thermal dehydrochlorination of poly(vinyl chloride), Polymer, Vol.51, Issue.17, pp.3998-4007, (2010). https://doi.org/10.1016/j.polymer.2010.06.020

[44] Zong H, Upcycling approach of polyvinycl chloride waste management, MSc Thesis, Johns Hopkins University, Maryland, (2020). http://jhir.library.jhu.edu/handle/1774.2/62755

[45] Gui B., Qiao Y., Wan D., Liu Sh., Han Z., Yao H., Xu M., Nascent tar formation during polyvinylchloride (PVC) pyrolysis, Proceedings of the Combustion Institute, Vol,34, Issue.2, pp.2321-2329, (2013). https://doi.org/10.1016/j.proci.2012.08.013

[46] Kanade Y., What causes PVC to degrade during processing and service?, Linkedin Article, (2019). https://www.linkedin.com/pulse/what-causes-pvc-degrade-during-processing-service-yashodhan-kanade/

[47] Zheng X-G., Tang L-H., Zhang N., Gao Q-H., Zhang Ch-F., Zhu Z-B., Dehydrochlorination of PVC materials at high temperature, Energy & Fuels, Vol.17, Issue.4, pp.896-900, (2003). https://doi.org/10.1021/ef020131g

[48] Onozuka M., Asahina M., On the dehydrochlorination and the stabilization of polyvinyl chloride, Journal of Macromolecular Science, Part C, Vol.3, Issue.2, pp.235-280, (2008). https://doi.org/10.1080/15583726908545924

[49] Hjertberg T., Sörvik E.M., Thermal degradation of PVC, In: Owen, E.D. (eds.) Degradation and stabilisation of PVC, Springer, Dordrecht, pp.21-79, (1984). https://doi.org/10.1007/978-94-009-5618-6_2

Ref.:
Al-Mosawi, Ali I.: *A novel conceptional approach for calculating the stability time related to converting the anticipated degradation from the curve of conductivity for flexible poly (vinyl chloride)*
Építőanyag – Journal of Silicate Based and Composite Materials, Vol. 74, No. 5 (2022), 188–195. p.
https://doi.org/10.14382/epitoanyag-jsbcm.2022.28

Material characterization and statistical evaluation of properties of hot mix asphalt concrete (HMAC) used in wearing course of road pavement; Southern Nigeria

Roland Kufre ETIM ▪ Department of Civil Engineering, Akwa Ibom State University, Ikot Akpaden, Nigeria ▪ rolandetm@aksu.edu.ng

Idorenyin Ndarake USANGA ▪ Department of Civil Engineering, Akwa Ibom State University, Ikot Akpaden, Nigeria

David Ufot EKPO ▪ Department of Civil Engineering, Akwa Ibom State University, Ikot Akpaden, Nigeria

Imoh Christopher ATTAH ▪ Department of Civil Engineering, Akwa Ibom State University, Ikot Akpaden, Nigeria

Érkezett: 2022. 04. 15. ▪ Received: 15. 04. 2022. ▪ https://doi.org/10.14382/epitoanyag-jsbcm.2022.29

Abstract

An investigative study was carried out on the assessment of engineering properties of asphaltic concrete used for pavement construction in Akwa Ibom State, South-south, Nigeria. A total of 225 compacted samples of wearing course asphaltic concrete were obtained from three different asphalt plants in Eket, Oron and Uyo designated as D, E, and G, respectively. The test results based on the outcome of the Marshal Stability for the three different asphalt plants ranged from 7.51-13.36 kN, 9.36-11.34 kN and 8.26-9.46 kN with corresponding flow values which ranged from 3.33-3.94 mm, 2.40-3.48 mm and 2.73-3.19 mm for asphalt plants D, E, and G, respectively. The test outcomes revealed that a good number of the test samples were within the benchmark of the Nigeria General Specifications for roads. Three predictive models were built for the estimation of Marshall Stability for the three different sites. Based on the outcome of t-test (paired two sample for means) and analysis of variance (ANOVA) single factor, there was no significant difference between the experimented values and model formulated results. Also, the formulated model yielded an excellent coefficient of determination (R^2) of 0.9513, 0.9777 and 0.9777 for the three sites. This excellent coefficient of determination reflect the models could be used in prediction of stability strength. The correlation statistic and their respective p-values of each of the independent variables, BIT, VIM and VFB has shown to contribute more than the other variables in building the established models and thus expedient in forecasting the performance of asphalt pavements.

Keywords: asphaltic concrete, stability flow, regression models, correlation statistics

Kulcsszavak: aszfaltbeton, stabilitási áramlás, regressziós modellek, korrelációs statisztikák

Roland K. ETIM
is a lecturer in the Department of Civil Engineering, Akwa Ibom State University, Ikot Akpaden, Nigeria. His research interest is in the field of geotechnical and geo-environmental engineering as well as sustainable cleaner materials for civil engineering infrastructures. He is a member of several professional societies.

Idorenyin N. USANGA
is a lecturer in the Department of Civil Engineering, Akwa Ibom State University, Ikot Akpaden. He is a registered Engineer with COREN and a corporate member of the Nigeria Society of Engineers. He has a Master's degree in Highway and Transportation Engineering with several well-known scholarly articles. He is currently working as a consultant in Akwa Ibom Roads and Other Infrastructure Maintenance Agency (AKROIMA).

David U. EKPO
is a lecturer in Akwa Ibom State University. He is a registered Engineer with COREN and a corporate member of the Nigeria Society of Engineers. He has a Master's degree in Civil Engineering with specialization in Geotechnical and Geo-environmental Engineering. He has published scholarly articles in Geotechnical and Geo-environmental Engineering.

Imoh C. ATTAH
is a lecturer in the Department of Civil Engineering, Akwa Ibom State University, Ikot Akpaden, Nigeria. His research focus is in: optimization of civil engineering materials, soil re-engineering, sustainable infrastructures and construction engineering. He is a member of several professional societies.

1. Introduction

Road infrastructure remains very fundamental in the modern day society because of the role it plays in urbanization. It makes sizeable investment concerning economic, social and cultural development of any country [1]. It also offers a platform that encourage the interchanging of goods, movement of human and as well include places that are difficult to access within a particular time [2]. However, distresses on our roads have resulted to various type of failure on our pavement. Pavement distresses ranging from rutting, shoving, raveling, transverse cracking, longitudinal cracking, potholes etc. are predominant on Nigerian roads. It is so disheartening that these roads are frequently being reconstructed overtime without making any frantic effort to examine the possible causes of their perpetual failures. Numerous factors which include but not limited to geotechnical, design and specifications, improper selection of materials, methods of construction, geomorphological etc. might influence the overall performance of highway pavement structures [3-7]. Also, studies have also shown that failure of wearing courses of road pavement are caused by the poor stability of sub-grade and sub-based materials. The stability is linked to the very low California bearing ratio (CBR) values which is a critical parameter to the design and stability of pavement structures. Therefore, researches on stabilization of poor soil materials to meet the benchmark for sub-grade and sub-base have being reported in several studies [8-17, 39-46]. Several studies have also reported poor quality of asphalt concrete as another main cause pavement failure [18-20].

However, wearing course of flexible pavement are built or design to withstand certain ups and downs in terms of physical climatic and environmental conditions during the pavement infrastructure life span. It is well known that some of our flexible pavements in this part of the country tend to experience some deterioration, cracks etc. due low quality of construction materials, poor supervision and climatic conditions. Also,

this layer (wearing course), being an essential part of the road structure is saddled with the responsibilities of enhancing even and stable distribution of axle wheel loads to all other layers below (i.e. binder coarse, base, subbase and subgrade) while ensuring that durability is not compromised. The hot mix asphalt (HMA) concrete is basically made of a combination of aggregates and asphalt cement (bitumen). The aggregate which consists of coarse and fine particles constitutes about 90% of the total volume of HMA. They usually act as the structural skeleton of the pavement. Ahmedzade and Sengoz [21] reported that the performance of asphalt pavement is largely dependent on the properties of the aggregates. The asphalt cement on the other hand, plays the role of bonding the mixtures together. The superior service performance in ensuring a stable, durable and water resistance pavement structures renders asphaltic concrete as one of the most utilized pavement materials [22].

Few studies that have examined the engineering properties of asphalt concrete with respect to its stability, flow, penetration, and viscosity in Nigeria has been in the Southwest. Recent studies by Akinleye and Tijani [23], concluded that; none of the samples met all the requirements specified by the Nigerian General Specifications (NGS) [24]. This might possibly be due to the use of poorly graded mineral aggregates coupled with poor and inadequate bitumen content that led to a mix with poor stability and excess voids. Osunkunle et al. [25] assessed the engineering properties of asphaltic concrete produced in the Southwestern region of Nigeria. The results of the test carried out on the bitumen and asphalt concrete were in conformity with the specifications of Federal Ministry of Works and Housing. However, the results of the water absorption fell below the minimum requirements. The authors therefore concluded that the water absorption might have impaired the strength of the asphalt concrete thereby leading to failure of the pavement structure before its design age in that region. The durability of flexible pavements was studied by Obeta and Njoku [26] and they concluded that the use of poor quality materials, inadequate thickness of pavement surface, improper mix design and lack of routine maintenance as the key factors responsible for low durability. The study by Alkawaaz and Qasim [27] revealed that low durability potential of the wearing course layer is one of the major reasons for distresses in asphalt pavement which reduced serviceability limit of highways.

Model generation from established data is one of the accurate process to corroborate as well as explain the usefulness of some highway laboratory results. Having said this, a mechanistic empirical approach was used to develop a model aimed at predicting the rutting performance of pavement structures [28]. Furthermore, Bala et al. [29] applied multivariable regression models for prediction of composite nano silica / polymer asphalt mixture of optimum binder content (OBC). Also, prediction equations of properties of asphalts material were achieved from large experimental data using statistical regression approach [30-33]. Baldo et al [34] numerically predicted the mechanical response of asphalt concretes for road pavement using artificial neural networks (ANN).

Asphaltic concrete pavement which has been otherwise used as flexible pavements is a complex system of multiple layers of various materials that combines irregular traffic loading and fluctuating environmental conditions which includes temperature, moisture and oxidation rates [35]. This makes it more challenging for highway engineers to build realistic models for predicting durability performance of asphaltic pavements. Since the performance of asphalt concrete pavement is closely related to the properties of the aggregates, it therefore becomes imperative to properly evaluate the performance and behaviour of asphalt concrete. The paucity of literatures on the assessment of the quality of asphalt pavement in the region under consideration needs an authoritative data to be established. Hence, the necessity of the studies. This study aims to critically examine the engineering properties of asphaltic concrete for basically Marshal Stability and flow and in turn compares it with the minimum benchmark of the NGS for wearing course. This is with a view of accessing its suitability for construction in Akwa Ibom State. Furthermore, since stability is a key parameter in asphaltic concrete mix design, a multiple variable regression model relating stability and flow will also be generated. The need to develop relevant models from laboratory results and data are central in engineering investigation and analysis. This is with the aim of saving time and or cost in certain aspect of evaluations. In the light of this, the model generated is expected to provide the pathway within the various processes of asphalt mix design, structural design, construction and rehabilitation of pavement structures. Therefore, if the stability and flow are known, the rigorous stress of the laboratory can be avoided thereby providing precise information as regards the performance of the asphalt pavement.

2. Materials and methods

2.1 Materials

2.1.1 Bitumen

Based on information available in the course of this study, the bitumen was obtained from Eleme petrochemical Port-Harcourt, Rivers State, Nigeria. The different test protocol used and the properties of bitumen that has been study is presented in *Table 1*.

2.1.2 Aggregates

Based on available information, the aggregate used in this study was collected at location outcrops of igneous rocks in Akampa quarry site (latitude; 5°0'30.64"N, longitude 7°53'22.84"E), Cross river state, Nigeria. The aggregates consist of fine aggregate having maximum sizes of 5 mm and coarse aggregate having maximum sizes of 5 mm and above. The various test properties and test protocols adopted for the aggregate is presented in *Table 2*.

Test	Standard
Penetration test	AASHTO D T-49
Specific gravity	BS 1377
Softening point	ASTM D36-95 or AASHTO D T-53
Flash point	AASHTO D T-48

Table 1 Characteristic properties of bitumen and standard of testing used
1. táblázat A bitumen jellemző tulajdonságai és az alkalmazott vizsgálati szabványok

Properties	Test code method
Gs (Coarse aggregate)	ASTM C127
Gs (fine aggregate)	ASTM C128
Sieve analysis	BS 1377
Los Angeles Abrasion test, %	ASTM C131/ EN 1097-8
Aggregate crushing value ACV, %	BS 812-114
Flakiness index %	EN 933-3

Table 2 Properties of aggregate and bitumen
2. táblázat Az aggregátum és a bitumen tulajdonságai

2.1.3 Marshall testing

The Marshall test was continuously carried out in a span of twelve months to cover all year-round season. The Marshall test involves using standard cylindrical molds (102 mm in diameter and 64 mm in height). Hot samples were intermittently collected from various batches of asphalt concrete samples from the asphalt plants. The hot mixture is placed in the mold and was compacted at regulated temperature of 130 °C by application of 75 blows of a Marshall hammer on each side of the specimen. It is generally expected that the average of three samples should be tested for each set. However, more than three samples test was considered because of the bulk of production which needed to be tested to ensure uniformity and consistency in batching and mixing that were maintained throughout the production process from the respective asphalt plants. Therefore, the report was based on the average of minimum of five samples whose values were very close. Tests results (Marshall stability and flow) was compared for quality based on pavement specifications of NGS [24] for wearing course. Marshall Stability and flow were determined according to ASTM D2172, ASTM C136 and ASTM D6927-05.

2.1.4 Formulation of regression model

The formulation of regression models follows the guiding principles in [36]. The Marshall stability is a very important parameter in asphaltic concrete mix design. The acceptable range in this study is based on the specification of NGS [24]. Generally, the Marshall properties depend on the volumetric analysis by weight of dense asphalt concrete obtained from Marshall Tests. Stability of dense asphaltic concrete (AC) is typically a factor for accepting optimal and adequate design of wearing course asphaltic concrete. Stability is thus selected in this study and modelled for various asphalt plant designated as D, E and G located in Eket, Oron and Uyo, respectively. Laboratory results was obtained from several batches of asphalts concrete (wearing course) collected from the three asphalts plant. Based on available information, the asphalts concrete collected from these plants were produced following adequate /optimum asphalt mix design that meets Marshall stability requirement according to NGS [24] specification for wearing course. The laboratory was maintained at room temperature during testing. The outcomes of the tests were used to assess the uniformity and consistency in the several batches of asphalt concrete paving mix produced for each unit and compared with the specifications provided by the Federal Ministry of Works, Nigeria. Consequently, the Marshall stability for each of the asphalt production unit were modelled using the concept of multiple variable regression with each variable having fifteen data points. Each of the fifteen data point was an average of five close values obtained during testing as stated earlier in this report.

2.1.5 Regression model for Marshall Stability

Independent variable (Y) identified and referred here as Marshall stability (S) was achieved based on identified independent variables x_1, x_2, x_3 and x_4 referred as bitumen content (BIT), void in the mix (VIM), void in total mix dry aggregates (VMA) and void filled with bitumen (VFB), respectively. x_1, x_2, x_3 and x_4 from i to nth number of various specimens of the selected asphalt production site was obtained from volumetric analysis (by weight) of specimen which was compacted to dense asphalt concrete (wearing course). The mode of compaction was is in accordance with ASTM D6927-15 with all other necessary laboratory conditions constant. Based on the multivariable factors considered in this study, the general formula for multilinear regression is presented as:

$$Y = a + b_1x_{1(i)} + b_2x_{2(i)} + b_3x_{3(i)} + b_4x_{4(i)} + \varepsilon; \quad (1)$$

Where: x_1, x_2, x_3 and x_4 is bitumen content (BIT), void in the mix (VIM), void in total mix dry aggregates (VMA) and void filled with bitumen (VFB), respectively; a, b_1, b_2, b_3, and b_4 are constants called regression constants. i = 1,2,3,...n data points for various asphalt production plant denoted as D, E and G. The laboratory study was done under steady condition with significant precision devoid of erratic or random error. Based on this, ε = zero random error due to the high level of accuracy with which the laboratory investigation was achieved. *Eq. (1)* is the linear form for the selected variables whose requirement are central to having good wearing course for sustainable pavement structure. The relationship of the SMRE for the different variables in the Marshall test is required to attain the stability that meets the wearing course specifications as required in design criterions for wearing course of HMAC. For the set of populated data points or results and introducing or as well as minimizing the sum of least square, we obtained from *Eq. (1)*;

$$\begin{aligned}
\sum y &= an + b_1\sum x_1 + b_2\sum x_2 + b_3\sum x_3 + b_4\sum x_4 \\
\sum yx_1 &= a\sum x_1 + b_1\sum x_1^2 + b_2\sum x_1x_2 + b_3\sum x_1x_3 + b_4\sum x_1x_4 \\
\sum yx_2 &= a\sum x_2 + b_1\sum x_1x_2 + b_2\sum x_2^2 + b_3\sum x_2x_3 + b_4\sum x_2x_4 \\
\sum yx_3 &= a\sum x_3 + b_1\sum x_1x_3 + b_2\sum x_2x_3 + b_3\sum x_3^2 + b_4\sum x_3x_4 \\
\sum yx_4 &= a\sum x_4 + b_1\sum x_1x_4 + b_2\sum x_2x_4 + b_3\sum x_3x_4 + b_3\sum x_4^2
\end{aligned} \quad (2)$$

However, *Eq. (2)* may well also be transformed to the format of a matrix which is now basically written in the form;

$$AX = B \quad (3)$$

where;

A = square matrix (5×5) that represent independent variables
B = column matrix that represent dependent variables
X = column matrix that represent linear regression constants so that,

$$\begin{bmatrix} \sum y \\ \sum yx_1 \\ \sum yx_2 \\ \sum yx_3 \\ \sum yx_4 \end{bmatrix} = \begin{bmatrix} n & \sum x_1 & \sum x_2 & \sum x_3 & \sum x_4 \\ \sum x_1 & \sum x_1^2 & \sum x_1x_2 & \sum x_1x_3 & \sum x_1x_4 \\ \sum x_2 & \sum x_1x_2 & \sum x_2^2 & \sum x_2x_3 & \sum x_2x_4 \\ \sum x_3 & \sum x_1x_3 & \sum x_2x_3 & \sum x_3^2 & \sum x_3x_4 \\ \sum x_4 & \sum x_1x_4 & \sum x_2x_4 & \sum x_3x_4 & \sum x_4^2 \end{bmatrix} \begin{bmatrix} a \\ b_1 \\ b_2 \\ b_3 \\ b_4 \end{bmatrix} \quad (4)$$

Using Gauss reduction method [48] or (MATLAB), *Eq. (4)* can be solved and a, b_1, b_2, b_3, and b_4 are established. Thus the MLR represented in *Eq. (1)* which expresses the Marshall Stability model could be expressed as;

$$S_i = a + b_1(BIT)_{(i)} + b_2(VIM)_{(i)} + b_3(VMA)_{(i)} + b_4(VFB)_{(i)}; i = 1, 2, 3, \ldots \ldots n \quad (5)$$

Additional statistical tool was deployed to check the adequacy of the models. The experimented and predicted responses from linear model were paired and subjected to t-test (paired two sample for means) and analysis of variance (ANOVA) single factor. The study is limited to laboratory-based performance of wearing course hot mix asphalt concrete with specified limit based on NGS [24] requirement.

3. Results and discussion

3.1 Characterization of materials used

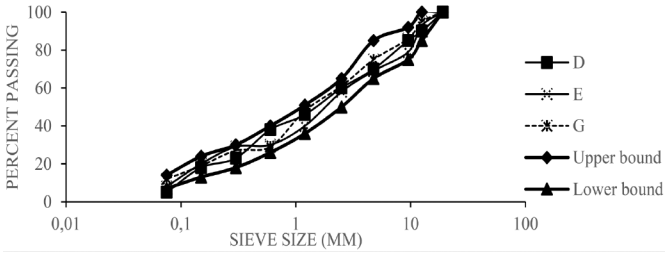

Fig. 1 Typical gradation of aggregates from binder course from site D, E and G
1. ábra A D, E és G helyszínről származó kötőanyagból származó aggregátumok tipikus osztályozása

Test	Site D	Site E	Site G	Specified limit by NGS [24]
Penetration test	64	67	65	60-70 at 25°C
Specific gravity	1.02	1.01	1.01	1.01-1.05 at 25°C
Softening point	49°C	53° C	51° C	48-50°C
Flash point	255	258	256	250 °C

Table 3 Characteristic properties of bitumen
3. táblázat A bitumen jellemző tulajdonságai

Aggregate properties	Asphalt concrete sites D	E	G	Specified limits NGS [24]
Gs (Coarse aggregate)	2.681	2.681	2.681	-
Gs (fine aggregate)	2.678	2.678	2.678	-
Average % passing 75um sieve	87	90	88	≥ 75%
Los Angeles Abrasion test, %	17	17.4	23	≤ 25%
Aggregate crushing value ACV, %	22	23	21.4	≤ 30%
Flakiness index %	18	20	20.5	≤ 35%

Table 4 Properties of aggregate and bitumen
4. táblázat Az adalékanyag és a bitumen tulajdonságai

The typical particle size gradation of aggregates from the three site presented in *Fig. 1.* It is observed that the results of sample D, E and G fell within the upper and lower boundary of the gradation envelope for wearing course asphaltic concrete. Typical properties of the bitumen and aggregate used in this study is shown in *Table 3* and *4.*

3.2 Asphalt concrete properties for wearing course

The wearing course properties of asphalt concrete mix for the three asphalt plants site denoted as D, E and G are presented in *Table 5-7*. The results of each samples revealed the following engineering properties of asphalt; marshal stability, flow, bitumen content, voids in total mixture and voids filled with bitumen. Based on the results, the volumetric properties, Marshall Stability and flow meet the pavement requirement for wearing course NGS (1997) (see *Table 8*). It is likely that the asphalt concrete from the three asphalt plants could withstand traffic load without getting cracked or easily failed. This is because the results suggest that if failure would occur on the pavement structure, it would not necessarily be linked to the quality of asphalt mix. Although the quality of hot mix asphaltic concrete may in some cased be compromised due to poor material handling/ preparation, efficiency of the asphalt plant, etc., therefore is also relevant to note that probable failure in service could be due to poor ground preparation (sub grade and subbase), excessive wheel load beyond that which the pavement was designed, drainage condition.

Sample description	BIT (%)	VIM (%)	VMA (%)	VFB (%)	S (kN)	F mm
D1	6.2	3.49	14.82	76.47	8.85	3.33
D2	6.13	3.3	15.24	78.33	8.05	3.78
D3	5.3	3.62	15.88	77.18	7.51	3.94
D4	6.4	2.78	15.31	81.82	9.66	3.80
D5	6.6	3.23	15.16	78.67	10.46	3.76
D6	5.75	3.49	14.89	76.57	7.78	3.70
D7	7.1	2.71	14.93	81.82	12.07	3.71
D8	6.8	2.61	14.36	81.81	11.27	3.56
D9	7.3	3.13	14.48	78.35	12.88	3.59
D10	6.5	2.68	14.59	81.64	10.06	3.62
D11	6.1	3.3	14.82	77.7	8.45	3.68
D12	5.7	3.08	15.01	79.51	7.65	3.72
D13	7.35	2.89	15.16	80.91	13.36	3.76
D14	6.57	3.11	15.12	79.42	10.25	3.75
D15	6.43	3.73	15.24	75.54	9.5	3.78

Table 5 Properties of compacted dense asphalt concrete specimens from site D
5. táblázat A D helyszínről származó tömörített sűrű aszfaltbeton próbatestek tulajdonságai

Sample description	BIT (%)	VIM (%)	VMA (%)	VFB (%)	S (kN)	F mm
E1	6.8	2.27	10.4	78.18	9.95	3.41
E2	7.6	1.98	10.4	80.97	10.87	2.50
E3	6.5	2.84	14.17	79.96	9.36	3.48
E4	7.3	2.26	15.12	85.06	10.55	2.84
E5	7.8	2.05	14.06	85.38	11.34	2.40
E6	6.7	2.87	15.2	81.14	9.62	3.38
E7	7.5	2.7	14.78	81.7	10.69	2.60
E8	7.3	1.81	14.48	87.51	10.4	2.80
E9	7.9	3.44	14.63	76.48	11.22	2.30
E10	6.8	3	14.74	79.63	9.81	3.39
E11	6.9	2	15.47	87.09	9.82	3.21
E12	7.1	2.35	15.58	84.9	10.18	2.97
E13	6.86	2.83	15.58	81.81	9.74	3.30
E14	7.43	2.86	15.58	81.67	10.72	2.70
E15	6.92	2.65	15.58	82.96	9.75	3.10

Table 6 Properties of compacted dense asphalt concrete specimens from site E
6. táblázat Az E helyszínről származó tömörített sűrű aszfaltbeton próbatestek tulajdonságai

Sample description	BIT (%)	VIM (%)	VMA (%)	VFB (%)	S (kN)	F mm
G1	5.86	4.16	16.07	74.14	9.39	3.15
G2	5.17	5.79	16.41	64.73	8.41	2.78
G3	5.61	4.61	16.78	72.52	9.04	3.01
G4	5.79	4.42	16.33	72.93	9.24	3.11
G5	5.53	4.97	16.67	70.18	9.11	2.97
G6	5.08	5.72	16.26	64.79	8.26	2.73
G7	5.92	4.07	16.82	75.82	9.44	3.18
G8	5.26	5.3	16.22	67.35	8.53	2.82
G9	5.88	4.33	16.74	74.16	9.37	3.16
G10	5.47	4.62	16.07	71.23	8.76	2.94
G11	5.76	4.55	17.56	74.11	9.25	3.09
G12	5.85	4.65	16.82	72.34	9.34	3.14
G13	5.94	4.76	14.24	66.61	9.46	3.19
G14	5.58	5.01	16.78	70.11	8.89	3.00
G15	5.18	5.38	14.43	62.75	8.41	2.78

BIT=Bitumen content in total weight of mix; VIM=Void in the mix; VMA=Void in total mix dry aggregate; VFB=Void filled with bitumen, S = Marshall stability, F = Marshall flow

Table 7 Properties of compacted dense asphalt concrete of specimens from site G
7. táblázat A G helyszínről származó minták tömörített sűrű aszfaltbetonjának tulajdonságai

Properties	Standards as per NGS (1997) [24]
Bitumen content, BIT (%)	4.5 - 6.5
Stability, S (kN)	≥3.5 KN
Flow, F (mm)	2 - 4
Voids in total mix, VIM (%)	3 -5
Voids filled with bitumen VFB (%)	75 -82

Table 8 Standard of asphalt concrete of wearing course
8. táblázat Az aszfaltbeton kopórétegének szabványa

3.3 Developing the regression models

The results of the Marshall test of the compacted hot mix asphaltic wearing course concrete presented in *Table 6-8*, was used in formulation of the multiple regression model equations that show a relationship between five of the variables (S, BIT, VIM, VMA and VFB). From these equations, stability (S) designated Y is the dependent variable and the independent variables are bitumen content (BIT) designated x_1; void in the mix (VIM) designated (x_2); void in total mix dry aggregates (VMA) designated x_3 and void filled with bitumen (VFB) designated x_4. Applying the least square for each of the site we thus have that for asphalt plant D

$$\begin{bmatrix} \sum y \\ \sum yx_1 \\ \sum yx_2 \\ \sum yx_3 \\ \sum yx_4 \end{bmatrix} = \begin{bmatrix} n & \sum x_1 & \sum x_2 & \sum x_3 & \sum x_4 \\ \sum x_1 & \sum x_1^2 & \sum x_1x_2 & \sum x_1x_3 & \sum x_1x_4 \\ \sum x_2 & \sum x_1x_2 & \sum x_2^2 & \sum x_2x_3 & \sum x_2x_4 \\ \sum x_3 & \sum x_1x_3 & \sum x_2x_3 & \sum x_3^2 & \sum x_3x_4 \\ \sum x_4 & \sum x_1x_4 & \sum x_2x_4 & \sum x_3x_4 & \sum x_4^2 \end{bmatrix} \begin{bmatrix} a \\ b_1 \\ b_2 \\ b_3 \\ b_4 \end{bmatrix} \quad (6)$$

Therefore

$$\begin{bmatrix} 147.8 \\ 963.14 \\ 459.2 \\ 2213.08 \\ 11713.4 \end{bmatrix} = \begin{bmatrix} 15 & 96.23 & 47.15 & 225.01 & 1185.74 \\ 96.23 & 622.11 & 300.83 & 1442.03 & 7615.7 \\ 47.15 & 300.83 & 149.97 & 708.18 & 3716.73 \\ 225.01 & 1442.03 & 708.18 & 3377.28 & 17783.7 \\ 1185.74 & 7615.7 & 3716.73 & 17783.7 & 93797 \end{bmatrix} \begin{bmatrix} a \\ b_1 \\ b_2 \\ b_3 \\ b_4 \end{bmatrix} \quad (7)$$

Solving a, b_1, b_2, b_3 and b_4 using Gaussian elimination method we have; a = -224.537; b_1 = 3.299; b_2 = 17.048; b_3 = -3.059; b_4 = 2.600. Thus;

$$Y_D = -224.537 + 3.2992X_1 + 17.0482X_2 - 3.059X_3 + 2.600X_4 \quad (8)$$

Also for asphalt plant E, *Table 5* refers

$$\begin{bmatrix} 154.02 \\ 1106.45 \\ 388.73 \\ 2212.87 \\ 12676.1 \end{bmatrix} = \begin{bmatrix} 15 & 107.41 & 37.91 & 215.77 & 1234.44 \\ 107.41 & 771.63 & 271.19 & 1543.92 & 8840.34 \\ 37.91 & 271.19 & 98.82 & 549.21 & 3104.61 \\ 215.77 & 1543.92 & 549.21 & 3144.14 & 17783.7 \\ 1234.44 & 8840.34 & 3104.61 & 17785 & 101731 \end{bmatrix} \begin{bmatrix} a \\ b_1 \\ b_2 \\ b_3 \\ b_4 \end{bmatrix} \quad (9)$$

Solving a, b_1, b_2, b_3 and b_4 using Gaussian elimination method we have; a = 4.717; b_1 = 1.422; b_2 = -0.3755; b_3 = 0.0469; b_4 = -0.0529

$$Y_E = 4.717 + 1.422X_1 - 0.3755X_2 + 0.0469X_3 - 0.0529X_4 \quad (10)$$

For asphalt plant G, *Table 6* refers;

$$\begin{bmatrix} 134.9 \\ 756.11 \\ 647.80 \\ 2197.19 \\ 9495.91 \end{bmatrix} = \begin{bmatrix} 15 & 83.88 & 72.34 & 244.2 & 1053.77 \\ 83.88 & 470.31 & 402.52 & 1366.22 & 5906.23 \\ 72.34 & 402.52 & 352.81 & 1176 & 5054.5 \\ 244.2 & 1366.2 & 1176 & 3986.56 & 17187.3 \\ 1053.77 & 5906.23 & 5054.5 & 17187.3 & 74261 \end{bmatrix} \begin{bmatrix} a \\ b_1 \\ b_2 \\ b_3 \\ b_4 \end{bmatrix} \quad (11)$$

Solving a, b_1, b_2, b_3 and b_4 using Gaussian elimination method we have; a = 1.158; b_1 = 1.4101; b_2 = -0.0128; b_3 = 0.0225; b_4 = -0.0051

$$\text{Thus, } Y_G = 1.1579 + 1.4101X_1 - 0.0128X_2 + 0.0225X_3 - 0.0051X_4 \quad (12)$$

3.4 Hypothesis using t- statistics and analysis of variance of paired outcome

The variables in experimented and predicted results (*Tables 9-10*) are paired and then subjected to t-test (paired two sample for means) and ANOVA (single factor). Two conditions hypothesis, the null and the alternative hypothesis is fixed. (1) The null hypothesis state that there is no significant difference between the experimental results and predicted

outcome of stability and (2) the alternative hypothesis state that there is a significant difference between the experimental test and predicted outcome of stability results. For a two-tail test (inequality), if t Stat < -t Critical two-tail or t Stat > t Critical two-tail, we reject the null hypothesis. Based on the outcome of experimental and predicted results of site D (*Table 9*) and *Table 12*, t Stat = 0.013595 and t Critical two-tail = 2.144787, so t Critical > t Stat. therefore we accept the null hypothesis. However, from the anova results on the experimental and predicted results of site D (*Table 13*), if F > F crit, we reject the null hypothesis. Accordingly, the result has shown that F = 4.61E-06 and F crit = 4.1959 thus F crit > F cal. It is then decided hereafter that we do not reject the null hypothesis. Therefore, the difference between the laboratory observed results and the model outcome was not significant. The model can be said to be adequate for use in predicting the possible stability which must be based on an optimum hot mix design. Similarly, the results of site E and G (*Table 10* and *11*) and verified with t-stat (*Table 13* for E and G) and ANOVA (*Table 14* and *15*) keep on with the same trend as adequacy is attained. The implication of this study is that rather than continuously carrying out design of asphalt concrete especially when the bitumen content is a significant determining factor, it will be necessary to adopt a model based on past laboratory performance of asphalt concrete manufactured based on satisfactory criteria of material specification and design requirement. This will of course save time and cost rather than going into the rigorous laboratory method of testing. It is now evident that simple multiple regression has proffer the opportunity of using other volumetric variables (independent) to predict the stability values of a compacted hot mixed asphalt concrete provided the quality of pavement mix prepared for wearing course meet the pavement service requirement as recommended by NGS (1997) [24].

Sample description	Sexp.	Spred.	Model	Abs. error	% error
D1	8.85	8.90	1	0.0054	0.54
D2	8.05	8.98	1	0.1154	11.54
D3	7.51	6.75	1	0.1015	10.15
D4	9.66	9.86	1	0.0212	2.12
D5	10.46	10.46	1	0.0005	0.05
D6	7.78	7.46	1	0.0412	4.12
D7	12.07	12.14	1	0.0061	0.61
D8	11.27	11.17	1	0.0092	0.92
D9	12.88	12.32	1	0.0436	4.36
D10	10.06	10.22	1	0.0163	1.63
D11	8.45	8.53	1	0.0091	0.91
D12	7.65	7.58	1	0.0090	0.90
D13	13.36	12.97	1	0.0294	2.94
D14	10.25	10.39	1	0.0139	1.39
D15	9.5	10.05	1	0.0574	5.74

Table 9 Experimental and predicted Marshall Stability of asphalt plant D
9. táblázat A D aszfaltgyár kísérleti **és** *előrejelzett Marshall-stabilitása*

Sample description	Sexp.	Spred.	Model	Abs. error	% error
E1	9.95	9.88	2	0.0066	0.66
E2	10.87	10.98	2	0.0104	1.04
E3	9.36	9.33	2	0.0036	0.36
E4	10.55	10.46	2	0.0089	0.89
E5	11.34	11.18	2	0.0142	1.42
E6	9.62	9.59	2	0.0036	0.36
E7	10.69	10.74	2	0.0044	0.44
E8	10.4	10.47	2	0.0063	0.63
E9	11.22	11.30	2	0.0069	0.69
E10	9.81	9.74	2	0.0075	0.75
E11	9.82	9.89	2	0.0075	0.75
E12	10.18	10.17	2	0.0012	0.12
E13	9.74	9.81	2	0.0072	0.72
E14	10.72	10.62	2	0.0097	0.97
E15	9.75	9.90	2	0.0156	1.56

Table 10 Experimental and predicted Marshall Stability of asphalt plant E
10. táblázat Az E aszfaltgyár kísérleti és előrejelzett Marshall-stabilitása

Sample description	Sexp.	Spred.	Model	Abs. error	% error
G1	9.39	9.36	3	0.0037	0.37
G2	8.41	8.42	3	0.0008	0.08
G3	9.04	9.02	3	0.0021	0.21
G4	9.24	9.26	3	0.0027	0.27
G5	9.11	8.91	3	0.0216	2.16
G6	8.26	8.29	3	0.0032	0.32
G7	9.44	9.45	3	0.0010	0.10
G8	8.53	8.53	3	0.0002	0.02
G9	9.37	9.40	3	0.0028	0.28
G10	8.76	8.81	3	0.0062	0.62
G11	9.25	9.24	3	0.0008	0.08
G12	9.34	9.36	3	0.0022	0.22
G13	9.46	9.46	3	0.0003	0.03
G14	8.89	8.99	3	0.0108	1.08
G15	8.41	8.40	3	0.0011	0.11

Sexp. = Stability (experimental); S = Stability (predicted); Abs. error = Absolute error

Table 11 Experimental and predicted Marshall Stability of asphalt plant G
11. táblázat A G aszfaltgyár kísérleti és előrejelzett Marshall-stabilitása

Descrip-tions	D		E	.	G	.
	Sexp.	Spred.	Sexp.	Spred.	Sexp.	Spred.
Mean	9.853333	5.008671	10.268	10.26934	8.993333	8.99298
Variance	3.570067	3.396386	0.372003	0.363711	0.176952	0.172989
Observ.	15	15	15	15	15	15
PC	0.975362		0.98878		0.988791	
HPC	0		0		0	
df	14		14		14	
t Stat	0.013595		-0.05716		0.021799	
P(T<=t) one-tail	0.494672		0.477611		0.491458	
t Critical one-tail	1.76131		1.76131		1.76131	
P(T<=t) two-tail	0.989345		0.955222		0.982916	
t Critical two-tail	2.144787		2.144787		2.144787	

Observ. = Observations; PC = Pearson Correlation; HPC = Hypothesized Mean Difference; df = Degree of freedom

Table 12 T-Test of D, E and G: Paired Two Sample for Means
12. táblázat D, E és G T-próbája: párosított kétmintás átlagértékek

Anova: Single Factor						
Summary						
Groups	*Count*	*Sum*	*Average*	*Variance*		
S	15	147.8	9.85333	3.57006		
Spred	15	147.7781	9.85187	3.39638		
ANOVA						
Source of Variation	*SS*	*df*	*MS*	*F*	*P-value*	*F crit*
Between Groups	1.61E-05	1	1.61E-05	4.61E-06	0.99830	4.19597
Within Groups	97.53033	28	3.48322			
Total	97.53035	29				

Table 13 Analysis of variance: Single factor for D
13. táblázat Varianciaanalízis a D telephelyhez

Anova: Single Factor						
Summary						
Groups	*Count*	*Sum*	*Average*	*Variance*		
S	15	154.02	10.268	0.37200		
Spred	15	154.0402	10.26934	0.36371		
ANOVA						
Source of Variation	*SS*	*df*	*MS*	*F*	*P-value*	*F crit*
Between Groups	1.36E-05	1	1.36E-05	3.69E-05	0.99519	4.19597
Within Groups	10.3	28	0.36785			
Total	10.30001	29				

Table 14 Analysis of variance: Single factor for E
14. táblázat Varianciaanalízis az E telephelyhez

Anova: Single Factor						
Summary						
Groups	Count	Sum	Average	Variance		
S	15	134.9	8.99333	0.17695		
Spred.	15	134.8947	8.99298	0.17298		
ANOVA						
Source of Variation	SS	df	MS	F	P-value	F crit
Between Groups	9.37E-07	1	9.37E-07	5.36E-06	0.99817	4.19597
Within Groups	4.89918	28	0.17497			
Total	4.89918	29				

Table 15 Analysis of variance: Single factor for G
15. táblázat Varianciaanalízis a G telephelyhez

3.5 Relationship between the experimented and predicted responses

The relationship between the experimented results and predicted responses of stability S obtained from the three models of *Eq. (8)*, *(10)* and *(12)* are presented in *Fig. 2a-c*. The results show a very high R-square values of up to 0.95 indicating that the models are adequate in predicting the stability of wearing course hot mixed asphalt concrete. These results provide further support for the hypothesis that the difference between the laboratory observed results and the model outcome was not significant.

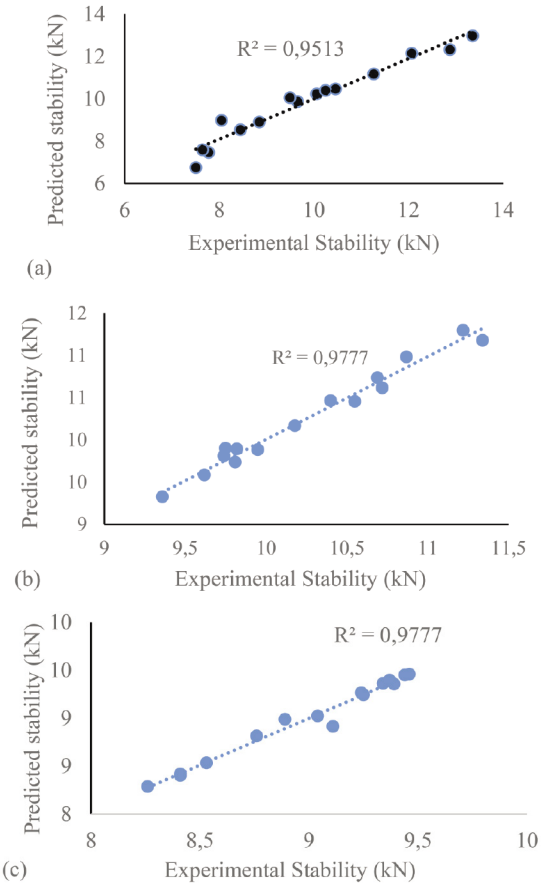

Fig. 2 Relationship between experimented and predicted results for (a) asphalt production plant D (b) asphalt production plant E and (c) asphalt production plant G
2. ábra A kísérleti és az előre jelzett eredmények közötti kapcsolat a) a D aszfaltgyártó üzem, b) az E aszfaltgyártó üzem és c) a G aszfaltgyártó üzem esetében

3.6 Correlation statistics

The correlation statistics (*Tables 16-18*) and their p-values (*Tables 19-21*) relationships between stability, S and other variables; BIT, VIM, VMA, VFB and F derived from Marshall tests, indicate various levels of associations. The results of asphalt plants D, indicate that the correlations between stability values S and BIT (0.9687 $P < 0.05$); VIM (-0.5747 $P < 0.05$); VMA (-0.4035 $P > 0.05$); VFB (0.5243 < 0.05) and F (-0.1778 > 0.05) show that BIT, VIM and VFB has high variable positive and negative correlations values with p-values less 0.05. Also, the correlation of asphalt plant E observed between S and BIT, VIM VFB, and F are (0.9859; $P < 0.05$), (-0.1342; $P > 0.05$); (-0.1833; $P > 0.05$), (0.0309; $P > 0.05$) and (-0.9623; $P < 0.05$), respectively

(See *Tables 9* and *12*). This indicate that bitumen content BIT and Marshall flow, F are well correlated with stability values of wearing course of hot mix asphalt concrete. This finding is in agreement with Bala et al., [29] findings which showed a good correlation between bitumen content Stability and flow. Similarly, the result of hot mix asphalt concrete tested for site G shows the correlation between stability S and BIT (0.9885 $P < 0.05$); VIM (-0.8886; $P < 0.05$); VMA (-0.1972 $P > 0.05$); VFB (0.7925 < 0.05) and F (-0.9885 < 0.05) is an indication that all variables except VMA correlated well with stability. Based on this study, it could be said that stability of wearing course of hot asphaltic concrete is undoubtedly a function of Marshall volumetric properties. Besides all variables showing various degree of relationship with stability for the three asphalts plant, one of the more significant findings to emerge from this study is that bitumen content BIT is a common significant factor that could influence the stability values of the wearing course of a compacted hot mix asphalt concrete. This is observed in the high positive correlation matrix between stability and bitumen (binder) for the three sites considered in this study. A possible explanation to this is based on the fact that the increase in bitumen content in a hot mix asphalt concrete; results in filling of the voids in total mix VIM thereby reducing percentage voids in total mix VIM. Also, it offers additional cohesive and adhesive bonding between the diverse aggregates within the mix thereby increasing percentage voids filled with bitumen VFB. This behavior agrees with the correlation statistics between stability and void variables (VIM and VFB) gotten for the threes asphalt plant site which indicate a negative and positive correlation statistics for VIM and VFB, respectively. Furthermore, the increase in bitumen or binder content stated in this study is based on optimum content which did not exceed the acceptable range or limits provided in the mix design of the project or job specifications. So, the performance of bitumen paving mixture or compacted/dense hot mixed asphaltic concrete is influenced by the unified and adhesive bonding between aggregates and bitumen (binder) [37]. Generally, this study has been able to show that these variables; BIT, VIM and VFB are very critical and pivotal to achieving adequate stability and must be strictly monitored so as to achieve stability S values that would meet the project specification based on optimum design of asphalt concrete. The test (correlation) was successful as it was able to identify critical variables whose contributions are very fundamental and should be looked out for during preliminary laboratory investigation so as to minimize error as well as achieve adequate quality of wearing course asphaltic concrete.

	S	BIT	VIM	VMA	VFB	F
S	1					
BIT	0.9687	1				
VIM	-0.5747	-0.5705	1			
VMA	-0.4035	-0.4820	0.4791	1		
VFB	0.5243	0.4988	-0.9768	-0.2813	1	
F	-0.1778	-0.2607	0.1470	0.7643	0.0263	1

Table 16 Correlation matrix (Pearson) for site D
16. táblázat Korrelációs mátrix (Pearson) a D helyszínhez

	S	BIT	VIM	VMA	VFB	F
S	1					
BIT	0.985909	1				
VIM	-0.13423	-0.09995	1			
VMA	-0.18327	-0.11264	0.353112	1		
VFB	0.030897	0.04936	-0.73694	0.369174	1	
F	-0.96225	-0.98837	0.114038	0.078405	-0.0907	1

Table 17 Correlation matrix (Pearson) for site E
17. táblázat Korrelációs mátrix (Pearson) az E helyszínhez

	S	BIT	VIM	VMA	VFB	F
S	1					
BIT	0.988471	1				
VIM	-0.88856	-0.90064	1			
VMA	0.197214	0.176472	-0.25973	1		
VFB	0.792468	0.793264	-0.90842	0.63736	1	
F	0.988471	1	-0.90064	0.176472	0.793264	1

Table 18 Correlation matrix (Pearson) for site G
18. táblázat Korrelációs mátrix (Pearson) a G helyszínhez

	S	BIT	VIM	VMA	VFB	F
S	0.000					
BIT	0.000	0.000				
VIM	0.025	0.026	0.000			
VMA	0.136	0.069	0.071	0.000		
VFB	0.045	0.058	0.000	0.310	0.000	
F	0.520	0.345	0.595	0.001	0.933	0.000

Table 19 P values of compacted asphalt concrete of site D
19. táblázat D telephely tömörített aszfaltbetonjának P értékei

	S	BIT	VIM	VMA	VFB	F
S	0.000					
BIT	0.000	0.000				
VIM	0.060	0.002	0.000			
VMA	0.380	0.161	0.024	0.000		
VFB	0.123	0.011	0.000	0.629	0.000	
F	0.083	0.000	0.002	0.152	0.011	0.000

Table 20 P values of compacted asphalt concrete of site E
20. táblázat E telephely tömörített aszfaltbetonjának P értékei

	S	BIT	VIM	VMA	VFB	F
S	0.000					
BIT	0.000	0.000				
VIM	0.000	0.000	0.000			
VMA	0.013	0.000	0.000	0.000		
VFB	0.000	0.000	0.261	0.009	0.000	
F	0.630	0.322	0.002	0.789	0.221	0.000

Table 21 P values of compacted asphalt concrete of site G
21. táblázat G telephely tömörített aszfaltbetonjának P értékei

4. Conclusions

The study on analysis of grade of asphalt and bitumen used in pavement construction clearly revealed that asphalt concrete from all the asphalt plant met the requirement for bitumen content, stability and flow when compared to general specification for roads and bridges from Federal Ministry of Works and Housing. The study has also shown that multiple linear regression models developed as a function of stability was adequate and could be used to predict the stability of HMAC designed for wearing course of a road pavement. The study and analysis also identify BIT, VIM and VFB as critical variables that contributed significantly to the stability of a hot mixed asphalt concrete and should be carefully observed in laboratory studies so as to minimize error and achieve optimum mix design that would realize adequate quality. Above all, to achieve good field performance of the asphalt concrete obtained through dedicated modelling from laboratory reports, relevant engineering procedure should be adopted during laying. This include but not limited to ensuring asphalt compaction thickness conform to design provision and also ensure that asphalt pavement surface is subjected to adequate drainage condition.

References

[1] O'Flaherty CA. Evolution of the transport task: C. A. O'Flaherty (ed): Transport planning and traffic engineering. Oxford: Elservier 1997.

[2] Gogoi R, Dutta B. (2020) Maintenance prioritization of interlocking concrete block pavement using fuzzy logic, Inter. J. Pavement Res. Technol. 2020; 13(2): 168-175.

[3] Aghamelu OP, Okogbue CO. Geotechnical assessment of road failure in the Abakaliki Area, Southeastern Nigeria. International Journal of Civil and Environmental Engineering. 2011; 11(2): 12 – 24.

[4] Jegede, G. Effect of soil properties on pavement failure along the F209 highway at Ado-Ekiti, Southwestern Nigeria. Construction and Building Materials. 2000; 14: 311- 315.

[5] Ofonime A, Aniekan E. Relationship between road pavement failures, engineering indices and underlying geology in a tropical environment. Global Journal of Geological Sciences. 2005; 4(2): 99 – 108.

[6] Akintorinwa OJ, Ojo JS, Olorunfemi MO. Appraisal of the causes of pavement failure along the Ilesa-Akure highway, Southwestern Nigeria using remotely sensed and geotechnical data. Ife Journal of Science. 2011; 13(1): 185-197.

[7] Osuolale OM, Oseni AA, Sanni IA. Investigation of highway pavement failure along Ibadan-Iseyin Road, Oyo State, Nigeria. International Journal of Engineering Research & Technology (IJERT). 2012; 1(8), 1-6.

[8] Etim RK, Eberemu AO, Osinubi K.J. Stabilization of black cotton soil with lime and iron ore tailings admixture. Journal of Transportation Geotechnics Elsevier. 2017; 10:85-95. http://dx.doi.org/10.1016/j.trgeo.2017.01.002

[9] Bassey OB, Attah IC, Ambrose EE, Etim RK. Correlation between CBR Values and Index Properties of Soils: A Case Study of Ibiono, Oron and Onna in Akwa Ibom State. Resources and Environment. 2017; 7(4): 94-102. http://dx.doi.org/10.5923/j.re.20170704.02

[10] Moses G, Etim RK, Sani JE, Nwude M. Desiccation effect of compacted tropical black clay treated with concrete waste. Leonardo Electronic Journal of Practices and Technologies. 2018; Issue 33: 69-88.

[11] Sani JE, Etim RK, Joseph A. Compaction behaviour of lateritic soil–calcium chloride mixtures. Geotechnical and Geological Engineering. Springer Nature Switzerland. 2019a; 37: 2343-2362. https://doi.org/10.1007/s10706-018-00760-6

[12] Sani JE, Yohanna P, Etim RK, Attah IC, Bayang, F. Unconfined compressive strength of compacted lateritic soil treated with selected admixtures for geotechnical applications. Nigerian Research Journal of Engineering and Environmental Sciences. 2019b; 4(2): 801-815.

[13] Etim RK, Attah IC, Eberemu AO, Yohanna P. Compaction behaviour of periwinkle shell ash treated lateritic soil for use as road sub-base construction material. Journal of GeoEngineering, Taiwan Geotechnical Society. 2019; 14(3): 179-190, http://dx.doi.org/10.6310/jog.201909_14(3).7

[14] Etim RK, Attah IC, Yohanna P. Experimental study on potential of oyster shell ash in structural strength improvement of lateritic soil for road construction. International Journal of Pavement Research Technology, Chinese Society of Pavement Engineering, Springer Nature Singapore. 2020. https://doi.org/10.1007/s42947-020-0290-y

[15] Attah IC, Agunwamba JC, Etim RK, Ogarekpe NM. Modelling and predicting of CBR values of lateritic soil treated with metakaolin for road material. ARPN Journal of Engineering and Applied Sciences. 2019; 14(20): 3606 – 3618.

[16] Moses G, Etim RK, Sani JE, Bobai YS. Geotechnical properties of crude oil incinerated lateritic soil for use in roadwork. FUW Trends in Science & Technology Journal, Federal University Wukari. 2019; 4(1): 69 – 74.

[17] Moses G, Etim RK, Sani JE, Nwude M. Desiccation-induced volumetric shrinkage characteristics of highly expansive tropical black clay treated with groundnut shell ash for barrier consideration. Civil and Environmental Research. 2019; 11(8): 58–74. https://doi.org/10.7176/CER/11-8-06

[18] Muench ST, Moomaw T. De-bonding of hot mix asphalt pavements in Washington State: An initial investigation. Technical report. Washington 146 State Department of Transportation, Office of Research & Library Services: Transportation Northwest Regional Center X (TransNow) 2008.

[19] Caro S, Masad E, Bhasin A, Little DN. Moisture susceptibility of asphalt mixtures, Part 1: mechanisms," International Journal of Pavement Engineering. 2008; (9): 81-98.

[20] Alhaji MM, Alhassan M. Effect of reclaimed asphalt pavement stabilization on the microstructure and strength of black cotton soil. International Journal of Technology. 2018; 9(4): 727–736.

[21] Ahmedzade P, Sengoz B. Evaluation of steel slag coarse aggregate in hot mix asphalt concrete. J Hazard Mater. 2009; 165:300–305.

[22] Uzun I, Terzi S. Evaluation of andesite waste as mineral filler in asphaltic concrete mixture. Constr Build Mater. 2012; 31:284–288.

[23] Akinleye MT, Tijani MA. Assessment of quality of asphalt concrete used in road construction in South West Nigeria. Nigerian Journal of Technology Development. 2017; 14(2): 51 – 54.

[24] Nigerian General Specifications, NGS: Roads and Bridges. Federal Ministry of Works, Abuja, Nigeria. 1997.

[25] Osunkunle A, Yusuf I, Ako T, Abolarin J. Assessment of engineering properties of asphaltic concrete produced in South Western Nigeria. Webs Journal of Science and Engineering Application. 2016; 5(1) 41-48.

[26] Obeta IN, Njoku JE. Durability of flexible pavements: A case study of South-Eastern Nigeria, Nigerian Journal of Technology. 2016; 35(2): 297-305.

[27] Alkawaaz NG, Qasim HA. Experimentally evaluation of durability characteristics for reclaimed local asphalt pavement mixtures. Imperial J Interdiscipl Res. 2016; 2(10).

[28] Erlingsson, S. Modelling of rutting development in pavement structures. Procedia-Social and Behavioral Sciences. 2012; 48: 321-330.

[29] Bala N, Napiah M, Kamaruddin I. Application of multivariable regression models for prediction of composite nanosilica/polymer asphalt mixture OBC. International Journal of GEOMATE. 2018; 14(45): 202-209. https://doi.org/10.21660/2018.45.94051

[30] Kim SH, Kim N. Development of performance prediction models in flexible pavement using regression analysis method. KSCE Journal of Civil Engineering. 2006; 10(2): 91–96.

[31] Laurinavi˘cius A, Oginskas R. Experimental research on the development of rutting in asphalt concrete pavements reinforced with geosynthetic materials. Journal of Civil Engineering and Management. 2006; 12(4): 311–317.

[32] Shukla PK, Das A. A re-visit to the development of fatigue and rutting equations used for asphalt pavement design. International Journal of Pavement Engineering, 2008; 9(5): 355–364.

[33] Asifur Rahman ASM, Mendez Larrain MM, Tarefder RA. Development of a nonlinear rutting model for asphalt concrete based on Weibull parameters. International Journal of Pavement Engineering. 2017; 1–10.

[34] Baldo N, Manthos E, Pasetto M. Analysis of the mechanical behaviour of asphalt concretes using artificial neural networks. Advances in Civil Engineering. Article ID 1650945, https://doi.org/10.1155/2018/1650945

[35] Igwe EA, Ayotamuno MJ, Okparanma RN. Road surface properties affecting rates of energy dissipation from vehicles. J Appl Energy. 2009; 86: 1692–1696.

[36] Agunwamba JC. 2007. Engineering Mathematical Analysis. De-Adroit Innovation, Enugu, Nigeria.Chap 16 and 17. ISBN 978-8137-08-3.

[37] Aboufoul M, Garcia A. Factors affecting hydraulic conductivity of asphalt mixture," Materials and Structures. 2017; 50, p. 116.

[38] Etim, R. K. Ekpo, D U. Ebong, UB, Usanga, I. N. (2021) Influence of periwinkle shell ash on the strength properties of cement-stabilized lateritic soil. International Journal of Pavement Research Technology, Chinese Society of Pavement Engineering, Springer Nature Singapore. https://doi.org/10.1007/s42947-021-00072-8

[39] Etim, R. K., Attah, I.C., Ekpo, D.U., Usanga, I.N. (2021) Evaluation on Stabilization Role of Lime and Cement in Expansive Black Clay - Oyster Shell Ash Composite. Transportation Infrastructure Geotechnology. https://doi.org/10.1007/s40515-021-00196-1

[40] Etim, R. K., Ekpo, D U. Etim, G.U., UB, Attah, I.C (2021) Evaluation of lateritic soil stabilized with lime and periwinkle shell ash (PSA) admixture bound for sustainable road materials. Innovative Infrastructure Solutions. https://doi.org/10.1007/s41062-021-00665-z

[41] Etim, R. K., Ekpo, D U., Attah, I.C. Onyelowe, K.C. (2021) Effect of micro sized quarry dust particle on the compaction and strength properties of cement stabilized lateritic soil. Cleaner Materials, https://doi.org/10.1016/j.clema.2021.100023

[42] Attah, I.C., Etim, R.K., Ekpo, D.U., Onyelowe, K.C. (2021) Understanding the impacts of binary additives on mechanical and morphological response of ameliorated soil for road infrastructures. Journal of King Saud University-Engineering Sciences, https://doi.org/110.1016/j.jksues.2021.12.001

[43] Yohanna, P., Etim, R.K., Ijimdiya, T.S., Osinubi, K.J., Buki, J.M. (2022) Reliability analysis of compaction characteristics of tropical black clay admixed with lime and iron ore-silica based dominant tailing. epitoanyag – Journal of Silicate Based and Composite Materials. Vol. 74 No.1; pp. 13-20. http://doi.org/10.14382/epitoanyag-jsbcm.2022.3

[44] Yohanna, P., Ibrahim, U.A and Etim, R. K. (2020) Compaction Behaviour of Black Cotton Soil Treated with Selected Admixtures: A Statistical Approach. Premier Journal of Engineering and Applied Sciences. Publication of Nigerian Society of Engineers, Ibadan Branch. Vol. 1, No. 1, pp. 35 – 44

[45] Yohanna, P., Kanyi, M. I., Etim, R. K., Eberemu, O. A., Osinubi, K. J. (2021) Experimental and Statistical Study on Black Cotton Soil Modified with Cement–Iron Ore Tailings. FUOYE Journal of Engineering and Technology (FUOYEJET), Vol. 6, Issue 1, http://dx.doi.org/10.46792/fuoyejet.vAiB.C

[46] Etim, R. K., Eberemu, A. O and Osinubi, K. J. (2014) Effect of Lime – Iron Ore Tailing Blend on the Expansive Behaviour of Black Cotton Soil. In: Proceeding of Nigeria Engineering Conference. Theme: Engineering and Technology for Economic Transformation. Faculty of Engineering, Ahmadu Bello University, Zaria, September 15-18, 2014. Zaria, Kaduna State. CR ROMs of Presentation; 2014: 864 – 874.

[47] Sani, J. E., Yohanna, P., Etim K. R., Osinubi, J. K. and Eberemu, O. A. (2017). Reliability Evaluation of Optimum Moisture Content of Tropical Black Clay Treated with Locust Bean Waste Ash as Road Pavement Sub-base Material. Geotechnical and Geological Engineering Springer. http://link.springer.com/article/10.1007/sl0706-017-0256-2

[48] Onyelowe, K.C., Bui Van, D (2018) Predicting strength behaviour of stabilized lateritic soil- ash matrix using regression model for hydraulically bound materials purposes, Int. J. Pavement Res. Technol. https://doi.org/10.1016/j.ijprt.2018.08.004

Ref.:
Etim, Roland Kufre – **Usanga**, Idorenyin Ndarake – **Ekpo**, David Ufot – **Attah**, Imoh Christopher: *Material characterization and statistical evaluation of properties of hot mix asphalt concrete (HMAC) used in wearing course of road pavement; Southern Nigeria*
Építőanyag – Journal of Silicate Based and Composite Materials, Vol. 74, No. 5 (2022), 196–205. p.
https://doi.org/10.14382/epitoanyag-jsbcm.2022.29

Üvegipari szakmai konferencia a Daniella Ipari Park Kft. Energocell hőszigetelő üveghabgyártó üzemében
2022. október 11.

A Szilikátipari Tudományos Egyesület Üveg Szakosztályának hagyományos őszi szakmai konferenciájára ezúttal a Daniella Ipari Park Kft. szíves közreműködésével a nemrég beüzemelt Energocell hőszigetelő üveghabgyártó üzemében került sor. A rendezvény előadásaiban kiemelt szerepet kaptak a 2022 – Az Üveg Éve aktuális eseményei, illetve a vendéglátó cég tevékenységének és legújabb üzemének bemutatása.

A 2022 - Az Üveg Éve az ENSZ dedikált, egy éven át tartó rendezvénye, melynek célja, hogy felhívja a társadalom és a döntéshozók figyelmét az üvegben rejlő lehetőségekre, a modern társadalomban betöltött, nélkülözhetetlen funkcióira, melyeket előrelátó tervezéssel fenntartható módon lehet előállítani.

A fenntarthatóságnak egyik fontos aspektusa az elsődleges nyersanyag-szükséglet csökkentése, másod-nyersanyagok minél nagyobb mértékű felhasználása a keletkező ipari melléktermékek, hulladékok hasznosítása révén. A megfelelő technológia és alapanyag-receptek kifejlesztésével környezetkímélőbb módon, a bányászott nyersanyagok mennyiségének csökkentésével, kevesebb energia felhasználásával állíthatunk elő termékeket. A Daniella Ipari Park Kft. terméke, az Energocell üveghab és annak gyártása eklatáns példái a tudatos, körforgásos gazdálkodásnak és a fenntartható nyersanyag gazdálkodásnak, melyhez kreatív és innovatív mérnöki-műszaki megoldásokra is láthattak a résztvevők példákat az előadásokat követő üzemlátogatás során.

A szakmai konferencia az értékes előadások mellett jó lehetőséget biztosított az ipari és akadémiai, kutatás – fejlesztési és felsőoktatási szakemberek részére együttműködési, fejlesztési lehetőségek megvitatására is. A rendezvény szervezői, a Szilikátipari Tudományos Egyesület Üveg Szakosztálya, illetve a Daniella Ipari Park Kft. valamennyi érdeklődőnek ezúton is köszönik a részvételt. Remélik továbbá, hogy immár véglegesen visszatér a jelenléti szakmai rendezvények lehetősége, és jövő tavasszal a hagyományaink szerint folytatódhat egy hasonlóan sikeres szakmai konferenciával a találkozók sora.

GUIDELINE FOR AUTHORS

The manuscript must contain the followings: title; author's name, workplace, e-mail address; abstract, keywords; main text; acknowledgement (optional)**; references; figures, photos with notes; tables with notes; short biography** (information on the scientific works of the authors).

The full manuscript should not be more than 6 pages including figures, photos and tables. Settings of the word document are: 3 cm margin up and down, 2,5 cm margin left and right. Paper size: A4. Letter size 10 pt, type: Times New Roman. Lines: simple, justified.

TITLE, AUTHOR

The title of the article should be short and objective.

Under the title the name of the author(s), workplace, e-mail address.

If the text originally was a presentation or poster at a conference, it should be marked.

ABSTRACT, KEYWORDS

The abstract is a short summary of the manuscript, about a half page size. The author should give keywords to the text, which are the most important elements of the article.

MAIN TEXT

Contains: materials and experimental procedure (or something similar), results and discussion (or something similar), conclusions.

REFERENCES

References are marked with numbers, e.g. [6], and a bibliography is made by the reference's order. References should be provided together with the DOI if available.

Examples:

Journals:

[6] Mohamed, K. R. – El-Rashidy, Z. M. – Salama, A. A.: In vitro properties of nano-hydroxyapatite/chitosan biocomposites. *Ceramics International.* 37(8), December 2011, pp. 3265–3271, http://doi.org/10.1016/j.ceramint.2011.05.121

Books:

[6] Mehta, P. K. – Monteiro, P. J. M.: Concrete. Microstructure, properties, and materials. *McGraw-Hill*, 2006, 659 p.

FIGURES, TABLES

All drawings, diagrams and photos are figures. The **text should contain references to all figures and tables**. This shows the place of the figure in the text. Please send all the figures in attached files, and not as a part of the text. **All figures and tables should have a title**.

Authors are asked to submit color figures by submission. Black and white figures are suggested to be avoided, however, acceptable.

The figures should be: tiff, jpg or eps files, 300 dpi at least, photos are 600 dpi at least.

BIOGRAPHY

Max. 500 character size professional biography of the author(s).

CHECKING

The editing board checks the articles and informs the authors about suggested modifications. Since the author is responsible for the content of the article, the author is not liable to accept them.

CONTACT

Please send the manuscript in electronic format to the following e-mail address: femgomze@uni-miskolc.hu and epitoanyag@szte.org.hu or by post: Scientific Society of the Silicate Industry, Budapest, Bécsi út 122–124., H-1034, HUNGARY

We kindly ask the authors to give their e-mail address and phone number on behalf of the quick conciliation.

Építőanyag – *Journal of Silicate Based and Composite Materials*, Quarterly peer-reviewed periodical of the Hungarian Scientific Society of the Silicate Industry, SZTE.
http://epitoanyag.org.hu